Fluorescently Labeled Carbohydrates as Targeted Tumor Imaging Probes and as pH Responsive Gelators

Thesis Submitted to AcSIR for the Award of the Degree of
DOCTOR OF PHILOSOPHY
in Chemical Sciences

By
Shimi M.
Registration No: 10CC13J39008

Under the combined guidance of

Dr. Suresh Das
and
Dr. K. V. Radhakrishnan

CSIR-NATIONAL INSTITUTE FOR INTERDISCIPLINARY SCIENCE AND TECHNOLOGY (CSIR-NIIST)
THIRUVANANTHAPURAM-695 019, KERALA, INDIA

June 2017

Dedicated to My Parents, Sister and Teachers……

DECLARATION

I hereby declare that the Ph.D. thesis entitled **"Fluorescently Labeled Carbohydrates as Targeted Tumor Imaging Probes and as pH Responsive Gelators"** is an independent work carried out by me at the Chemical Sciences and Technology Division, CSIR-National Institute for Interdisciplinary Science and Technology (CSIR-NIIST), Thiruvananthapuram under the combined supervision of Dr. Suresh Das and Dr. K. V. Radhakrishnan, and it has not been submitted anywhere else for any other degree, diploma or title.

Shimi M.

Thiruvananthapuram
June 2017

NATIONAL INSTITUTE FOR INTERDISCIPLINARY SCIENCE & TECHNOLOGY

Council of Scientific & Industrial Research

GOVERNMENT OF INDIA

Thiruvananthapuram-695 019, India

CERTIFICATE

This is to certify that the work incorporated in this Ph.D. thesis entitled ***"Fluorescently Labeled Carbohydrates as Targeted Tumor Imaging Probes and as pH Responsive Gelators"*** *submitted by* ***Mrs. Shimi M.*** *to Academy of Scientific and Innovative Research (AcSIR), New Delhi, in partial fulfillment of the requirements for the award of the* ***Degree of Doctor of Philosophy in Chemical Sciences,*** *embodies original research work under our combined supervision and guidance at the Chemical Science and Technology Division, CSIR-National Institute for Interdisciplinary Science and Technology (CSIR-NIIST), Thiruvananthapuram. We further certify that this work has not been submitted to any other University or Institution in part or full for the award of any degree or diploma.*

Dr. Suresh Das ***Dr. K. V. Radhakrishnan***

(Thesis Supervisor) ***(Thesis Supervisor)***

Thiruvananthapuram

June 2017

ACKNOWLEDGEMNTS

*It is my great pleasure to express my deep sense of gratitude to my research supervisors **Dr. Suresh Das** and **K. V. Radhakrishnan** for suggesting the research problem and for the guidance, constant support and encouragement that led to the successful completion of this work.*

I thank Dr. A. Ajayaghosh, and Dr. Gangan Prathap present and former Directors of CSIR-NIIST, Thiruvananthapuram, for providing me the necessary facilities and infrastructure of the institute for carrying out this work.

My Sincere thanks are also due to

- ✓ *Dr. Mangalam S. Nair and Dr. R. Luxmi Varma former and present AcSIR programme coordinators at CSIR-NIIST for timely help and advice for the academic procedures of AcSIR*
- ✓ *Dr. K. R. Gopidas, Dr. D. Ramaiah, Former Head, Chemical Sciences and Technology Division for their support*
- ✓ *Dr. Bhoje Gowde, and Dr. Narayanan Unni, (DAC members) for their valuable suggestions throughout the research period*
- ✓ *Prof. M. V. George and Dr. G. Vijay Nair, for their inspiring presence*
- ✓ *Dr. A. Jayalekshmy, Dr. Kaustabh Kumar Maiti, Dr. L. Ravisankar and Dr. B. S. Sasidhar, Scientists of Organic Chemistry Section, for their help and support extended to me*
- ✓ *Dr. Jubi John and Dr. Ganesh Chandra Nandi for their valuable suggestions and support*
- ✓ *Dr. Sunil Varughese, for Single Crystal X-ray analysis*
- ✓ *Dr. Raghu K. G. and Dr. Vandana Sankar, Agroprocessing and Technology Division for the biological imaging studies*
- ✓ *Ms. Saranya Jayaram for conducting the cytotoxicity studies*
- ✓ *Mrs. Saumini Mathew, Mr. B. Adarsh, Mr. Arun, Mr. Vipin M. G., Mr. Saran P. Raveendran, Mr. Syam and Mr. Rakesh Gokul for recording NMR spectra. Thanks are also due to Mrs. S. Viji and Ms. Aathira for mass spectral analysis*
- ✓ *Mr. Chandrakanth C. K., Mr. Chandran, Mrs. Soumya, Mr. Aswin and Mr. Vishnu for the SEM and AFM analysis*
- ✓ *Dr. K. V. Ratheesh, Dr. K. M. Shafeekh, Dr. Abdul Rahim, Dr. Deepak D. Prabhu, Dr. P. S. Aneesh Mr. Rahul Ongungal, and Mrs. Kanya B. Nair, for giving me the basic ideas of research and immense support*
- ✓ *Ms. P. R. Nitha for assisting me in conducting some of the experiments reported in this thesis*
- ✓ *Dr. Nayana Joseph, Dr. Ajish K. R., Dr. Praveen Prakash, Dr. E. Jijy and Dr. Sarath Chand S, Mr. Preethanuj Preethalayam, Dr. Saranya. S., Mr. Ajesh Vijayan, Ms. Aparna P. S., Ms. Dhanya B. P., Ms. Santhini P. V., Mrs. Remya Raj, Mr.*

Sasikumar P., Ms. Greeshma Gopalan, Ms. Prabha B. Ms. Sharathna Sivan, Ms. Neethu, Mr. Madhu Balakrishnan, Mrs. Meenu, Ms. Ummu Jumaila, Mr. Guruprasad for their companionship and great support

- ✓ *Dr. Suchitra M. V., Dr. Anupriya S., Dr. Jisha Babu, Ms. Maya R. J., Mrs. Athira Krsihna, Ms. Santhi S., Mr. Rajeev K. K., Dr. Dhanya S. R., Dr. Sajin Francis K., Dr. Parvathy Ratnam, Dr. Sinu C. R., Dr. Anu Jose, Dr. Rony Rajan Paul., Dr. Seethalakshmi, Mr. Jagadheesh, Mr. Jayakrishnan A., Ms. Sreedevi P., and Ms. Jyothi for their friendship*
- ✓ *I express my sincere gratitude to Dr. Anil Kumar, Director, and Mr. V. V. Sivan, M. S. Swaminathan Research Foundation-Community Agro biodiversity Centre (MSSRF-CAbC), Kalpetta, Wayanad, Kerala Mr. Sajeev (Managing Director, Ayurvasthra, Thiruvananthapuram) for the successful completion of my CSIR-800 project*
- ✓ *I am grateful to UGC and DST New Delhi, for the financial assistance*
- ✓ *I would like to extend my sincere thanks to all my friends at CSIR-NIIST*

I am deeply and forever indebted to my parents, sister and my husband for their constant source of love, inspiration and support. Finally I would like thank my teachers and friends starting from my school days to those at NIIST, who motivated and blessed me.

Above all, I bow to Almighty for bestowing his blessings upon me.

Shimi M.

CONTENTS

Abbreviations

Ac	Acetyl
AcOH	Acetic acid
ATP	Adenosine triphosphate
AFM	Atomic force microscopy
BSA	Bovine serum albumin
BzCl	Benzoyl chloride
δ	Chemical shift
CD	Circular dichroism
J	Coupling constant
°C	Degree celsius
BODIPY	4,4-Difluoro-4-bora-3a,4a-diazo-8-indacane
d	Doublet
DIPEA	*N*,*N*-diisopropylethylamine
DMAP	4-Dimethyl aminopyridine
DMSO	Dimethyl sulfoxide
DMEM	Dulbecco's mediated eagle's medium
DLS	Dynamic light scattering
ESI	Electrospray ionization
EtOH	Ethanol
EtOAc	Ethyl acetate
Equiv.	Equivalent
FRET	Fluorescence resonance energy transfer
FT-IR	Fourier transform infrared
Φ_f	Fluorescence quantum yield
Gal	Galactose
Glu	Glucose
GLUT	Glucose transporter
GSH	Glutathione
g	Gram

Gul	Gulose
HBSS	Hanks balanced salt solution
Hz	Hertz
HPLC	High pressure liquid chromatography
HRMS	High resolution mass spectroscopy
h	Hour
HeLa	Human cervical cancer cell line
HepG2	Human liver hepatocellular carcinoma
pH	Hydrogen ion concentration at logarithmic scale
ICT	Intramolecular charge transfer
LMOGs	Low molecular weight organo gelators
m	Multiplet
Man	Mannose
MALDI	Matrix assisted laser desorption/ionisation-time of flight
MHz	Mega hertz
MeOH	Methanol
MTT	Methyl thiazolyl tetrazolium bromide
Mg	Microgram
μM	Micromolar
mM	Millimolar
mmol	Millimoles
M	Molar
ε	Molar extinction coefficient
MS	Molecular sieves
nm	Nanometer
NIR	Near-infrared
NAD	Nicotinamide adenine dinucleotide
N	Normality
NMR	Nuclear magnetic resonance
ppm	Parts per million
PBS	Phosphate buffer saline

PET	Positron emission tomography
KOH	Potassium hydroxide
Py	Pyridine
rpm	Revolutions per minute
RNA	Ribonucleic acid
Ribo	Ribose
rt	Room temperature
SEM	Scanning electron microscope
t	Triplet
TBAB	Tetrabutyl ammonium bromide
THF	Tetrahydrofuran
TGA	Thermo gravimetric analysis
TLC	Thin layer chromatography
TEM	Transmition elelctron microscopy
TEA	Triethyl amine
TFA	Trifuoroacetic acid
TMS	Trimethylsilane
UV	Ultraviolet
Vis	Visible
λ_{abs}	Wavelength of absorption
λ_{em}	Wavelength of emission
λ_{ex}	Wavelength of excitation
Xylo	Xylose

PREFACE

Fluorescent labeling of biomolecules is an excellent tool for understanding biological events like receptor-ligand interaction, protein structures and enzyme activity. Fluorescent labeling/tagging involves binding biomolecules chemically or biologically to it. Most commonly used biomolecules are antibodies, proteins, aminoacids and peptides which are amenable to structural modification. Carbohydrates are naturally abundant, ecofiriendly, economical scaffolds which play a critical role in many biological events like cell-cell recognition, cell growth regulation, immune response, cancer cell metastasis, and also as energy source. But the structural modification of carbohydrates is a tiresome process mostly functionalization led to alteration in the structure and their binding properties. Therefore, fluorescently labeled glycans/ carbohydrates are less exploited and a challenging topic in the clinical diagnostics and chemical biology. An overview of the synthetic aspects and varied applications of fluorescent labeled glycoconjugates developed in recent years is discussed in chapter 1.

Chiral supramolecular self-assembly recently received considerable attention in the field of designing of chiroptical devices. In the second chapter, we present the investigation conducted on the aggregation properties of sugar conjugated squaraine dyes in aqueous solution. We synthesized, SSqβGl (symmetrical) bis-sugar appended and mono-sugar appended, ASqβGl (unsymmetrical) squaraine dyes. In the structural designing, we have chosen sugar moiety as hydrophilic chiral ligand and biocompatible triazoles as linkers which connect the squaraine dye and sugar moiety. Both the squaraine dyes SSqβGl and ASqβGl formed H- and J- aggregates in water which lead to non-emissive transition and caused the fluorescence quenching. Symmetrical squaraine dye-SSqβGl formed preferably H-aggregates in aqueous solution while J-aggregate fraction was high for unsymmetrical squaraine dye-ASqβGl which indicates the favourable end to end orientation of ASqβGl in water. CD measurements and morphological analysis clearly evidenced the formation of chiral H-type self-assembly from SSqβGl in water. These squaraine dyes also showed fluorogenic

response in the presence of the enzyme β-glucosidase, a lysosomal lipid hydrolase, membrane-associated glycoprotein that facilitates the cleavage of the glycosidic linkage. H-aggregates formed from SSqβGl underwent cleavage and lead to the fluorescence enhancement. These results support the utility of non-fluorescent aggregates as fluorogenic probes in aqueous solution to overcome the aggregation caused quenching that restricts the biological application of squaraine dyes.

An ideal fluorophore for the specific and sensitive cancer detection requires a cancer cell targeting agent conjugated chemically or biologically to it. Glucose molecules as tumor targeting ligands evoked great interest among researchers in the biomedical field. The application of the glyco-conjugated squaraine dyes for targeted tumor imaging is described in the third chapter. We have utilized the squaraine dyes SSqβGl & ASqβGl and the α-glucose analogue of unsymmetrical squaraine dye ASqαGl for the imaging studies. In order to understand the mechanism and to confirm the stereospecific binding of the glucose transporters, two model compounds; α-mannose and α-galactose analogues of the unsymmetrical squaraine dyes ASqαGa and ASqαM were also synthesised. All the squaraine dyes were internalized in HeLa cell lines, but the cellular uptake of ASqαGl and ASqβGl was only occurring through the glucose transporters. Also, there exist a huge difference in the fluorescence intensity from the cells incubated with ASqβGl and ASqαGl. Glucose transporter mediated uptake of the squaraine dyes were confirmed by competitive assay with D- and L-glucose. ASqαGl was found to be the efficient candidate as an imaging probe which showed better results compared to the commercially available glucose bioprobe, 2-NBDG.

Carbohydrate molecules are excellent hydrogen bond donors and are biocompatible to yield functional materials with significant application in biology. The fourth chapter of the thesis deals with the design and synthesis of pyrene-sugar orthoester conjugates and their application as pH responsive gelator. Orthoesters are important intermediates in the carbohydrate chemistry which are highly sensitive to acid whereas well stable in basic medium. This factor leads to usage of orthoester as pH responsive materials, and the fluorescent pH-responsive

materials based on sugar orthoesters are scarcely studied in the literature. We synthesized two pyrene-sugar orthoester conjuagtes PMO from mannose and PGO from glucose. These materials were able to form fluorescent gels in aromatic solvents like toluene and xylene upon heating and sonication. The study of pH responsive nature of the gel was conducted using trifluoroacetic acid (TFA). The gels formed were found to be unstable even in the presence of a catalytic amount of TFA which leads to the breakage of the gel. The TFA catalysed gel breakage is attributed to the cleavage of orthoester linkage which was further confirmed by NMR studies. The gel formed from pyrene-sugar orthoesters underwent cleavage in the presence of catalytic amount of TFA. Photophysical properties of the synthesized pyrene-carbohydrate conjugates were measured in various solvents and they exhibited characteristic absorption and emission properties of pyrene. SEM analysis was conducted to investigate the morphology of the xerogels prepared by drying the gels formed from toluene. These results disclosed the potency of carbohydrate orthoesters as new functional materials for biological studies.

In summary, we explored carbohydrate scaffolds toward developing supramolecular architectures and designing selective bioimaging probes. In the second chapter we synthesized two glucose conjugated squaraine dyes (Mono-sugar appended, ASqβGl and bis-sugar appended, SSqβGl). These squaraine dyes showed aggregate formation in aqueous solvents associated with fluorescence quenching. Fluorogenic response towards an analyte- β-glucosidase was also proved using the squaraine dye SSqβGl. Selective tumor optical imaging was demonstrated using monosugar appended squaraine dyes ASqβGl and ASqαGl and explained in the third chapter. Fourth chapter describes the application of sugar molecules as low molecular weight pH responsive fluorescent organogelators were made out of pyrene-sugar orthoester conjugates.

CHAPTER 1

Fluorescently labeled carbohydrates: An overview

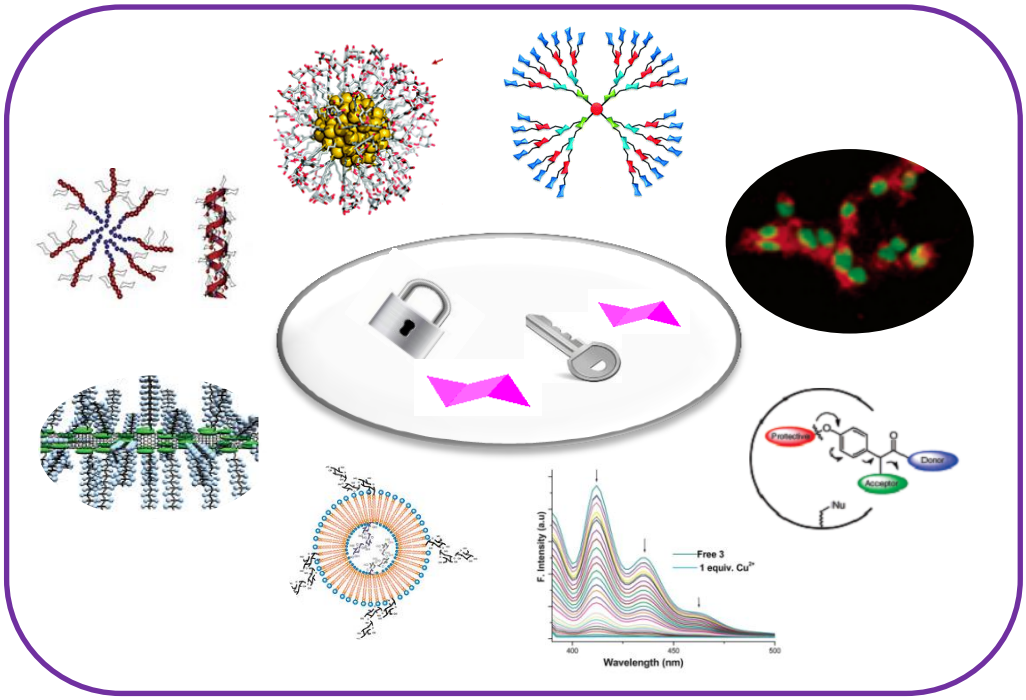

Abstract

The design of small glycoconjugated organic molecules is one of the hot topics in current research due to their possible practical applications in biology as well as in material chemistry. Fluorescently labeled glycoconjugates provide ease of access toward biological events at the molecular level with high selectivity and sensitivity and are widely employed in diagnostic tool development. Moreover, sugar units are excellent building blocks in the supramolecular chemistry owing to their chirality and hydrogen bond forming ability. Various applications and recent developments in the fluorescently labeled glycoconjugates are discussed in the introductory chapter. Finally, objectives of the present work are presented.

1.1. Introduction

Carbohydrates are the fundamental class of organic molecules that are distributed widely in nature and are also known as saccharides. They are mainly classified into two classes- monosaccharides and oligosaccharides. Oligosaccharides are found on cell surfaces in the form of glycoproteins, glycolipids, and glycocalyx which are involved in important life processes such as cell growth regulation, immune response, inflammation by viruses and bacteria, cancer cell metastasis and fertilization.[1] Whereas monosaccharides form the constituent of significant biomolecules like NAD, FAD, RNA and also glucose represent the major energy source for live cells and stored as the metabolite. Because of these factors, carbohydrates play a crucial role in the development of efficacious drugs and diagnostic tools. Combinatorial chemistry explores thousands of synthetic carbohydrates as potential ligands for biological receptors, and rigorous research has been devoted to the development of glycoconjugates for therapeutics as well as diagnostic tools.[2] Consequently, numerous glycomaterials with variable valency, topology, and modes of ligand presentation have been introduced. These glycomaterials include nanoparticles,[3] peptides,[4] dendrimers,[5] polymers,[6] liposomes,[7] cyclodextrins,[8] fullerenes,[9] calixarenes,[10] fluorescent labeling agents,[11] biological sensors[11] and chemosensors[11] for trafficking and as diagnostic probes. In addition to this, glycans are excellent hydrogen bond donors and are widely exploited as building blocks in material chemistry for the construction of supramolecular architectures.

Fluorescence technique offers advantageous features like high sensitivity and less toxicity over other conventional methods which work based on the radiolabeled probes. Fluorescent probes are brilliant tools for monitoring the cellular events at the molecular level with extremely low concentrations of chemical species, and therefore

the development of novel fluorescent probes is a vibrant research field.[12] To accelerate the detection of positive hits and for improving the target selectivity and biocompatibility, carbohydrates can serve as a reliable detecting tool. The structural complexity of the carbohydrates makes the functionalization difficult compared to the presently used nucleic acids and proteins. Functionalization of carbohydrates may cause an alteration in the structure and their binding properties. Thus fluorescently labeled carbohydrates have been less explored and remain as a challenging area of research. However, there have been extensive efforts on understanding interactions and functions of carbohydrate structures in the biological system.

1.2. Covalent labeling of carbohydrates with fluorescent probes

Carbohydrates do not possess any chromophores, and they remain to be non-fluorescent. This makes the carbohydrate analysis which has great significance in biomedicinal chemistry a difficult task. Earlier methods used for carbohydrate detection are gel electrophoresis, and high-performance liquid chromatography (HPLC). *In situ* covalent labeling of the carbohydrates was employed in these analytical techniques.[13] Reducing end of the sugar, which contains masked aldehyde undergo reductive amination in the presence of amines or hydrazines to form corresponding imines or hydrazones. Subsequent reduction of these moieties with sodium cyanoborohydride yield stable amines or hydrazine derivatives. Therefore utilizing a fluorescent amine or hydrazine will lead to the formation of a stable fluorescent product which will light the way to carbohydrate detection. In the case of non-reducing sugars, periodate oxidation of vicinal diols followed by condensation with amine or hydrazine functional group and subsequent sodium cyanoborohydride reduction affords stable amines or hydrazines. Enzymes were also employed in the

oxidation of diols. Various fluorescent amines or hydrazines (Figure 1.1) such as dansyl hydrazine (**1**),[14] dansylamine (**2**),[15] 7-aminonaphthalne-1,3-sulphonic acid (**3**),[16] 2-aminopyridine (**4**),[17] 2-aminobenzoic acid (**5**),[18] fluorescein amine (**6**) and 9-aminoacridine (**7**)[19] have been commonly employed in carbohydrate analysis. Despite these factors, there are restrictions on the probes that can be utilized in this protocol.[15] The pH of the amine should be near or less than the cellular media for an amine to be available in the reactive unprotonated form. Therefore, aliphatic amines and most of the aromatic amines are eliminated from the list of fluorescent labeling agents. Another restriction is regarding the solubility and hydrophobicity of the fluorophore which makes the detection procedure difficult. Additionally, this protocol can be applied only for the detection of monosaccharides; oligosaccharide detection is a tiresome job.

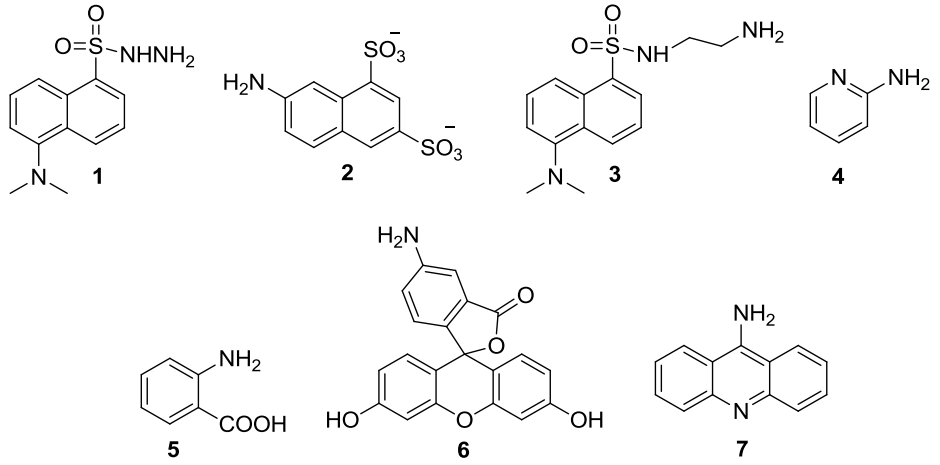

Figure 1.1. Fluorescent probes used for the covalent labeling of carbohydrates.

Recently, Andreana and co-workers demonstrated the structural elucidation and degree of loading of the cancer antigen to a carrier with the aid of fluorescent probe Alexa Fluor488.[20] Chemically oxidized form of the polysaccharide PS A1 is conjugated to the cancer antigen, Thomsen-nouveau (Tn = α-D-GalNAc-OSer/Thr). This vaccine construct Tn-PS A1 linked fluorophore through indirect oxime linkage

(Figure 1.2). The structural characteristics and degree of loading of the cancer antigen, Tn were also studied using circular dichroism and UV absorbance.

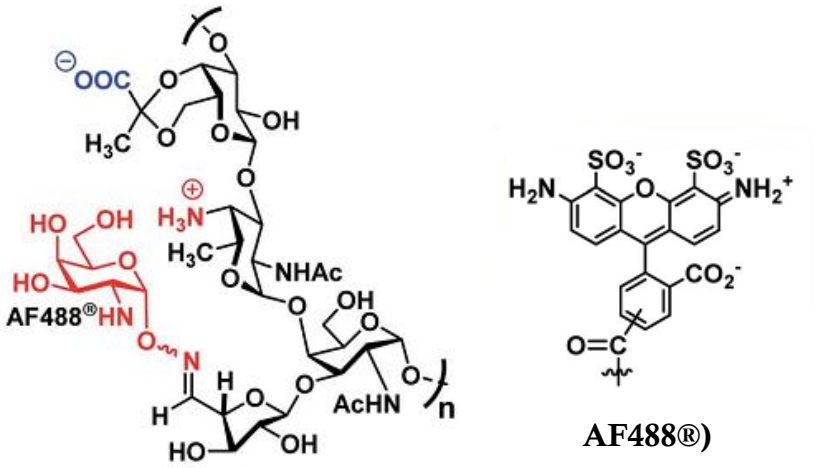

Tn (AF488®)-PS A1 oxime **AF488®)**

Figure 1.2. Structure of the vaccine construct Tn (AF488®)–PS A1 oxime and the fluorophore AF488® used for determining percentage of Tn loading.

Reactivity of the boronic acid with 1,2- or 1,3-diols has been well exploited in the designing of fluorescent probes for carbohydrate detection. Boronic acid forms cyclic boronate esters by reacting with diols, and this complexation renders boronic acid more acidic and reduces the pH from 8.8 to 5.9.[21] Thus, the boronic acid in aqueous solution get readily converted to the corresponding anionic species. These anionic species participate in photoinduced electron transfer and induce changes in the emission profile. This emission changes associated with carbohydrate binding are utilized to detect carbohydrate. Numerous boronic acid based saccharide detectors have been developed.[22]

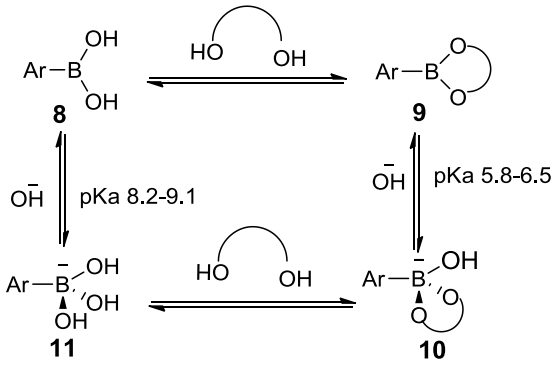

Scheme 1.1. Reaction of boronic acids with diols.

Boronic acid derived fluorescent glucose sensors (**12** and **13**) was first developed by Yoon and Czarnik in 1992.[23] Excited state internal charge transfer (ICT) induced changes in the emission profile of anthracene boronic acid was explored toward saccharide detection in aqueous solution. Photoinduced electron transfer,[24] twisted internal charge transfer,[25] aggregation induced emission,[26] *cis-trans* isomerisation[27] and hydrogen bonding were utilized to read-out boronate ester formation *via* emission profile variation. Mohr *et al.* developed a longer wavelength emitting glucose sensor (**16**, Figure 1.3).[28] Specific detection of saccharides was also demonstrated with pyrene boronic acid conjugate system (**17**, Figure 1.3).[29]

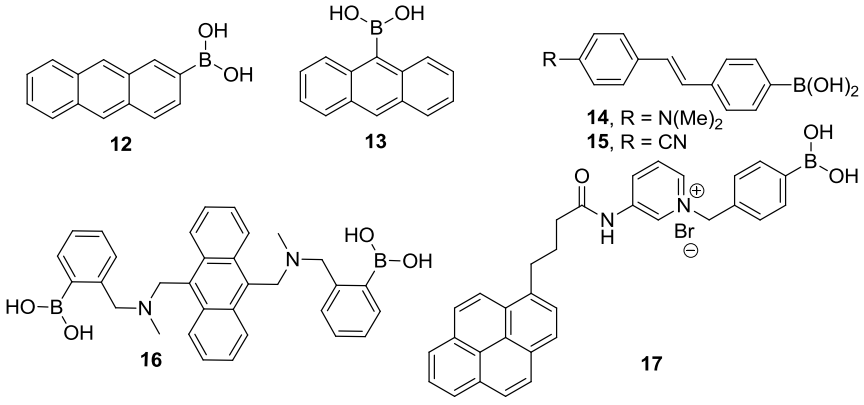

Figure 1.3. Boronic acid based fluorescent saccharide sensors.

Recently, Glass and co-workers introduced a turn-on optical sensor (**18**). The structure of the glucosamine sensor contains coumarin aldehyde-boronic acid system

and they used compound **18** for the selective detection of amino sugar-glucosamine over other biological molecules under physiological pH.[30] The co-operative binding of diols and amine in the glucosamine with boronic acid and aldehyde present in the coumarin core lead to excellent selectivity (Scheme 1.2). The cavity size of the functional group in the designed probe plays a critical role in the sensing activity. However, boronic acid coupled fluorescence sensing is restricted to few fluorophores, and this strategy is effective only for the detection of simple monosaccharides.

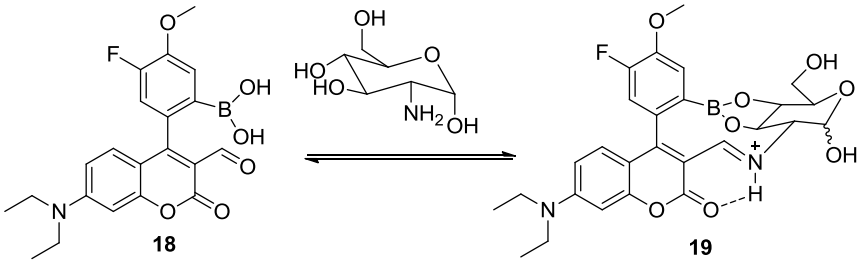

Scheme 1.2. Co-operative binding mechanism for the amino-sugar-glucosamine detection.

1.3. Fluorescently labeled carbohydrates as ion chelators/receptors

The significant role of metal ions such as zinc, magnesium, calcium, potassium, *etc.* in various biological process, diseases and the environmentally toxicity of certain other metal ions like mercury, cadmium, lead, *etc.* are evident from the literature.[31] Fluorescent sensors enable the sensitive detection of the metal ions even at the lower concentration. Therefore active research has been carried out in the design and synthesis of efficient fluorescent sensors for the detection of environmentally toxic ions in aqueous solution and biologically benign ions in the cellular environment.[32] These sensing agents generally contain three major blocks in the structure, one receptor unit/ligand, the other signaling unit/fluorophore and a linker which connect the fluorophore and ligand. The binding unit will react with the

targeted species and will make changes in the absorption and emission spectra. The challenges involved in the design strategy of molecular sensors are their water solubility[33] and biocompatibility.[34]

Tailoring carbohydrate moiety, the naturally abundant scaffolds, to the fluorophores is a promising strategy for sensing. This approach helps to improve the hydrophilicity of the probe. Moreover, in some cases, the hydroxyl group oriented in specific directions will aid these sugar moieties to take the role of binding unit or function as targeting ligands. Glycoligands are scarcely explored in the development of fluorescent sensors for transition metal ions due to the structural complexity and rigidity of the carbohydrate scaffold before past two decades. However, recent literature reports unveiled the versatility of the glycoligands and chemists have come up with a plethora of fluorescent glycans in which monosaccharide or oligosaccharide is connected to different chromophores. Three hydroxyl groups at the suitable steric arrangement in carbohydrates will function as suitable co-ordination sites for the metal ions.

Sugars generally exist in the chair confirmation of pyranose form with three hydroxyl groups axial-equatorial-axial (*ax-equat-ax*) sequence or *ax-ax-ax* or in the furanose form with *cis-cis* alignment of the adjacent hydroxyl groups, and they behave as excellent coordinating ligands (Figure 1.4).[35] Also, the conformational differences of the hydroxyl groups have a crucial role in identifying the chirality of the metal ion and the complexes.[36] Appending suitable anchoring groups at the appropriate position on carbohydrate scaffold enhance the co-ordination ability.

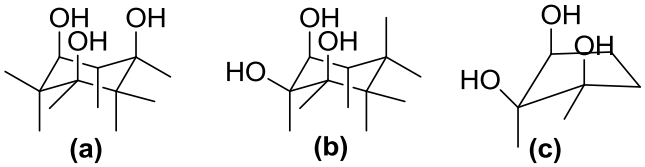

Figure 1.4. The possible steric arrangements of the hydroxyl groups available for metal coordination in pyranose form of sugar moiety (a) 1,3,5-*ax-ax-ax* triol (b) 1,2,3-*ax-eq-ax* triol and (c) *cis-cis* triol in furanose form.

Policar and co-workers conducted a detailed investigation on polydentate ligands based on sugar scaffolds exploiting the chelating ability of hydroxyl groups.[37] Three finger claw chelating ligands **20** and **21** were developed by attaching a Lewis base, pyridine on the 3,4,5-*cis* hydroxyl groups of galactose, which are capable of co-ordinating Co (II) ion and Ni (II) ion.[38]

Later then fluoroionophores (**22-24**, Figure 1.5) based on different stereoisomers of glycofuranoside (C3 epimers) were designed, and their fluorescence properties were used for monitoring the metal cation complexation.[39] Recently, the same group demonstrated live cell fluorescence imaging with the benzothiadiazole grafted glycoligand **22'** in the visible region.[40] These fluorescent probes are cell permeable and are accumulated inside the cells through passive uptake. Also, their presence in the cells induced chemical stress.

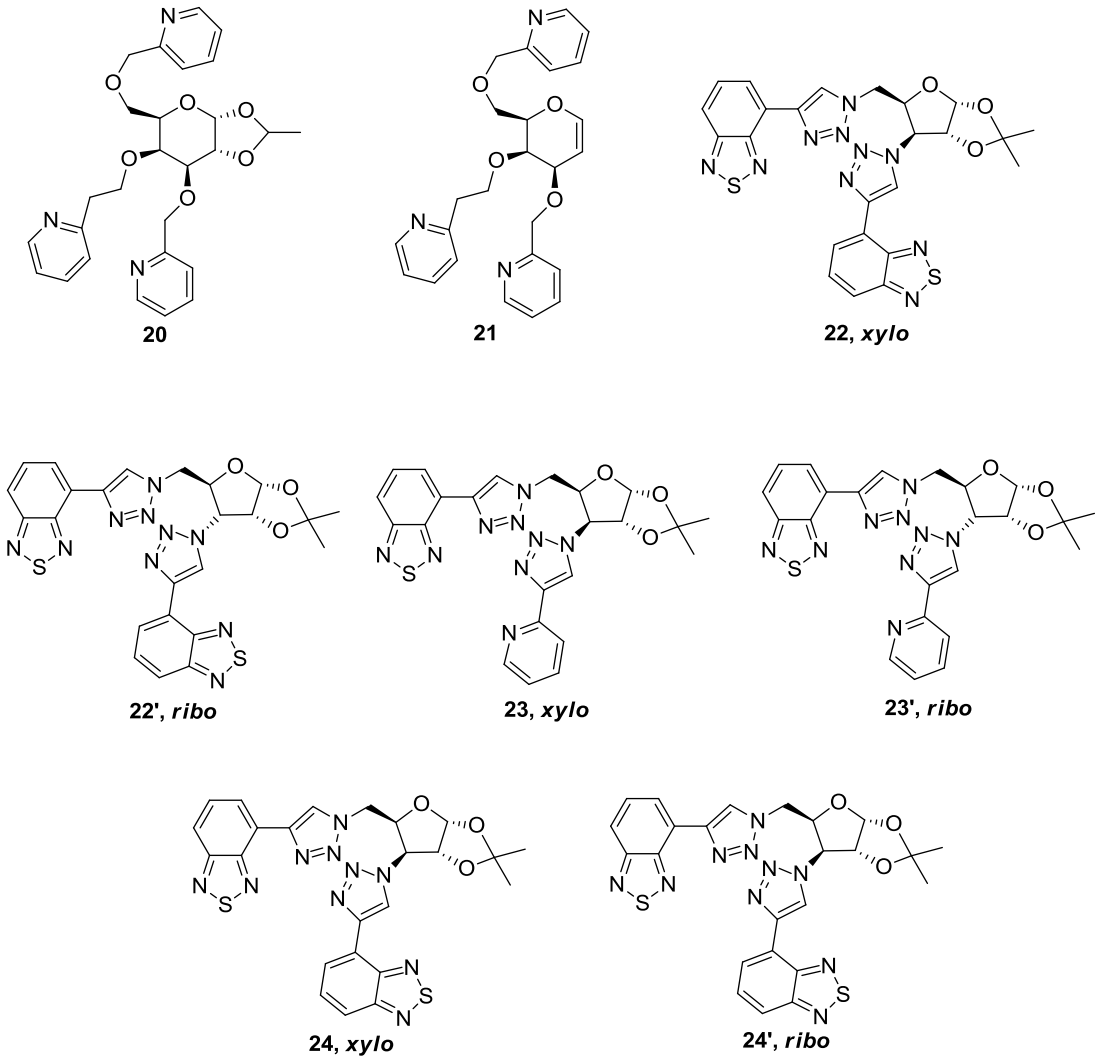

Figure 1.5. Polydendate glycoligands developed by Policar *et al.* for the metal chelation.

Rao and co-workers conducted a detailed investigation on carbohydrate appended fluorescent receptors. Naphthyl imino galactose probe **25** (Figure 1.6) was used for the selective and sensitive detection of Cu^{2+} ions in HEPES buffer solution under physiological pH.[41] The O-N-O linkage including carbohydrate moiety in the molecular skeleton acts as the binding unit and the presence of Cu^{2+} was elicited by the switch on fluorescence. When the galactose unit was replaced by glucose moiety selective binding of the fluorophore turned towards Zn^{2+} instead of Cu^{2+}.[42] Schiff's base conjugates derived from glucosamine (**27**, Figure 1.6) have proven to be an

effective chelator for Hg^{2+} detection in aqueous solution in which the sugar part also contribute to its water solubility.[43] The aromatic core also plays a critical role in the chelation process. Selectivity towards Hg^{2+} was reduced while changing the aromatic core from anthracene to naphthalene. Anthracenyl iminoglycoconjugate (28) detects Hg^{2+} ions through the imine moiety binding as well as the aromatic moiety, cation-π interaction to form a 2:1 (Ligand:Hg^{2+}) complex.[44] A minimum detection limit of 110 ± 16 nM was demonstrated in biological fluids over a pH range of 5-10.

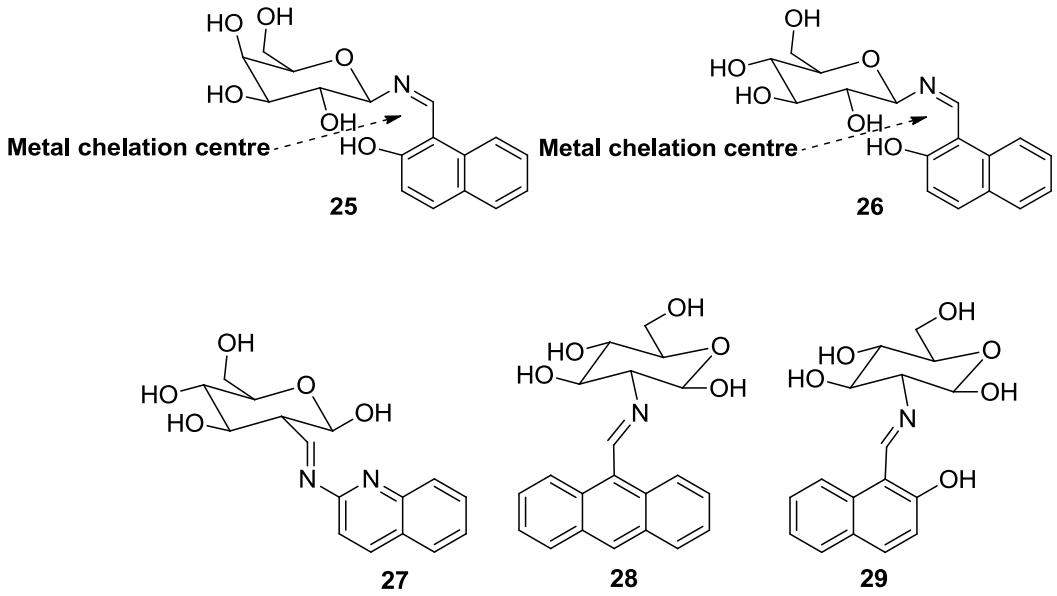

Figure 1.6. Structure of the fluorescent glycoconjugated receptors (**25-29**).

Water solubility is a major obstacle encountered in designing of fluoroionophores. Carbohydrates which are rich in hydroxyl groups will considerably enhance the water solubility of the chemical entity. Aminoanthraquinone cored carbohydrate molecular receptor (**30**) for Hg^{2+} have developed and demonstrated the sensing propensity of the probe in the presence of albumin proteins in blood serum and in solid silica support.[47] Thiourea functional group present in the molecular sensor acts as receptor ligand and the attached carbohydrate unit enhances water solubility and bio-compatibility. In the absence of Hg^{2+} ion, the probe exists as

thioenolate anion and efficiently quenched the fluorescence *via* photo induced electron transfer (PET) and remained non-fluorescent. Co-ordination of the Hg^{2+} ion to the thiourea through sulfur linkage inhibits the PET and led to the fluorescence turn-on.

Triazolyl glycoconjugates received much attention owing to their biological and optical properties.[48] Moreover, triazolyl bidentate glycoconjugates are proven to be an excellent chemical moiety for the metal ion detection.[49] Stereochemistry of the hydroxyl groups on pyranose ring had a great impact on the sensitivity and selectivity of the fluorescent probe.[48] For example, two triazolyl coumarin moieties installed at different positions of the same glucose nucleus (**31-33**, Figure 1.7) produced reversed optimal response in presence of Ag (I) over a wide range of metal ions in aqueous solution. The *C*-3,4-ligand (**32**) showed fluorescence quenching whereas *C*-2,3-(**33**) and *C*-4,6-ligand (**31**) exhibited fluorescence enhancement upon metal binding.[49] Also, the *C*-2,3-ligand showed less cytotoxicity and increased cell permeability, and that can be successfully applied in living cells.

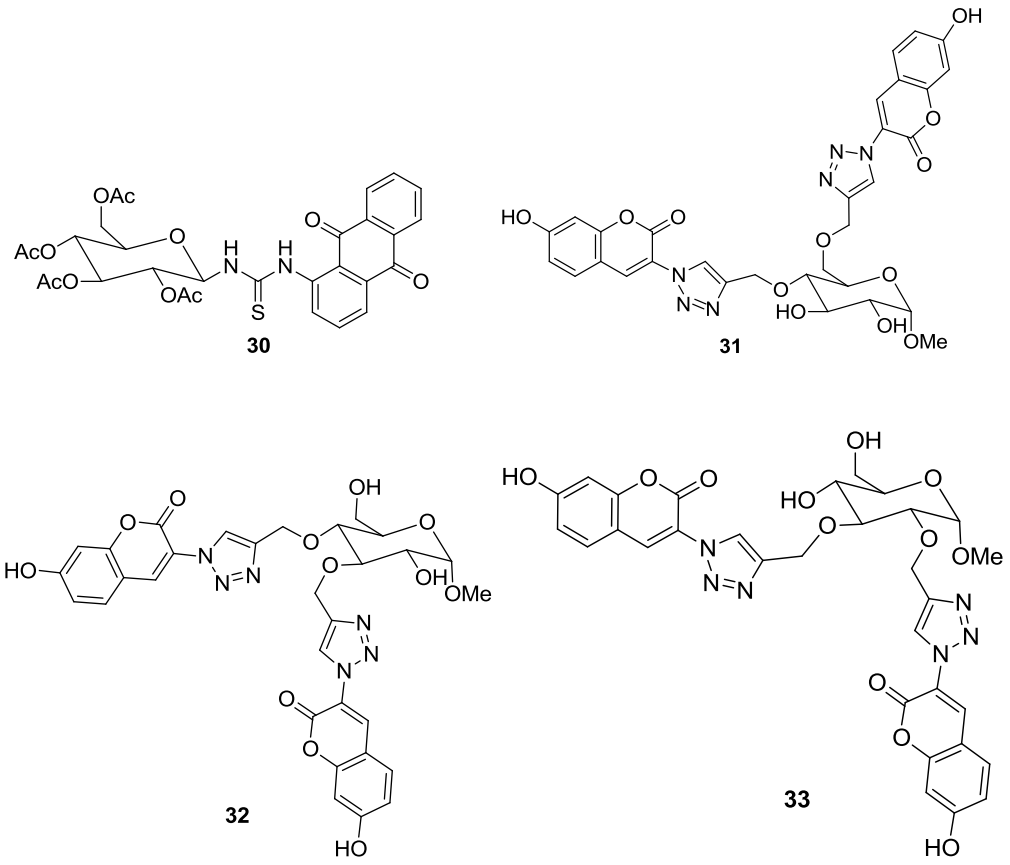

Figure 1.7. Structure of aminoanthraquinone conjugated glycan based receptor (**30**) and bis-triazolyl coumarin glycosides (**31-33**).

Glycosyl naphthalimide-dansyl dyad system (**34**, Figure 1.8) with triazolyl moiety as linker was demonstrated as a ratiometric probe for the detection of environmentally toxic thiophenol in aqueous solution.[50] Recently, Rao and co-workers introduced a triazole linked quinoline conjugate of glucopyranose (**35**, Figure 1.8).[51] The quinoline-glycoconjugate detects Zn^{2+} and Cd^{2+} with respective 30±2 and 14±1-fold fluorescence enhancement and Hg^{2+} with a fluorescence quenching response in the aqueous media. Comparative studies with the model compounds (which do not possess sugar) indicate that the sugar conjugation caused significant improvement in the selectivity, water solubility and biocompatibility. The metal ions Zn^{2+} and Cd^{2+} exhibited 1:2 complexation with the glycoconjugate and Hg^{2+} ion showed 1:1 stoichiometry.

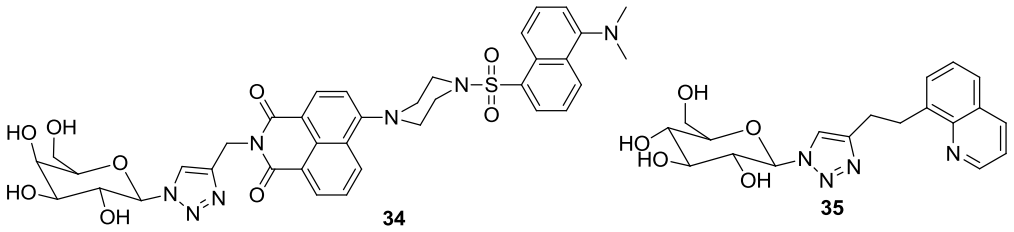

Figure 1.8. Structure of glycosyl naphthalimide-dansyl dyad system (**34**) and quinonline glycoside (**35**).

Hinge sugar was explored as a recognition unit in the development of fluorescent receptors. Pyrene based excimer fluorescence sensor (**36**, Figure 1.9) was designed for the detection of Zn^{2+} and Cd^{2+}, ring flip of the hinge sugar unit upon chelation with the metal ions lead to the excimer formation, and the excimer emission helps to read out the presence of metal ions.[52]

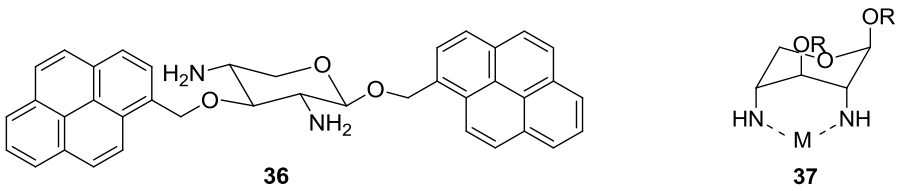

Figure 1.9. Structure of the pyrene based hinge sugar sensor (**36**) and the ring flipped confirmation after metal binding (**37**)

Sugar aza crown (SAC) ethers were also utilized for the design of fluoroionophores toward detection of trace metal ions in which sugar moiety plays the role of receptor. Xie *et al*. demonstrated the fluorescence sensing of Cu^{2+} ion with a SAC based bis-pyrenyl compound **38** (Figure 1.10).[53] Cu^{2+} ion chelation to the fluroinophore induces fluorescence quenching ascribed to PET from excimer to the Cu^{2+} ion. Among the fluorogenic probes developed for sensing, the "turn-on" fluorophores are superior to "turn-off" fluorophores. Wu and co-workers introduced a SAC based fluorogenic chemosensors (**39** and **40**, Figure 1.10) for the selective

detection of Cu^{2+} and Hg^{2+}. Here, the fluorescence enhancement was displayed upon chelation of the nitrogen atoms on the pyrene ring with Cu^{2+} and Hg^{2+}.[54]

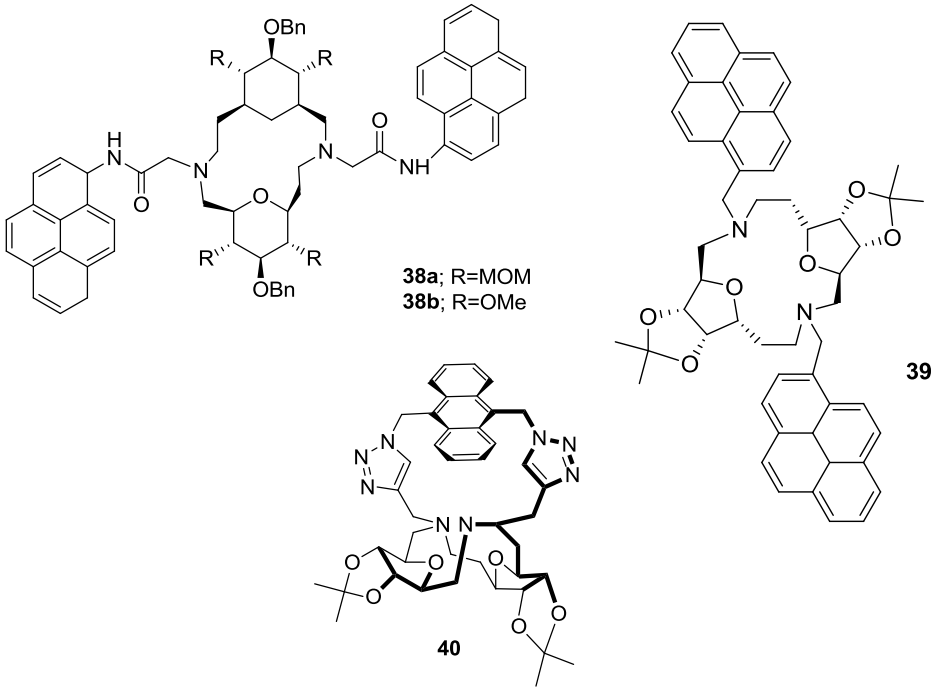

Figure 1.10. Structure of the hinge sugar based receptors **38-40**.

1.4. Fluorescently labeled carbohydrates as biomolecule receptors

Fluorescence based detection methods have also been extensively applied to the detection of biologically relevant ions, bio-molecules and metabolites.[55] Selective detection of biologically relevant thiols is of particular interest, and enormous attempts have been reported in the literature.[56] The interaction of carbohydrate molecules with various polyfunctional molecules and metal ions in the living organism are also well studied. For example, metal ion transport across the cell membrane. Because of all these factors, glycoligand based fluorescent probes for biomolecule sensing are at the centre stage of research that can be extended to the therapeutics.

Near-infrared emitting fluorophores attracted great interest as fluorescent sensor owing to their unique advantages favorable for biological applications.[57] Tae and co-workers introduced a "turn-on" chemosensing ensemble based on the

rhodamine-sugar probe (**41**) for the detection of thiol containing aminoacids in the aqueous system (Scheme 1.3). The gold complex, **41**-Au^{+} acts as the chemosensing ensemble in which the addition of thiol containing aminoacids like cysteine and homocysteine enhance the emission intensity of the **41**-Au^{+}. The basic tetrahydrofuran ring in the furanose form of sugar enhances the metal binding affinity of the probe.

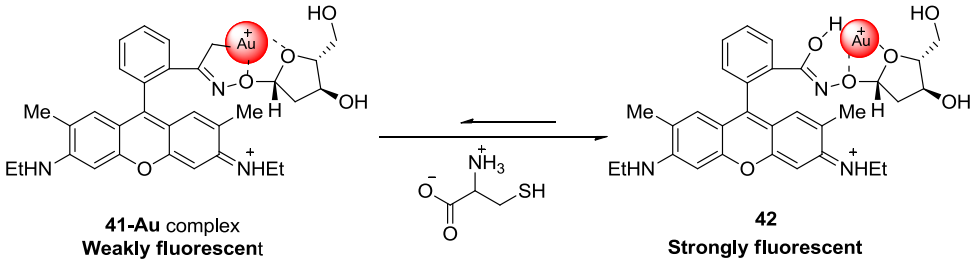

Scheme 1.3. Sensing mechanism operative for the chemosensing ensemble **41**-Au^{+}.

C-S/C-O bond cleavage followed by nucleophilic substitution has been widely utilized for the selective detection of thiols. Selenocysteine is the 21st aminoacid and its inappropriate level cause cardiovascular and neurodegenerative diseases. Rao *et al.* introduced a dansyl derivatized triazole linked glucopyranosyl conjugate **43** for the selective detection of selenocysteine (Cys-SeH) over cysteine and other bio-thiols.[58] Increased nucleophilicity of the Cys-SeH favoured the selective detection with a 210-fold enhancement of fluorescence (Scheme 1.4). Biological application of this probe was established by the *in vitro* analysis in human liver hepatocarcinoma cells (HepG2) using fluorescence microscopy.

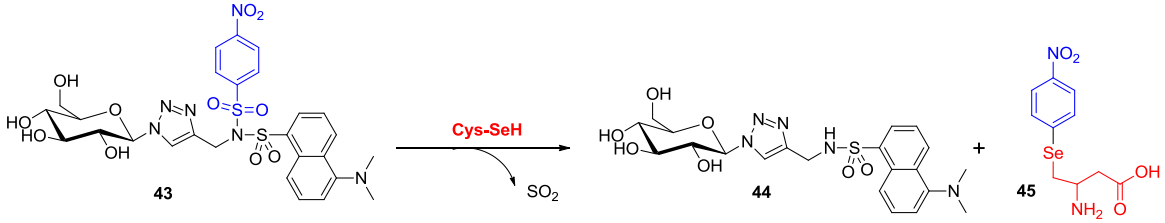

Scheme 1.4. Sensing mechanism of selenocysteine using glucopyranosyl probe (**43**).

Wang *et al*. designed a non-cytotoxic sugar functionalized fluorescent probe **46** for the detection of intracellular fluoride ion based on a de-silylation reaction in the aqueous medium (Scheme 1.5).[59] De-silylation, specifically in the presence of fluoride ion generated 30 fold enhancement in emission intensity.

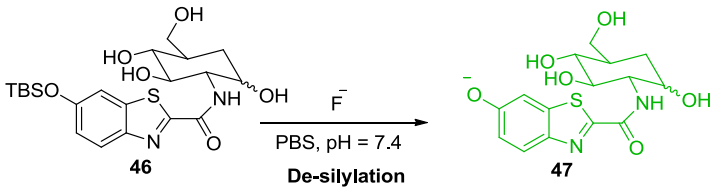

Scheme 1.5. Fluoride ion catalysed de-silylation reaction.

1.5. Enzyme based sensors

Glycoproteins are the major class of glycoconjugates distributed in the human body, and they mainly exist in the glycosylated form.[60] Glycosidase enzymes are catalytic machinery for the hydrolytic cleavage of the glycosidic bond. The rate of the enzyme catalyzed hydrolysis is 10^7 fold higher compared to the spontaneous hydrolysis and are extremely substrate specific.[61] Glycosidase enzymes are of different types depending on their site of glycosidic cleavage, catalytic mechanism and substrate specificity.[62] Attributed to the varying and pivotal role of glycans in cellular biology, glycosidase enzymes are also linked with a wide array of biological applications.[63] Deviation and deficiency in the glycosidase enzyme production cause several pathological conditions such as Gaucher and Parkinson's disease.[64] Therefore, glycoconjugated probes for the real-time assays of enzymes have been attracted a great deal of attention in biomedical research which helps in early stage detection of diseases. A broad spectrum of activatable chromogenic and fluorogenic probes and lanthanide glycoconjugates for MRI analysis have been developed for the glycosidase enzyme assay.[65] Early reports were based on small molecule fluorophores

such coumarins. A vast array of fluorophores based on umbeliferones, fluoresceins, rhodamines and NIR emitting squaraine dyes were also explored in this direction.[65]

Numerous chromogenic[66] and fluorogenic probes[67] have been developed for monitoring the β-galactosidase enzyme activity, the most widely employed reporter gene in enzyme immunoassays.[68] However, recent research have been focused on to develop fluorogenic substrates with high emission wavelengths to avoid background fluorescence from the intracellular molecules.

Tung and co-workers introduced an acridine-based NIR emitting dye (**48**) for the *in vivo* β-galactoside detection.[69] Galactose moiety was conjugated to 7-hydroxy-9H-(1,3-dichloro-9,9-dimethylacridin-2-one) and the resultant conjugate (**48**) showed far red fluorescence properties, with a red shift in emission (50 nm) in response to the enzyme catalyzed cleavage (Scheme 1.6). But the overlap of excitation-emission spectra limits their application for optical imaging. Later, the same research group reported a water soluble self-immolative probe (**51**) for the β-galactoside monitoring. Disulfonated benzo[a]phenoxazine fluorophore core was connected to sugar moiety through a self immolative spacer 4-hydroxy-3-nitrobenzyl alcohol and glycine. Seven-fold increase in fluorescence intensity was observed at the time of enzymatic cleavage (Scheme 1.6).

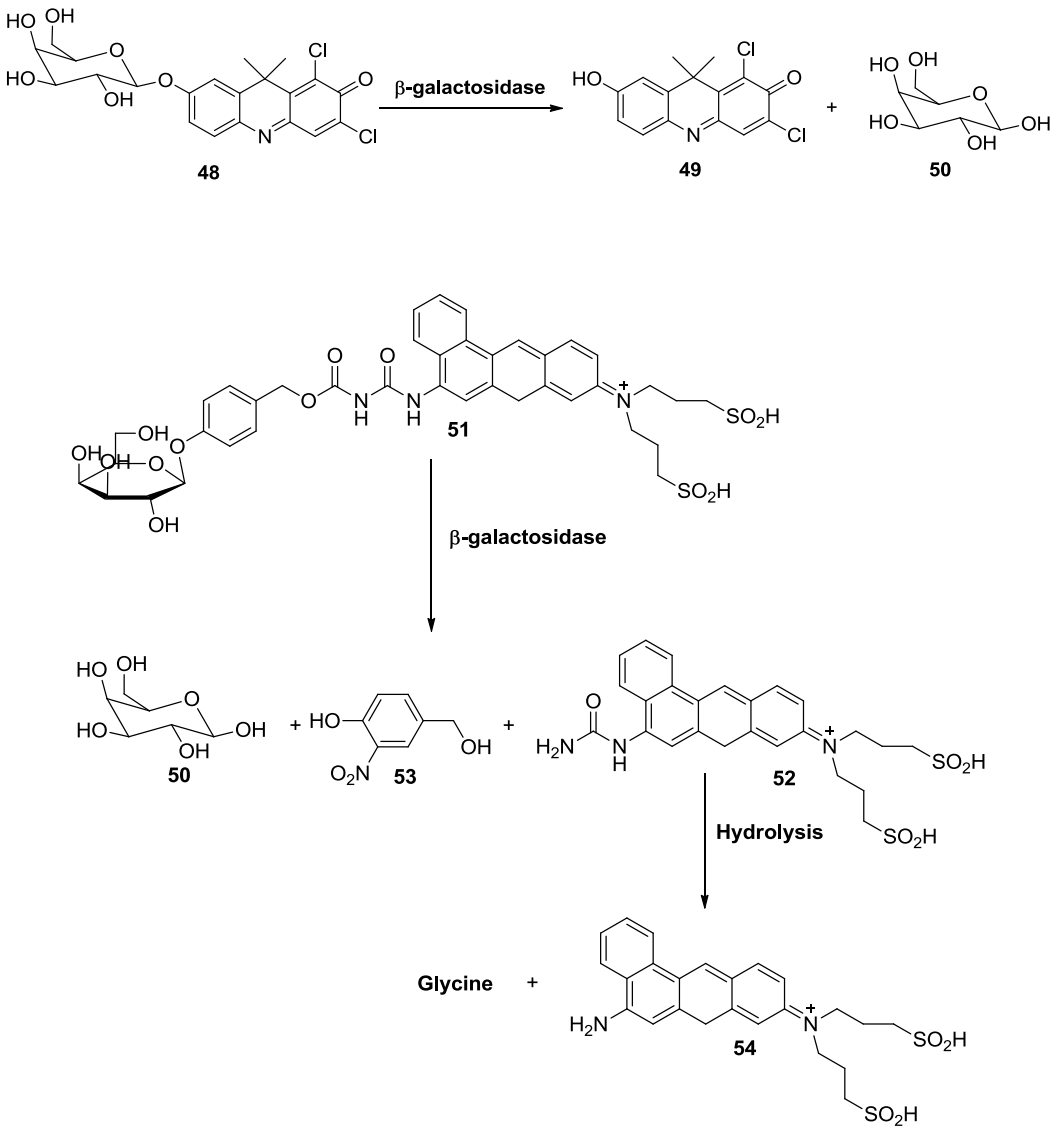

Scheme 1.6. Structure and reactivity of the compounds **48** and **51** with β-galactosidase.

Nagano and co-workers set out an NIR-fluorescent probe **55** (Figure 1.11a) based on squarylium dye scaffold to visualize β-galactosidase enzyme activity.[70] They exploited a protein (fetal bovine serum albumin, FBS that is ubiquitously distributed in the living organism) to activate the fluorescence of the probe. The squarylium dye connected to a functional group, galactose which reduces the protein affinity of the dye and emission intensity. β-Galactosidase enzyme cleaves the galactoside linkage,

which restores the protein binding affinity of the squarylium dye and enhances the fluorescence (Figure 1.11).

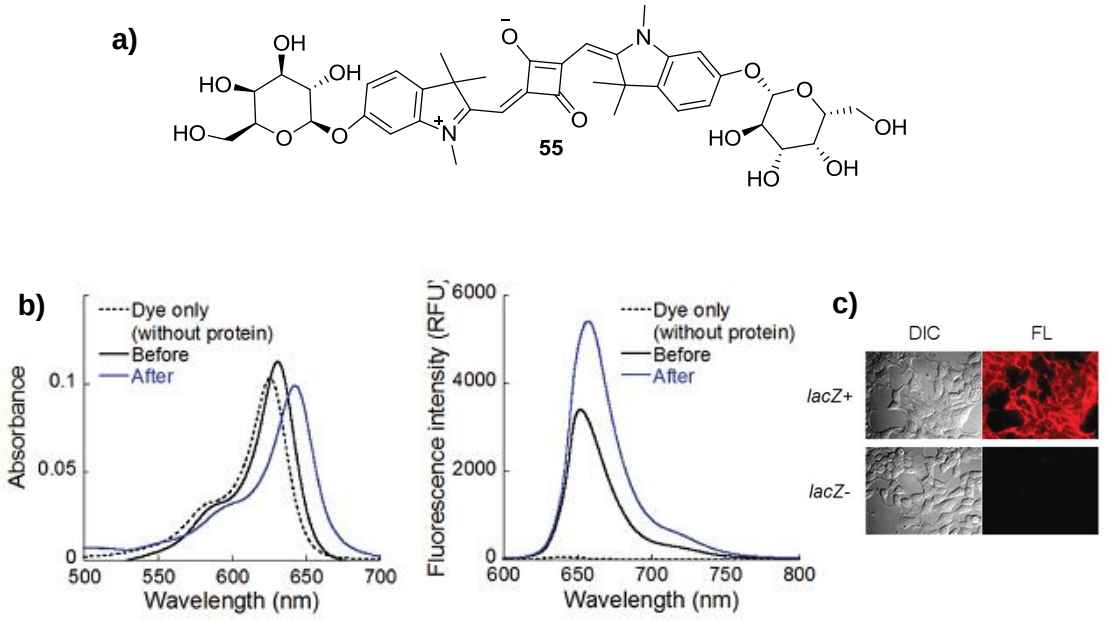

Figure 1.11. (a) Structure of the compound **55**, (b) UV-Vis absorption spectra of the dye **55** in the absence and presence of protein, (c) fluorescence and differential interference contrast (DIC) images of *lac*Z-positive or *lac*Z-negative HEK293 cells loaded with **55.**

Fluorescent probe for the effective detection of α-glucosidase and α-mannosidase enzyme activity were also developed.[71] Recently, Vocaldo and co-workers reported a fluorescence resonance energy transfer (FRET) based glucocerebrosidase (GCase) enzyme substrate (**56**, Figure 1.12).[72] This compound is non-fluorescent before enzyme action and the emission quenching is attributed to FRET. Black hole quencher is attached at the anomeric centre of the glucose through a spacer and boron dipyrromethene (BODIPY) fluorophore is attached at the 6th position of glucose moiety. NIR emission of BODIPY is retained upon hydrolytic cleavage by the endogenous glucocerebrosidase enzyme (Figure 1.12). This probe also exhibited excellent localization in lysosomes.

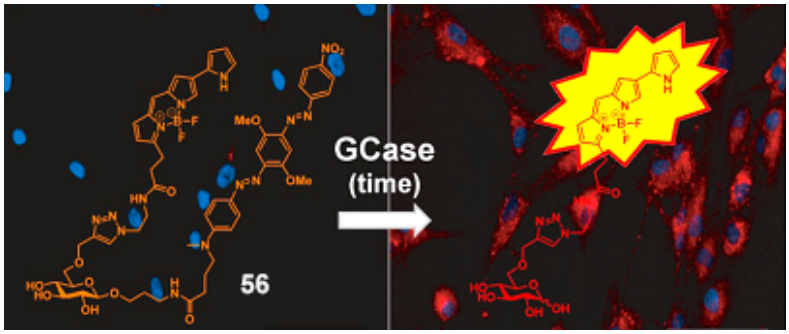

Figure 1.12. Structure of the compound **56** and the schematic representation of fluorescence turn-on in the presence of glucocerebrosidase (GCase) enzyme

1.6. Intracellular application/Imaging

Fluorescence imaging of the biological events at the molecular level provides the most precise approach toward disease diagnosis and treatment. However, selective imaging of the analytes in the cell remains as a challenging task. Carbohydrates have a significant role in the cell surface signalling and hence modulate the physiological and pathological function through specific carbohydrate-receptor recognition. The additional advantage is that the hydroxyl groups present in sugar molecules will increase the water solubility of the system. These factors make carbohydrate molecules as promising ligands in imaging probes and carries for the target specific drug delivery. Large numbers of fluorescent as well as phosphorescent glucose-bioprobes were reported recently for the bioimaging applications.[73]

Utilizing the receptor-mediated endocytosis strategy, Kim *et al.* developed a hepatocyte targeting bioprobe **57** (Figure 1.13).[74] Asialoglycoprotein receptor (ASGP R) is predominantly expressed in the hepatocytes, which selectively recognize the terminal galactose residue of the substrate. Single galactose appended naphthalimide probe was designed with thiol specific cleavable disulfide bond. In the absence of glutathione (GSH), the compound **57** exhibited weak emission features centred

around 473 nm due to strong ICT character. Exposure to thiols leads to a red shift in emission spectra, λ_{em} = 540 nm with fluorescence intensity enhancement.

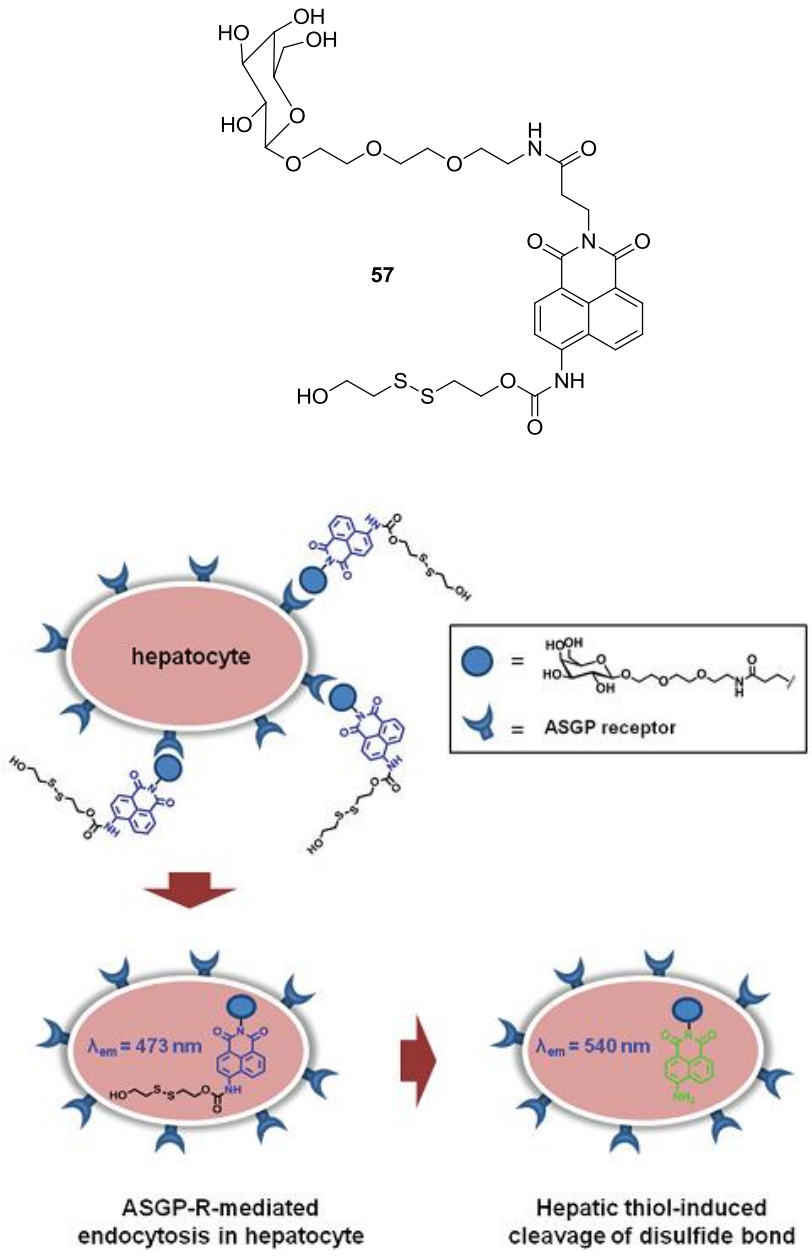

Figure 1.13. Structure of the compound **57** and the mechanism of action in the presence of GSH (cleavage induced fluorescence enhancement)

Exploiting the similar strategy (ASGP-R mediated endocytosis) He *et al.* synthesized a water soluble galactosyl-rhodamine probe **58** for the selective detection of mercury ions in the hepatoma cells over other cancer cells.[75] The spirocyclic ring

opening consequent to the mercury complexation leads to the fluorescence enhancement (Scheme 1.7), and this fluorescence enhancement is used to read out the mercury (II) ions in hepatoma cells.

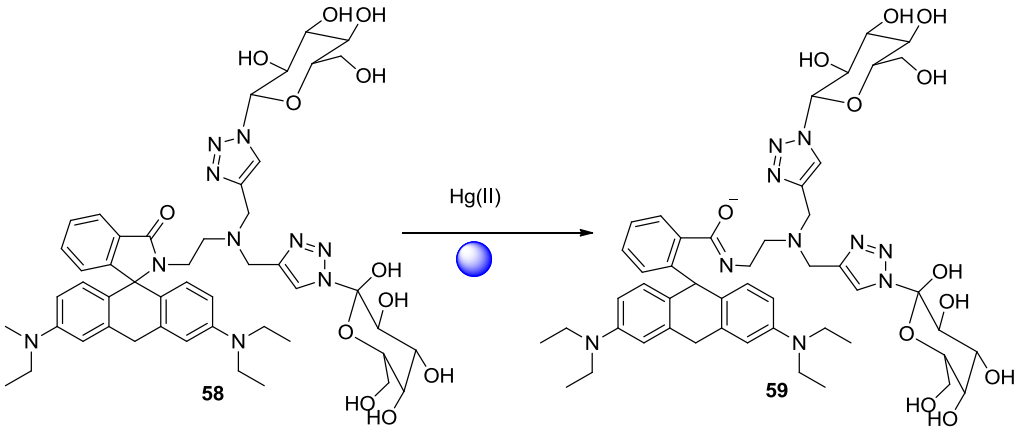

Scheme 1.7. Proposed ligand-ion co-ordination and release of the fluorescent probe for the compound **58.**

Chambert and co-workers synthesized a series of fluorescent glycoconjugated probes (**60-66**, Figure 1.14), mimicking the natural glycolipids and optimized their membrane affinity.[76] Red emitting, push-pull chromophore based on dicyanoionosphere (λ_{em} = 650 nm) was used as fluorescent core and the non-reducing, commercially available di- or trisaccharide units are connected to it. These compounds exhibited varying internalization efficiency according to their size and number of chromophore units present in it. Glycoconjugates bearing single chromophore, with limited size of carbohydrate moiety displayed best results.

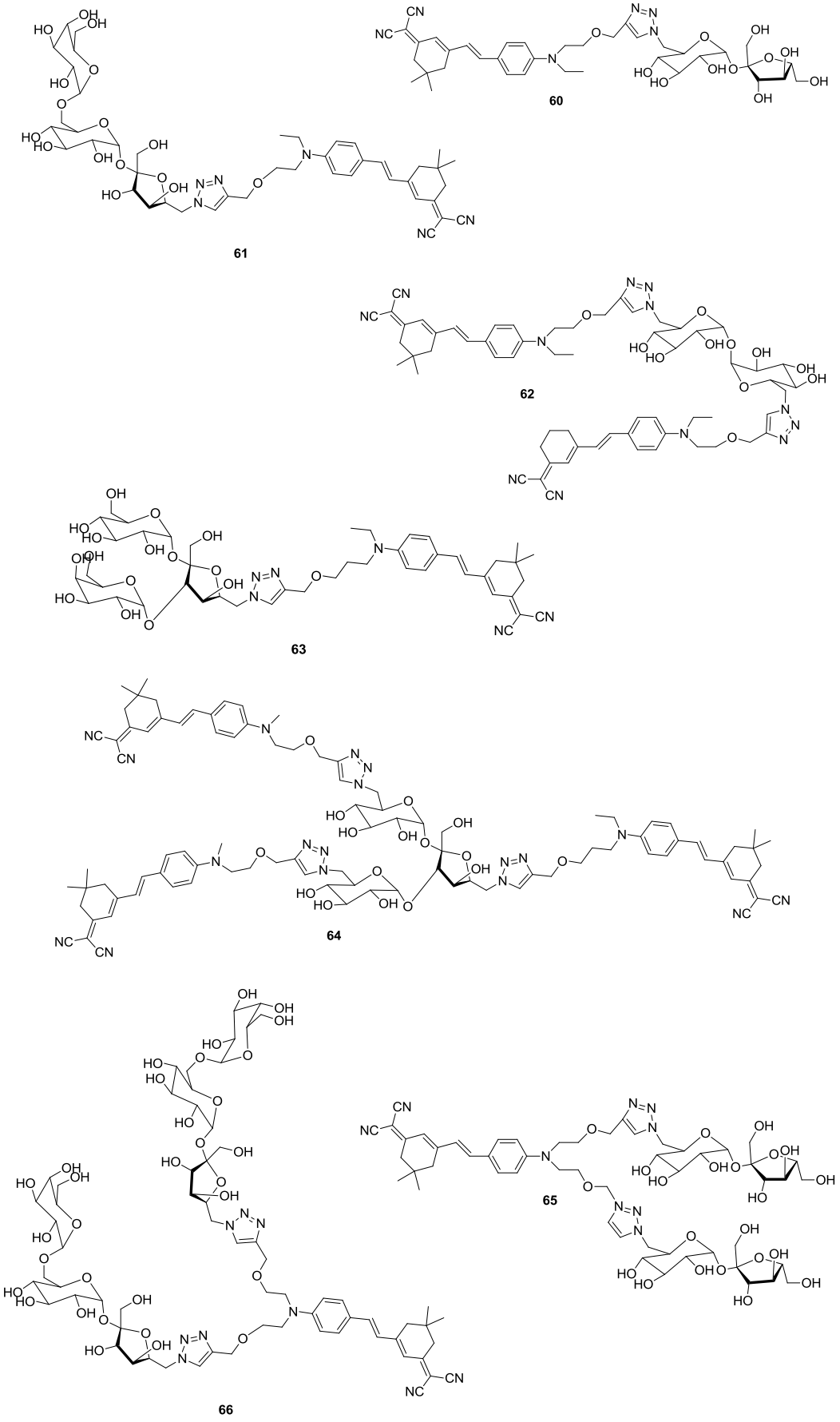

Figure 1.14. Structure of glycoconjugated probes **60-66**.

Simple sugar units also function as excellent cancer targeting ligands and there are many therapeutic agents and optical imaging tracers developed based on this principle.[77] The and cancer cells consume an excess amount of glucose compared to normal cells and this strategy is known as "Warburg effect".[78] As a result, uptake of glucose in cancer cells will remain high. Beginning form 1985, first fluorescent glucose anlogue-2-NBDG [2-(*N*-(7-Nitrobenz-2-oxa-1,3-diazol-4-yl)Amino)-2-Deoxyglucose] large number of glycoconjugated probes were designed for monitoring the glucose uptake. Monitoring the glucose uptake also helps to assess the function of brain cells and muscle cells. Details of the glycoconjuagted fluorescent probes for targeted tumor optical imaging is discussed in Chapter 3.

1.7. Material applications

The biological significance of carbohydrates and their applications were evidenced from the earlier discussions. Availability of chiral centres and large number of hydroxyl groups to form hydrogen bonds make them attractive building blocks in supramolecular chemistry. Sugar based supramolecular systems can be classified mainly according to the number of sugar units attached such as mono-valent and multi-valent ligands. Multi-valent ligands are mainly utilized in designing host-guest complex forming systems which play a major role in the biochemical process. The multiple valency present in the ligands enhance their complex forming ability.[79] Different types of systems have been designed by utilizing these multi-valent sugar ligands which include macromolecules, dendrimers, polymers, nanomaterials, *etc*. Simple mono-sugar appended building blocks are mainly used to optimize the gelation behaviour in organo and aqueous media. These sugar derivatives may be amphiphiles (containing a polar/hydrophilic head at the end of a non-polar/hydrophobic tail)[80] or bolamphiphiles (Two polar/hydrophilic heads on each

ends of a nonpolar, hydrophobic group).[81] Shinkai and co-workers synthesized a library of organic and hydrogels from chiral-sugar derivatives.[82] However, fluoescently labeled sugar-based gelators are very less.

Sugar decorated nanofibres were synthesized by Kitaoka and co-workers.[83] They synthesized three compounds with different sugar moieties such as lactose, maltose and cellobiose connected to azobenzene unit **67a-c** (Figure 1.15). These carbohydrate derivatives exhibited variable chiral behaviour attributed to the glycosidic linkages and steric arrangement of hydroxyl groups present in it. Hydrogels formed from the compounds **67a** and **67b** exhibited photoresponsive reversible sol-gel transition and thus they are suitable candidates for cell-culture engineering applications.

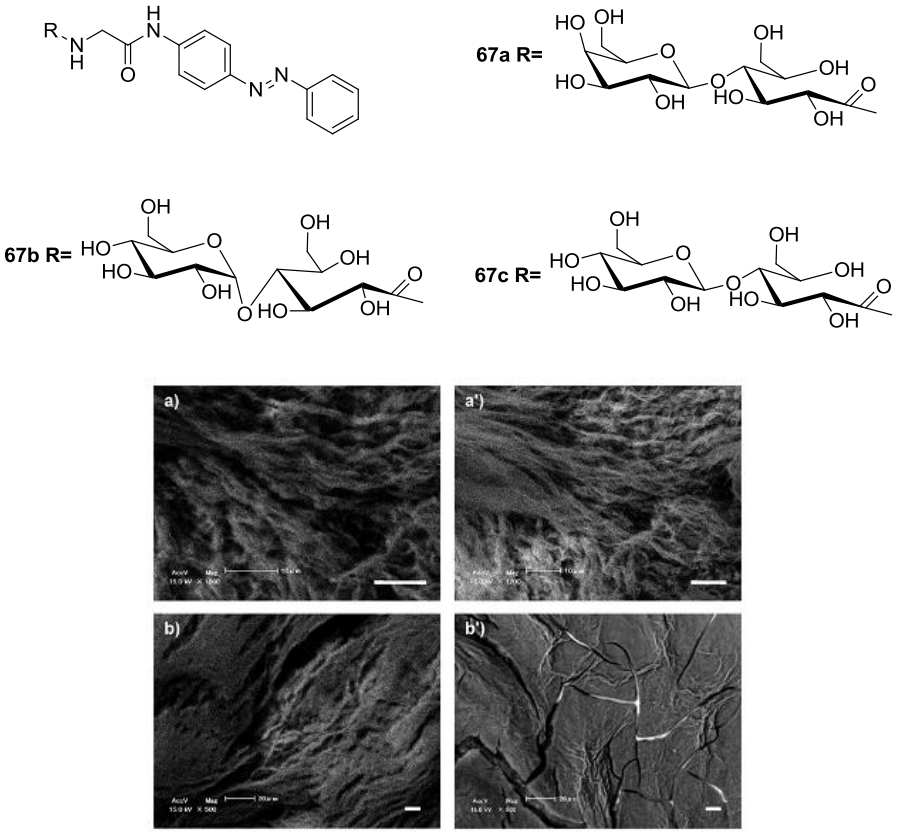

Figure 1.15. Structure of the azobenzene cored glycoconjugates and the SEM images of the gel obtained from **67a** and **67b**.

Recently, a supramolecular ensemble was developed and demonstrated for the selective fluorogenic detection of receptor proteins at the molecular level.[84] This supramolecular ensembles **68** and **69** (Figure1.16) were formed between charged conjugated polymers [positively and negatively charged diazo benzene containing poly(p-phenylethynylenes), PPEs] and fluorescent glycoligands [fluorescein (negatively charged) and rhodamine B (positively charged)] as fluorophores through electrostatic interaction. Conjugated polymers act as amplified quenchers and the fluorescence of the ensemble was in "*off*" mode in the absence of protein receptors. But fluorescence recovery was observed in the presence of specific protein receptors [Galactose residue with Peanut agglutinin (PNA), Glucose with Concanavalin A (Con A) and GalNAc with Soybean agglutinin (SBA)]. This fluorogenic ensemble was also successfully applied in live cells.

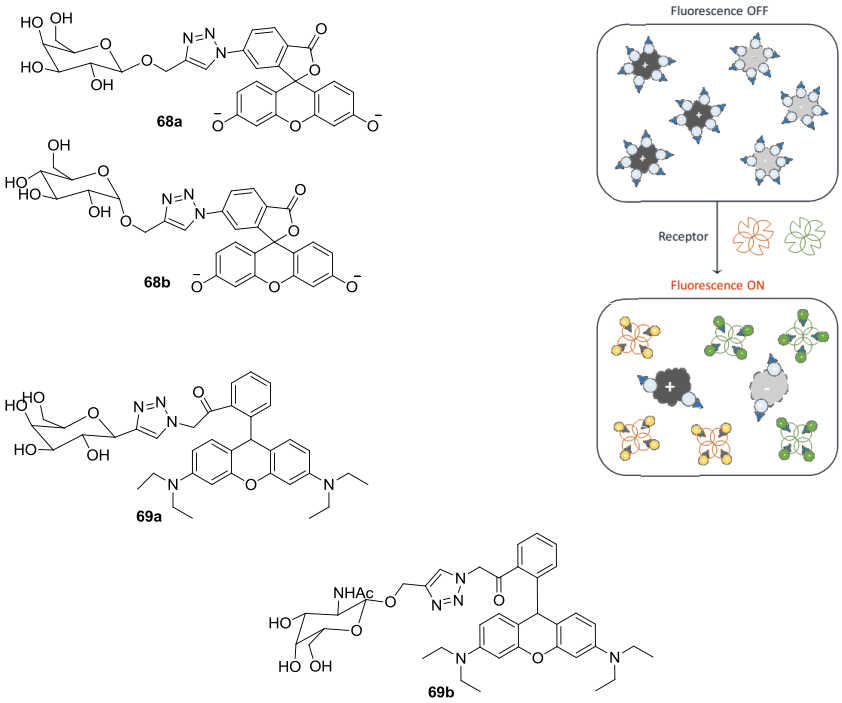

Figure 1.16. Structure of the fluorescein (**68a** & **68b**) rhodamine B (**69a** & **69b**) labeled glycoprobes and scheme representing the fluorescence switch on.

Yan and co-workers were successful in mimicking nature by constructing liposomes from glycoconjugates (Figure 1.17).[85] Liposomal supramolecular assembly was created from a BODIPY-glycan conjugate. The glycan core was linked to BODIPY *via* triazole linker. Out of the four derivatives synthesized, **70a** (Figure 1.17) showed liposomal formation while hydrating. This system can be effectively employed for monitoring lectin interaction and labeling.

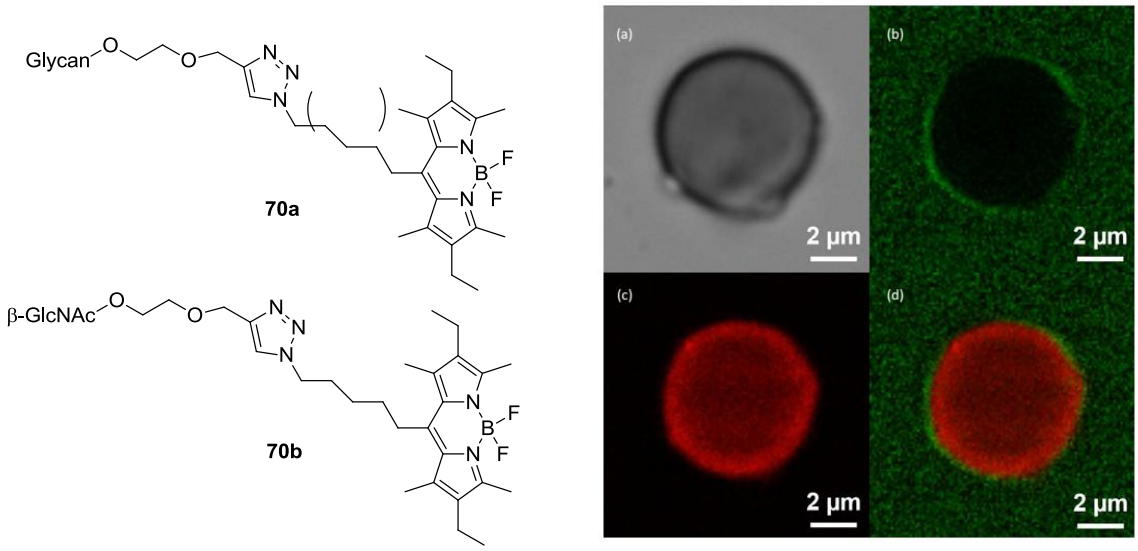

Figure 1.17. Structure of BODIPY glycans and the microscope images of a single lysosome formed from **69a**, (a) bright field, (b) green fluorescence, (c) red fluorescence and (d) overlay of the green and red fluorescence channels.

1.8. Conclusion and present work

Recent progress towards the development of fluorescence-tagged glycoprobes for sensing, cell imaging and material applications have been discussed. It has been recognized that the sugar conjugation imparts (a) increased water solubility (b) less toxicity and (c) target selectivity for the fluorophores. The main objective of the present thesis is to synthesize various sugar conjugated fluorophores and conduct a detailed study of these fluorophores towards biological as well as material applications. Aggregation behaviour of the sugar appended squaraine aggregates in

water was subjected to detailed study in the second chapter and response of this aggregate towards β-glucosidase enzyme was also monitored. Sugar moiety is an important targeting ligand to monitor glucose uptake and are widely exploited to target cancer cells due to the phenomenon known as "*Warburg effect"* observed at the cancer site. The third chapter describes the application of sugar appended squaraine dyes as NIR probes for the selective optical imaging of cancer cells. Carbohydrate molecules exhibited increased tendency to form hydrogen bonds and hence they promote the supramolecular self-assembly formation. This feature of sugar unit is utilized to construct a pH responsive fluorescent organogel from pyrene-sugar orthoester conjugate and discussed in fourth chapter.

1.9. References

1. (a) R. A. Dwek, *Chem. Rev.* **1996**, *96*, 683-720.; (b) S. -I. Hakomori, Y. Zhang, *Chem. Biol.* **1997**, *4*, 97-104.; (c) H. Lis, N. Sharon, *Chem. Rev.* **1998**, *98*, 637-674.; (d) P. M. Rudd, T. Elliott, P. Cresswell, I. A. Wilson, R. A. Dwek, *Science* **2001**, *291*, 2370-2376.; (e) J. Alper, *Science* **2003**, *301*, 159-160.; (f) N. Sharon, H. Lis, *Glycobiology* **2004**, *14*, 53R-63R.
2. (a) W.-C. Haase, P. H. Seeberger, *Curr. Org. Chem.* **2000**, *4*, 481-511.; (b) O. Ramstrom, J. M. Lehn, *Chembiochem.* **2000**, *1*, 41-48.; (c) P. Arya, A. Barkley, K. D. Randell, *J. Comb. Chem.* **2002**, *4*, 193-198.
3. A. K. Adak, B.-Y. Li, C.-C. Lin, *Carbohydr. Res.* **2015**, *405*, 2-12.
4. P. H. Seeberger, W.-C. Haase, *Chem. Rev.* **2000**, *100*, 4349-4394.
5. A. Imberty, Y. M. Chabre, R. Roy, *Chem. Eur. J.* **2008**, *14*, 7490-7499.
6. L. L. Kiessling, J. E. Gestwicki, L. E. Strong, *Angew. Chem. Int. Ed.* **2006**, *45*, 2348-2368.
7. N. Jayaraman, K. Maiti, K. Naresh, *Chem. Soc. Rev.* **2013**, *42*, 4640-4656.
8. A. Martinez, C. Ortiz Mellet, J. M. Garcia Fernandez, *Chem. Soc. Rev.* **2013**, *42*, 4746-4773.
9. O. Renaudet, R. Roy, *Chem. Soc. Rev.* **2013**, *42*, 4515-4517.
10. A. Dondoni, A. Marra, *Chem. Rev.* **2010**, *110*, 4949-4977.
11. X.-P. He, Y. Zang, T. D. James, J. Li, G.-R. Chen, J. Xie, *Chem. Commun.* **2017**, *53*, 82-90.
12. M. Dowlut, D. G. Hall, O. Hindsgaul, *J. Org. Chem.* **2005**, *70*, 9809-9813.
13. H. Yan, R. S. Yalagala, F. Yan, *Glycoconj. J.* **2015**, *32*, 559-574.

14. (a) P. Weber, L. Hof, *Biochem. Biophys. Res. Commun.* **1975**, *65*, 1298-1302.; (b) P. Weber, F. W. Harrison, L. Hof, *Histochemistry* **1975**, *45*, 271-277.
15. K. C. Ingham, S. A. Brew, *Biochim. Biophys. Acta, Protein Struct.* **1981**, *670*, 181-189.
16. Y. Mechref, G. K. Ostrander, Z. El Rassi, *J. Chromatogr. A* **1995**, *695*, 83-95.
17. E. Coles, V. N. Reinhold, S. A. Carr, *Carbohydr. Res.* **1985**, *139*, 1-11.
18. K. R. Anumula, P. Du, *Anal. Biochem.* **1999**, *275*, 236-242.
19. G. Abraham, P. S. Low, *Biochim. Biophys. Acta* **1980**, *597*, 285-291.
20. K. R. Trabbic, R. A. De Silva, P. R. Andreana, *MedChemComm.* **2014**, *5*, 1143-1149.
21. J. P. Lorand, J. O. Edwards, *J. Org. Chem.* **1959**, *24*, 769-774.
22. (a) H. Cao, M. D. Heagy, *J. Fluoresc.* **2004**, *14*, 569-584.; (b) H. S. Mader, O. S. Wolfbeis, *Microchim. Acta* **2008**, *162*, 1-34.; (c) R. W. Sinkeldam, N. J. Greco, Y. Tor, *Chem. Rev.* **2010**, *110*, 2579-2619.; (d) X. Sun, T. D. James, *Chem. Rev.* **2015**, *115*, 8001-8037.; (e) H.-C. Wang, A.-R. Lee, *J. Food Drug Anal.* **2015**, *23*, 191-200.
23. J. Yoon, A. W. Czarnik, *J. Am. Chem. Soc.* **1992**, *114*, 5874-5875.
24. J. D. Larkin, J. S. Fossey, T. D. James, B. R. Brooks, C. W. Bock, *J. Phys. Chem. A* **2010**, *114*, 12531-12539.
25. (a) S. Arimori, L. I. Bosch, C. J. Ward, T. D. James, *Tetrahedron Lett.* **2001**, *42*, 4553-4555.; L. I. Bosch, M. F. Mahon, T. D. James, *Tetrahedron Lett.* **2004**, *45*, 2859-2862.
26. Y. Liu, C. Deng, L. Tang, A. Qin, R. Hu, J. Z. Sun, B. Z. Tang, *J. Am. Chem. Soc.* **2011**, *133*, 660-663.

27. A. J. Pearce, D. S. Walter, C. S. Frampton, T. Gallagher, *J. Chem. Soc. Perkin Trans. 1* **1998**, 847-852

28. S. Trupp, A. Schweitzer, G. J. Mohr, *Microchim. Acta* **2006**, *153*, 127-131.

29. Y.-J. Huang, W.-J. Ouyang, X. Wu, Z. Li, J. S. Fossey, T. D. James, Y.-B. Jiang, *J. Am. Chem. Soc.* **2013**, *135*, 1700-1703.

30. T. M. Tran, Y. Alan, T. E. Glass, *Chem. Commun.* **2015**, *51*, 7915-7918.

31. (a) T. Dudev, C. Lim, *Chem. Rev.* **2003**, *103*, 773-788.; (b) W. N. Lipscomb, N. Sträter, *Chem. Rev.* **1996**, *96*, 2375-2434.; (c) T. Dudev, C. Lim, *Chem. Rev.* **2003**, *103*, 773-788.; (d) J.-N. Rebilly, B. Colasson, O. Bistri, D. Over, O. Reinaud, *Chem. Soc. Rev.* **2015**, *44*, 467-489.; (e) K. P. Carter, A. M. Young, A. E. Palmer, *Chem. Rev.* **2014**, *114*, 4564-4601. (f) G. Aragay, J. Pons, A. Merkoçi, *Chem. Rev.* **2011**, *111*, 3433-3458.

32. (a) Rice, T. E. *Chem. Rev*.**1997**, *97*, 1515-1566.; (b) C. M. Lytle, F. W. Lytle, N. Yang, J.-H. Qian, D. Hansen, A. Zayed, N. Terry, *Environ. Sci. Technol.* **1998**, *32*, 3087-3093.; (c) S. Loutseti, D. B. Danielidis, A. Economou-Amilli, C. Katsaros, R. Santas, P. Santas, *Bioresour. Technol.* **2009**, *100*, 2099-2105. (d) S. E. Wolkenberg, D. L. Boger, *Chem. Rev.* **2002**, *102*, 2477-2495.; (e) R. B. Lauffer, *Chem. Rev.* **1987**, *87*, 901-927.

33. (a) G. Hennrich, W. Walther, U. Resch-Genger, H. Sonnenschein, *Inorg. Chem.* **2001**, *40*, 641-644.; (b) B. Liu, H. Tian, *Chem. Commun.* **2005**, 3156-3158.; (c) Z. Guo, W. Zhu, M. Zhu, X. Wu, H. Tian, *Chem. Eur. J.* **2010**, *16*, 14424-14432.

34. (a) C.-Y. Wu, C.-C. Lin, T.-M. Fu, C.-R. Yang, Y.-P. Yen, *Aust. J. Chem.* **2010**, *63*, 329-335.;

35. B. Gyurcsik, L. Nagy, *Coord. Chem. Rev.* **2000**, *203*, 81-149.

36. Z. Damaj, F. Cisnetti, L. Dupont, E. Henon, C. Policar, E. Guillon, *Dalton Trans.* **2008**, 3235-3245.

37. Z. Damaj, F. Cisnetti, L. Dupont, E. Henon, C. Policar, E. Guillon, *Dalton Trans.* **2008**, 3235-3245.

38. (a) F. Bellot, R. Hardre, G. Pelosi, M. Therisod, C. Policar, *Chem. Commun.* **2005**, 5414-5416.; (b) G. Charron, F. Bellot, F. Cisnetti, G. Pelosi, J.-N. Rebilly, E. Riviere, A.-L. Barra, T. Mallah, C. Policar, *Chem. Eur. J.* **2007**, *13*, 2774-2782.

39. L. Garcia, S. Maisonneuve, J. Oudinet-Sin Marcu, R. Guillot, F. Lambert, J. Xie, C. Policar, *Inorg. Chem.* **2011**, *50*, 11353-11362.

40. L. Garcia, M. Lazzaretti, A. Diguet, F. Mussi, F. Bisceglie, J. Xie, G. Pelosi, A. Buschini, D. Baigl, C. Policar, *New J. Chem.* **2013**, *37*, 3030-3034.

41. N. K. Singhal, B. Ramanujam, V. Mariappanadar, C. P. Rao, *Org. Lett.* **2006**, *8*, 3525-3528.

42. A. Mitra, V. K. Hinge, A. Mittal, S. Bhakta, P. Guionneau, C. P. Rao, *Chem. Eur. J.* **2011**, *17*, 8044-8047, S8044/8041-S8044/8022.

43. S. Ou, Z. Lin, C. Duan, H. Zhang, Z. Bai, *Chem. Commun.* **2006**, 4392-4394.

44. A. Mitra, A. K. Mittal, C. P. Rao, *Chem. Commun.* **2011**, *47*, 2565-2567.

45. S. Areti, D. S. Yarramala, K. Samanta, V. K. Hinge, J. Khedkar, C. P. Rao, *RSC Adv.* **2014**, *4*, 16290-16297.

46. L. Lin, Q. Shen, G.-R. Chen, J. Xie, *Bioorg. Med. Chem.* **2008**, *16*, 9757-9763.

47. Z. Song, X.-P. He, X.-P. Jin, L.-X. Gao, L. Sheng, Y.-B. Zhou, J. Li, G.-R. Chen, *Tetrahedron Lett.* **2011**, *52*, 894-898.

48. X. P. He, Y. L. Zeng, Y. Zang, J. Li, R. A. Field, G. R. Chen, *Carbohydr. Res.* **2016**, *429*, 1-22.

49. D.-T. Shi, X.-L. Wei, Y. Sheng, Y. Zang, X.-P. He, J. Xie, G. Liu, Y. Tang, J. Li, G.-R. Chen, *Sci. Rep.* **2014**, *4*, 4252/4251-4252/4256.

50. K.-B. Li, D. Zhou, X.-P. He, G.-R. Chen, *Dyes Pigm.* **2015**, *116*, 52-57.

51. S. Areti, S. Bandaru, C. P. Rao, *ACS Omega* **2016**, *1*, 626-635.

52. (a) H. Yuasa, N. Miyagawa, T. Izumi, M. Nakatani, M. Izumi, H. Hashimoto, *Org. Lett.* **2004**, *6*, 1489-1492.; (b) H. Yuasa, N. Miyagawa, M. Nakatani, M. Izumi, H. Hashimoto, *Org. Biomol. Chem.* **2004**, *2*, 3548-3556.

53. J. Xie, M. Ménand, S. Maisonneuve, R. Métivier, *J. Org. Chem*. **2007**, *72*, 5980-5985.

54. (a) Y.-B. Chen, Y.-J. Wang, Y.-J. Lin, C.-H. Hu, S.-J. Chen, J.-L. Chir, A.-T. Wu, *Carbohydr. Res.* **2010**, *345*, 956-959.; (b) Y.-C. Hsieh, J.-L. Chir, H.-H. Wu, C.-Q. I. Guo, A.-T. Wu, *Tetrahedron Lett.* **2010**, *51*, 109-111.; (c) Y.-C. Hsieh, J.-L. Chir, S.-T. Yang, S.-J. Chen, C.-H. Hu, A.-T. Wu, *Carbohydr. Res.* **2011**, *346*, 978-981.

55. (a) Y.-K. Yang, K.-J. Yook, J. Tae, *J. Am. Chem. Soc.* **2005**, *127*, 16760-16761.; (b) S.-K. Ko, Y.-K. Yang, J. Tae and I. Shin, *J. Am. Chem. Soc.* **2006**, *128*, 14150-14155.; (c) Y.-K. Yang, S.-K. Ko, I. Shin and J. Tae, *Nat. Protoc.* **2007**, *2*, 1740-1745.; (c) Y.-K. Yang, H. J. Cho, J. Lee, I. Shin and J. Tae, *Org. Lett.* **2009**, *11*, 859-861.; (d) S.-K. Ko, I. Shin and J. Tae, *Org. Biomol. Chem*. **2009**, *7*, 4590-4593.; (e) S. Kang, S. Kim, Y.-K. Yang, S. Bae and J. Tae, *Tetrahedron Lett.* **2009**, *50*, 2010-2012.; (f) K.-S. Moon, Y.-K. Yang, S. Ji and J. Tae, *Tetrahedron Lett.* **2010**, *51*, 3290-3293.

56. (a) P. K. Pullela, T. Chiku, M. J. Carvan Iii, D. S. Sem, *Anal. Biochem.* **2006**, *352*, 265-273.; (b) N. Shao, J. Jin, H. Wang, J. Zheng, R. Yang, W. Chan, Z.

Abliz, *J. Am. Chem. Soc.* **2010**, *132*, 725-736.; (c) X. Chen, Y. Zhou, X. Peng, J. Yoon, *Chem. Soc. Rev.* **2010**, *39*, 2120-2135.

57. (a) J. V. Frangioni, *Curr. Opin. Chem. Biol*. **2003**, *7*, 626-634.; (b) Worms, B. D. Smith, *J. Am. Chem. Soc.* **2006**, *128*, 16476-16477.; (c) C. Li, T. R. Greenwood, Z. M. Bhujwalla, K. Glunde, *Org. Lett.* **2006**, *8*, 3623-3626.; (d) Z. R. Zhang, S. Achilefu, *Org. Lett.* **2004**, *6*, 2067-2070.
58. S. Areti, S. K. Verma, J. Bellare, C. P. Rao, *Anal. Chem.* **2016**, *88*, 7259-7267.
59. O. Motabar, Z.-D. Shi, E. Goldin, K. Liu, N. Southall, E. Sidransky, C. P. Austin, G. L. Griffiths, W. Zheng, *Anal. Chem.* **2009**, *390*, 79-84.
60. R. Apweiler, H. Hermjakob, N. Sharon, *Biochim. Biophy. Acta, Gen. Subj.* **1999**, *1473*, 4-8.
61. D. L. Zechel, S. G. Withers, *Acc. Chem. Res.* **2000**, *33*, 11-18.
62. (a) G. J. Davies, M. L. Sinnott, *Biochemistry.* **2008**, *30*, 26-32.; (b) J. D. McCarter, G. Stephen Withers, *Curr. Opin. Chem. Biol.* **1994**, *4*, 885-892.; (c) D. E. Koshland, *Biol. Rev. Cambridge Philos. Soc*. 1953, 28, 416-436.; (d) C. S. Rye, S. G. Withers, *Curr. Opin. Chem. Biol.* **2000**, *4*, 573-580.; (e) K. A. Stubbs, *Carbohydr. Res.* **2014**, *390*, 9-19.; (f) B. Henrissat, G. Davies, *Curr. Opin. Struct. Biol.* **1997**, *7*, 637-644.
63. (a) M. L. Sinnott, *Chem. Rev.* **1990**, *90*, 1171-1202.; (b) D. G. Naumoff, *Biochemistry* **2011**, *76*, 622-635.; (c) Fabrega, S.; Lehn, P.; Mornon, J.-P.; Davies, G. *Proc. Natl. Acad. Sci. U.S.A*. **1995**, *92*, 7090-7094.
64. (a) G. A. Grabowski, S. Gaft, M. Horowitz, E. H. Kolodny, *Crit.Rev. Biochem. Mol. Biol.* **1990**, *25*, 385-414.; (b) Keutzer, F. Zacchello, M. Scarpa, *Clin. Chim. Acta* **2009**, *402*, 38-41.; (c) T. D. Butters, R. A. Dwek, F. M. Platt,

Chem. Rev. **2000**, *100*, 4683-4696.; (d) K. Ohtsubo, J. D. Marth, *Cell* **2006**, *126*, 855-867.

65. H. M. Burke, T. Gunnlaugsson, E. M. Scanlan, *Chem. Commun.* **2015**, *51*, 10576-10588.
66. (a) A. Yamamoto, S. Adachi, S. Kawamura, M. Takahashi, T. Kitani, *Arch. Intern. Med.* **1974**, *134*, 627-634.; (b) N. G. Asp, A. Dahlqvist, *Anal. Biochem.* **1971**, *42*, 275-280.
67. (a) J. Lo, K. Mukerji, Y. C. Awasthi, E. Hanada, K. Suzuki, S. K. Srivastava, *J. Biol. Chem.* **1979**, *254*, 6710-6715.; (b) J. H. a. M. Sernetz, *Anal. Chim. Acta* **1984**, *163*, 67-72.; (c) T. Komatsu, K. Kikuchi, H. Takakusa, K. Hanaoka, T. Ueno, M. Kamiya, Y. Urano, T. Nagano, *J. Am. Chem. Soc.* **2006**, *128*, 15946-15947.; (d) M. Kamiya, H. Kobayashi, Y. Hama, Y. Koyama, M. Bernardo, T. Nagano, P. L. Choyke, Y. Urano, *J. Am. Chem. Soc.* **2007**, *129*, 3918-3929.; (e) O. Motabar, Z.-D. Shi, E. Goldin, K. Liu, N. Southall, E. Sidransky, C. P. Austin, G. L. Griffiths, W. Zheng, *Anal. Biochem.* **2009**, *390*, 79-84.
68. (a)M. Rose, M. J. Casadaban, D. Botstein*, Proc. Natl. Acad. Sci. USA* **1981**, *78*, 2460-2464.; (b) J. Alam, J. L. Cook, *Anal. Biochem.***1990**, *188*, 245-254.
69. C.-H. Tung, Q. Zeng, K. Shah, D.-E. Kim, D. Schellingerhout, R. Weissleder, *Cancer Research* **2004**, *64*, 1579-1583.
70. Takakura, T. Nagano, *Anal. Chem.* **2012**, *84*, 4404-4410.
71. (a) O. Motabar, Z.-D. Shi, E. Goldin, K. Liu, N. Southall, E. Sidransky, C. P. Austin, G. L. Griffiths, W. Zheng, *Anal. Chem.* **2009**, *390*, 79-84.; (b) D. J. Coleman, D. A. Kuntz, M. Venkatesan, G. M. Cook, S. P. Williamson, D. R. Rose, J. J. Naleway, *Anal. Biochem.* **2010**, *399*, 7-12.

72. A. K. Yadav, D. L. Shen, X. Shan, X. He, A. R. Kermode, D. J. Vocadlo, *J. Am. Chem. Soc.* **2015**, *137*, 1181-1189.

73. K. Y. Zhang, K. K.-S. Tso, M.-W. Louie, H.-W. Liu, K. K.-W. Lo, *Organometallics*, **2013**, *32*, 5098-5102.

74. M. H. Lee, J. H. Han, P.-S. Kwon, S. Bhuniya, J. Y. Kim, J. L. Sessler, C. Kang, J. S. Kim, *J. Am. Chem. Soc.* **2012**, *134*, 1316-1322.

75. K.-B. Li, Y. Zang, H. Wang, J. Li, G.-R. Chen, T. D. James, X.-P. He, H. Tian, *Chem. Commun.* **2014**, *50*, 11735-11737.

76. S. Redon, J. Massin, S. Pouvreau, E. De Meulenaere, K. Clays, Y. Queneau, C. Andraud, A. Girard-Egrot, Y. Bretonnière, S. Chambert, *Bioconjug. Chem.* **2014**, *25*, 773-787.

77. (a) W. H. Kim, J. Lee, D.-W. Jung, D. R. Williams, *Sensors* **2012**, *12*, 5005-5027.; (b) E. C. Calvaresi, P. J. Hergenrother, *Chem. Sci.* **2013**, *4*, 2319-2333.

78. M. G. Vander Heiden, L. C. Cantley, C. B. Thompson, *Science* **2009**, *324*, 1029-1033.

79. M. Delbianco, P. Bharate, S. Varela-Aramburu, P. H. Seeberger, *Chem. Rev.* **2016**, *116*, 1693-1752.

80. K. Soundarajan, R. Periyasamy, T. Mohan Das, *RSC Adv.* **2016**, *6*, 81838-81846.

81. (a) I. Nakazawa, M. Masuda, Y. Okada, T. Hanada, K. Yase, M. Asai, T. Shimizu, *Langmuir* **1999**, *15*, 4757-4764.; (b) S. Abraham, S. Paul, G. Narayan, S. K. Prasad, D. S. S. Rao, N. Jayaraman, S. Das, *Adv. Funct. Mater.* **2005**, *15*, 1579-1584.; (c) S. Das, N. Gopinathan, S. Abraham, N. Jayaraman, M. K. Singh, S. K. Prasad, D. S. S. Rao, *Adv. Funct. Mater.* **2008**, *18*, 1632-1640.

82. (a) J. H. Jung, S. Shinkai, T. Shimizu, *Chem. Eur. J.* **2002**, *8*, 2684-2690.; (b) H. Kobayashi, A. Friggeri, K. Koumoto, M. Amaike, S. Shinkai, D. N. Reinhoudt, *Org. Lett.* **2002**, *4*, 1423-1426.; (c) J. H. Jung, G. John, M. Masuda, K. Yoshida, S. Shinkai, T. Shimizu, *Langmuir* **2001**, *17*, 7229-7232.; (d) O. Gronwald, S. Shinkai, *J. Chem. Soc. Perkin Trans. 2* **2001**, 1933-1937.
83. Y. Ogawa, C. Yoshiyama, T. Kitaoka, *Langmuir* **2012**, *28*, 4404-4412.
84. W.-T. Dou, Y.-L. Zeng, Y. Lv, J. Wu, X.-P. He, G.-R. Chen, C. Tan, *ACS Appl. Mat. Int.* **2016**, *8*, 13601-13606.
85. R. S. Yalagala, S. A. Mazinani, L. A. Maddalena, J. A. Stuart, F. Yan, H. Yan, *Carbohydr. Res.* **2016**, *424*, 15-20.

CHAPTER 2

Design, synthesis and aggregation studies of glycoconjugated squaraine dyes

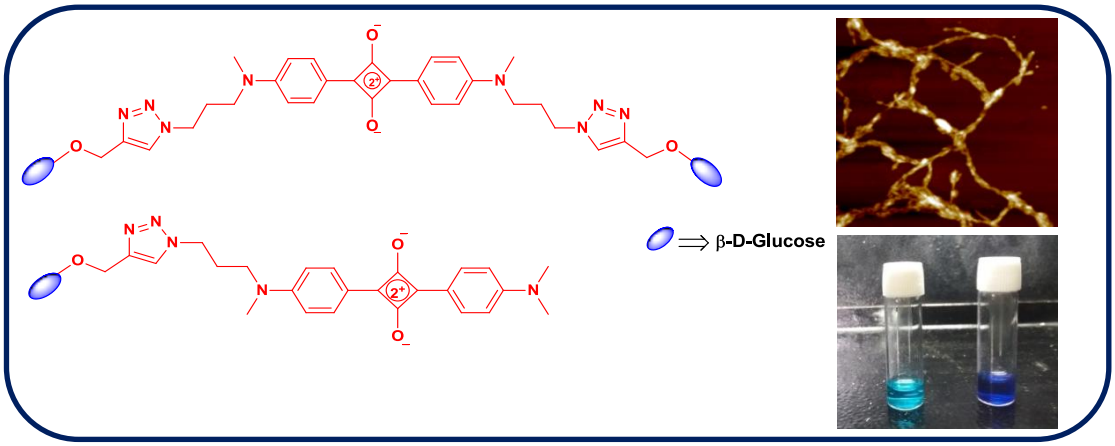

Abstract

Squaraine dyes, an interesting class of organic dyes, are widely explored in the optical field owing to their outstanding photophysical properties. Squaraine dyes are known to exhibit aggregation-caused quenching (both H- and J-aggregates) in the solid state as well as in solution (depending upon the medium and structure) and have been extensively studied. However, there are only limited reports on the construction of hierarchical architectures via supramolecular self-assembly from squaraine dyes. In particular, the chiral supramolecular self-assembly recently received considerable attention in the field of designing of chiroptical devices. The aggregation behavior of squaraine dyes associated with fluorescence quenching in aqueous solution limited their application in the biomedical field. Efforts are also directed to circumvent this detriment by supramolecular encapsulation, forming squaraine rotaxanes and squaraine adducts.

Recently, aggregation caused quenching is widely explored to design brilliant fluorogenic probes with excellent contrast. We conducted a detailed investigation of the aggregation properties of novel glycoconjugated squaraine dyes in aqueous solution and their applicability as a fluorogenic probe in aqueous solvent.

2.1. Introduction

There is a rapid development in the optical information technology and optical absorbing materials have got immense attention owing to their potential applications in the fields of nonlinear optics, photodynamic therapy, optical data storage, laser printing, biological probes, infrared photography, solar cells, etc.[1] A large number of functional dyes, π-conjugated molecules and chromophore based systems have been developed in this direction including phthalocyanine, polymethine cyanine, polyacetylenes, squaraines, radical dyes, azo dyes, and their derivatives. Among these, squaraine dyes are an interesting group of organic molecules owing to their unique optical properties. Squaraines possess broad applications ranging from material to biology, and some of the relevant applications can be listed as nonlinear optics,[2] light-emitting diodes,[3] bio-imaging,[4] solar cells,[5] fluorescence probes,[6] photodynamic therapy,[7] protein labeling[8] and as surface enhanced raman scattering (SERS) reporters.[9]

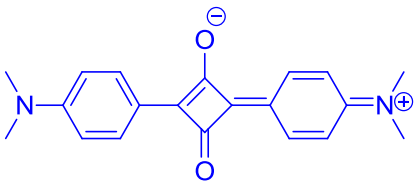

Figure 2.1. General structure of squaraine dye

Squaraine dyes have a unique rigid zwitterionic structure (Figure 2.1) with two donor units connected to an electron deficient cyclobutane dione ring. They possess sharp, strong absorption (Molar absorption coefficient, $\varepsilon \geq 10^5$ $cm^{-1}M^{-1}$) and

emission in the near infrared region ascribed to the intramolecular charge transfer (ICT). The interesting properties of squaraine dyes such as facile and scalable synthesis of different derivatives, tunable absorption and emission in the near infrared (NIR) region and environmental sensitive optical properties make them promising NIR emitting fluorescent probes among other chromophores. However, squaraine molecules undergo aggregation in solid state and in solutions containing poor solvents attributed to the strong dipole-dipole and π-π stacking interactions between the adjacent molecules. This aggregation leads to strong optical quenching and restricts their practical applications in water, particularly in the biomedical field. Great effort has gone in this direction to overcome the aggregation caused quenching, to effectively increase the interplanar distance between the adjacent molecules (> 3.5 Å) and thereby reducing the intermolecular charge transfer.[10] Successful attempts that have been done to solve this problem include supramolecular encapsulation,[11] incorporating squaraine molecules to rotaxanes,[12] supramolecular adducts of squaraine with protein,[13] by developing squaraine-inorganic hybrid systems, *etc.*[14]

Aggregation properties of squaraines have been extensively studied in mixed solvents, organized media, and in the presence of metal ions and are well documented in the literature.[15] However, there are only very few reports on the formation of extended supramolecular architectures of functional squaraine derivatives. The aggregation behaviour plays a critical role in electron- and energy-transport processes,[16] hence the control over aggregation and their effective utilization in the field of optical imaging and material chemistry remains to be a hot topic. Würthner and co-workers conducted a detailed investigation on the aggregation properties of the squaraine dyes in non-polar solvents.[17]

Ajayaghosh and co-workers demonstrated the formation of metallo-supramolecular self-assembly from squaraine dimers with flexible alkyl chains.[18] Complexation of Ca^{2+} with squaraine dye (**1**) facilitate the formation of folded H-type aggregates (Figure 2.2). The electrostatic interaction between the negatively charged oxygen atom in the central cylobutenoate ring of squaraine to Ca^{2+} lead to the successful complexation and H-type aggregate formation. The binding of Ca^{2+} induced the formation of one-dimensional spherical micellar self-assembly was also demonstrated with flexible alkyl chain linked bis-squaraine dye, **2** (Figure 2.3).[19] This supramolecular hierarchical structure possesses strong molecular absorptivity and thermal stability.

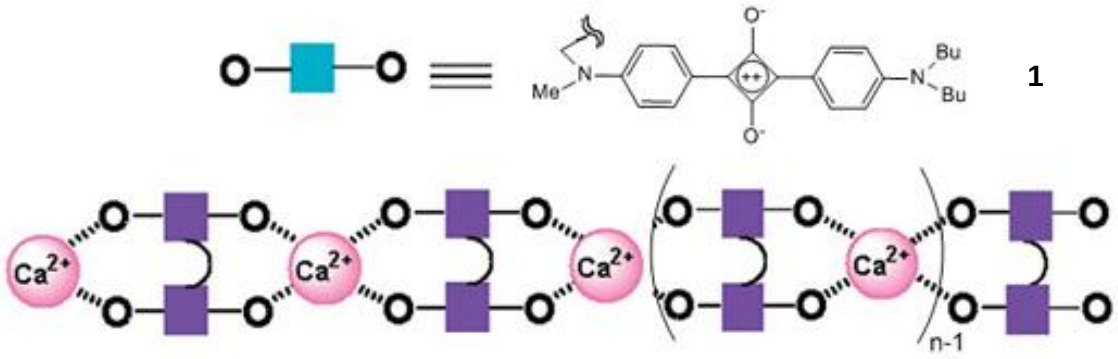

1

Figure 2.2. Schematic representation of cation induced metallo-supramolecular assemblies from squaraine dimers

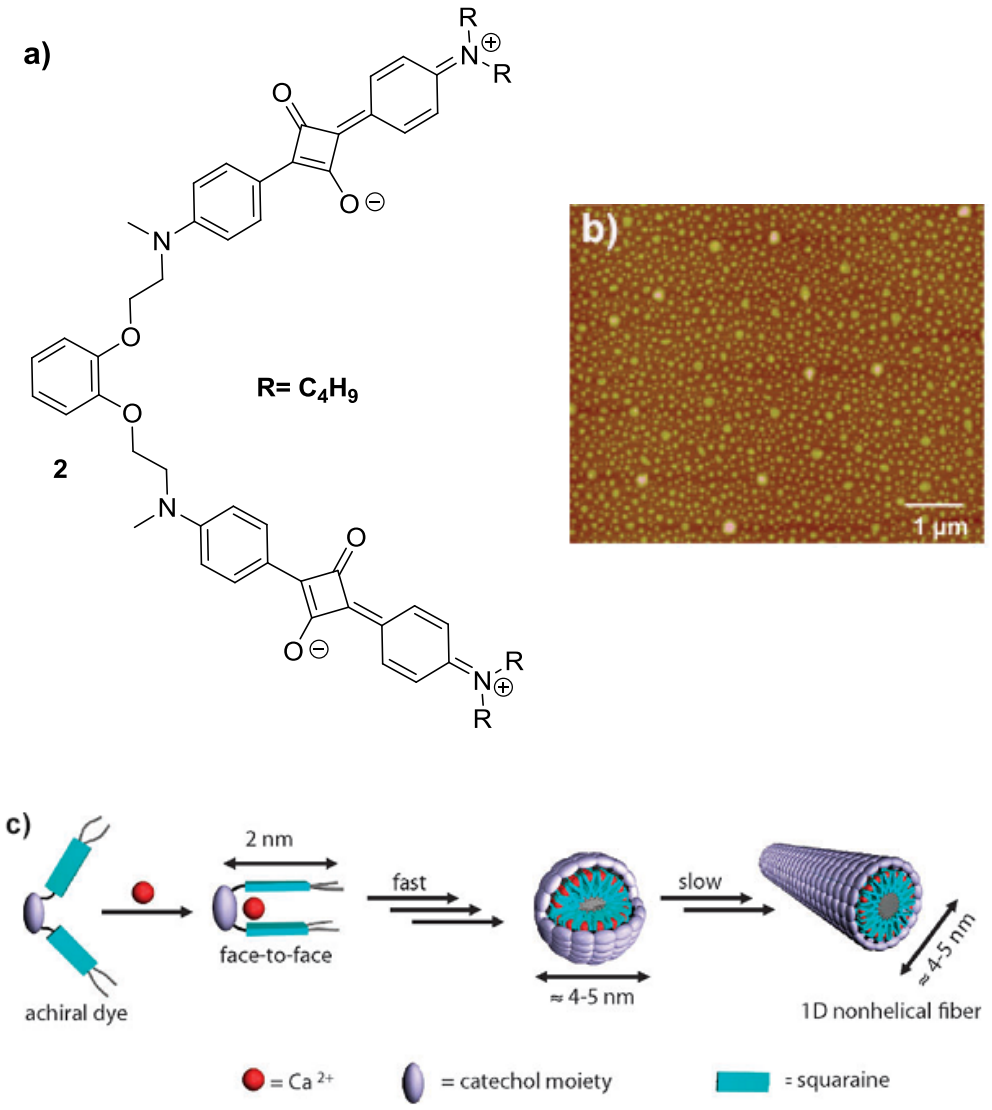

Figure 2.3. (a) Molecular structure, (b) schematic representation of cation induced spherical micellar self-assembly formation of bis-squaraine and (c) AFM image of the micellar structure.

Recently, Liu and co-workers reported that self-assemblies could be effectively controlled by rational molecular design.[20] They designed a few zwitterionic squaraine dyes **3-5** (Figure 2.4) with different hydrogen-bonding (H-bond) abilities and conducted a detailed investigation of the synergistic effect of H-bond and π-π stack interaction on optical properties and morphologies of squaraine aggregates. The morphologies of the resultant self-assemblies could be effectively tuned from nanoparticles, 1D nanowire to 2D nanoribbon (Figure 2.4). Increasing number of

hydrogen bond donors at the end of squaraine skeleton influence the optical properties as well as morphology. The proposed electrostatic interaction between the adjacent molecules based on the theoretical experiments is shown in the Figure 2.5. The electrostatic attraction will be high when the hydrogen bond formed between O-atom in the central (C_4O_2) cyclobutane dione bridge ring and H-atom of the terminal methyl group.

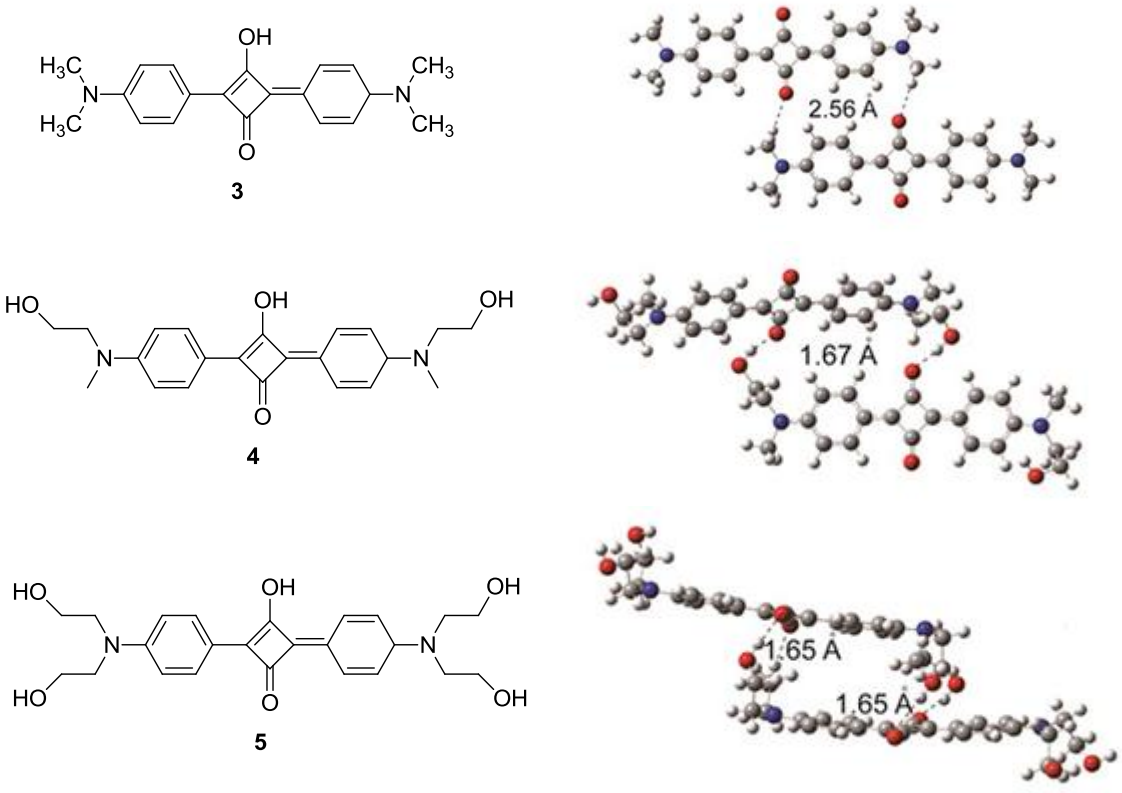

Figure 2.4. Structure of the squaraine dyes **3-5**, their molecular arrangements and hydrogen bonding distributions implemented on Gaussian 03 program suite.

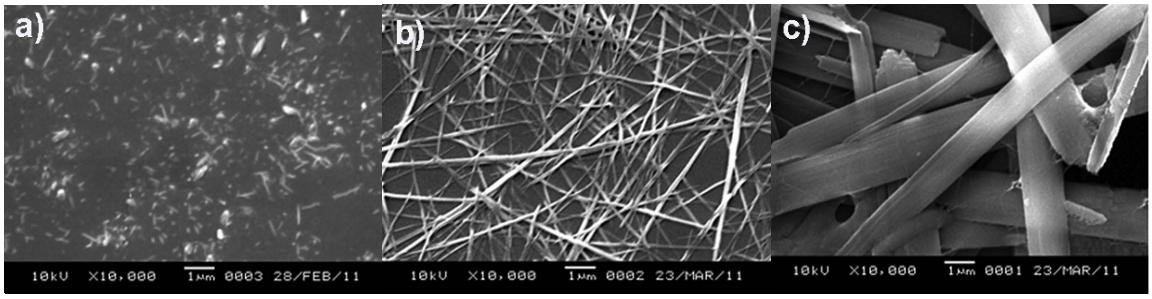

Figure 2.5. SEM images of the assembly formed from squaraine dyes **3-5** (a-c).

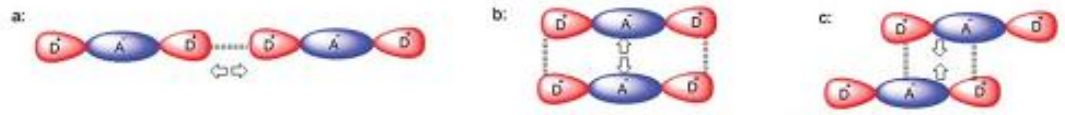

Figure 2.6. Schematic representation of the electrostatic interaction between adjacent molecules of squaraine dyes based on theoretical experiment.

Chirality has been identified as a guiding element in the self-assembly process and widely exploited in the design of supramolecular architectures.[21] Chiral supramolecular assemblies seek researchers attention due to the similarity with natural biological structures and application in designing chiroptical devices.[22] Though chiral supramolecular architectures based on squaraine skeleton is very few.

Chiral squaraine dyes can be constructed by tailoring chiral ligands on the squaraine skeleton. Hescht and co-workers synthesized chiral squaraine dye for the first time by attaching a chiral ligand, natural amino acid L-proline on both ends of the aniline based squaraine skeleton (**6**) and their aggregation properties was elucidated in solution and in solid state.[23] This squaraine dye exhibited unique chiral self-assembling behaviour in aqueous solution and in the solid state. Helical self-assembly of the squaraine dye in aqueous solution was purely attributed to the hydrophobic interaction.[24] The negative Cotton effect was observed in the circular dichroism (CD) spectra for the squaraine dye (**6**) in acetonitrile-water mixtures which coincide with red shifted absorption band of squaraine aggregate.

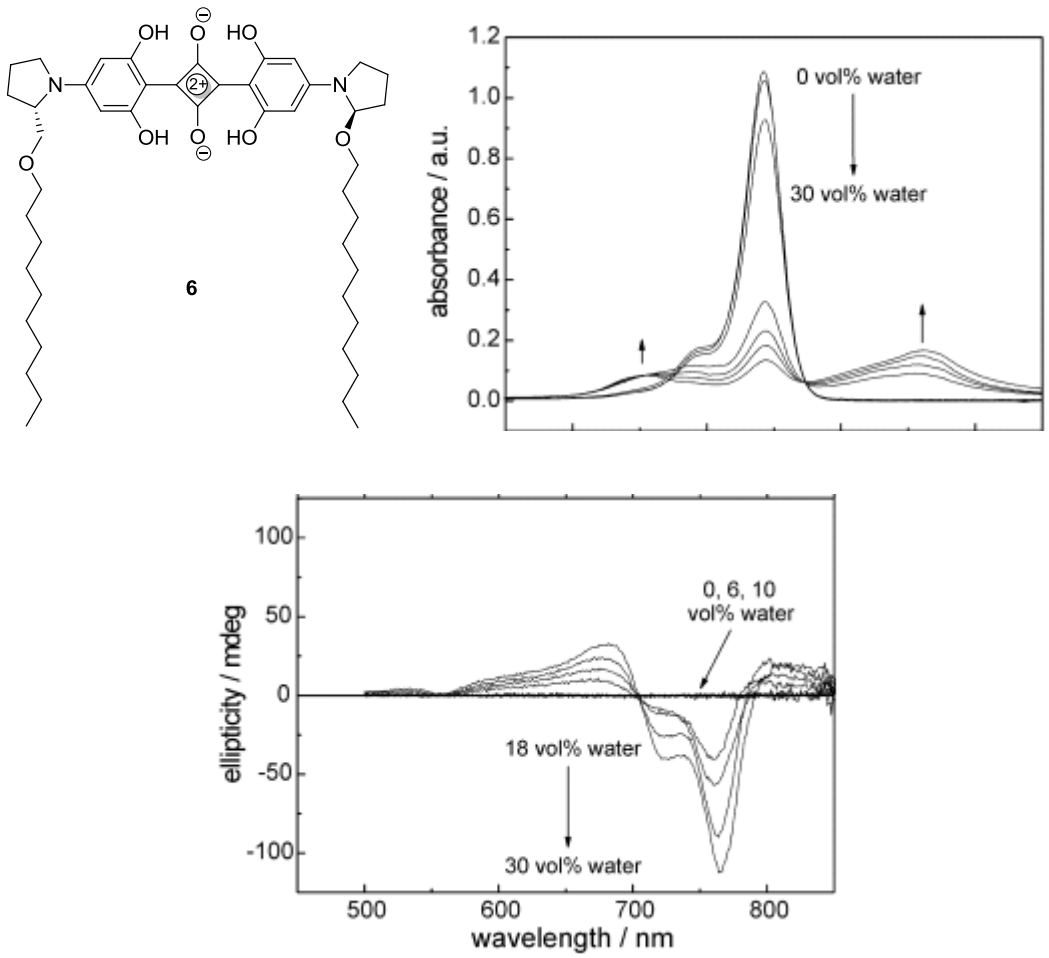

Figure 2.7. Molecular structure of chiral squaraine dye, **6** and self-assembly properties of compound **6** in aqueous solution

Later, Ramaiah and co-workers demonstrated the formation of two chiral (both *M* and *P*) H-type supramolecular assemblies with opposite phases from the cholesterol appended quinoline based squaraine dye (**7**, Figure 2.8).[25] Influence of chiral ligand, the cholesterol moiety, in the self-assembly process was confirmed by comparing the results with that of a model compound (**8**), which lacks cholesterol moiety. The model compound (**8**) exhibited only achiral J-type aggregate formation in poor solvent. The chiral aggregates derived from cholesterol appended squaraine dye were found to be switchable with response to temperature, concentration and solvent ratio.

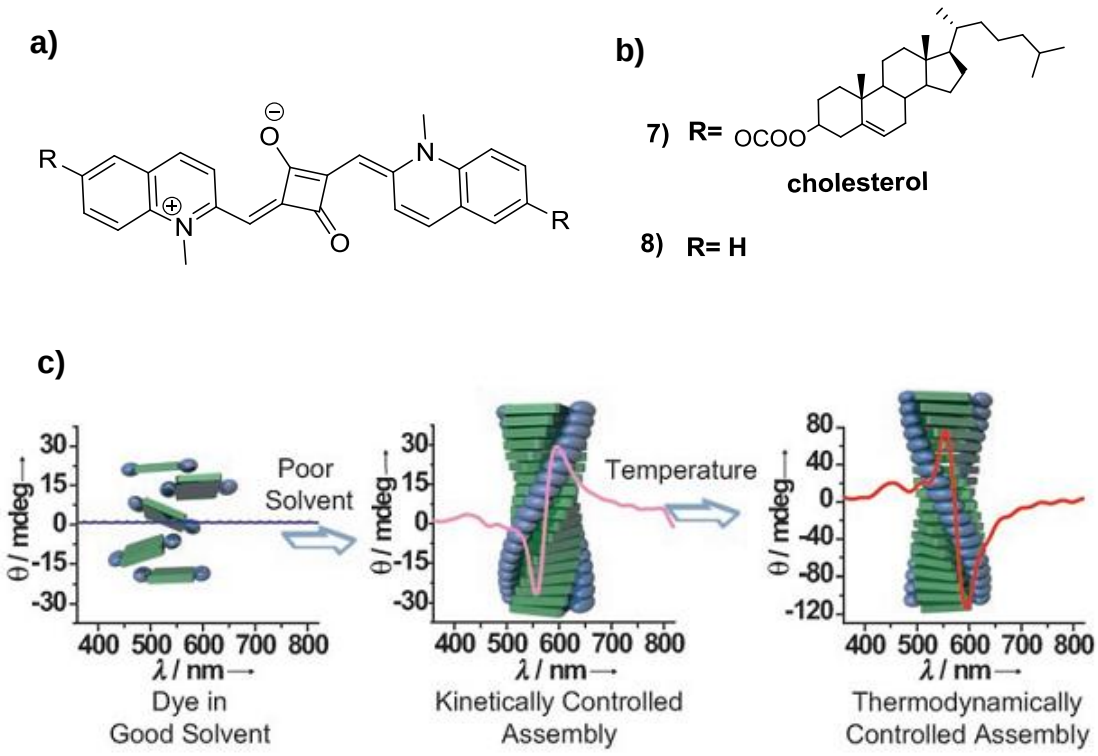

Figure 2.8. (a) Molecular structure of cholesterol linked squaraine dye **7**, (b) model compound **8** and (c) schematic representation of the two chiral self-assemblies and their CD spectra.

Cation induced formation of helical supramolecular architectures was demonstrated by developing a tripodal squaraine dye containing flexible chiral alkyl chain (**9**) (Figure 2.9).[26] Aggregates derived from the chiral squaraine dye in acetonitrile-water mixture solvent was CD inactive and showed agglomerated morphology in AFM analysis. Cation complexation with the squaraine skeleton was necessary for the CD amplification and supramolecular helicity. The complexation was reported to be reversible in the presence of ethylenediaminetetraacetic acid (EDTA).

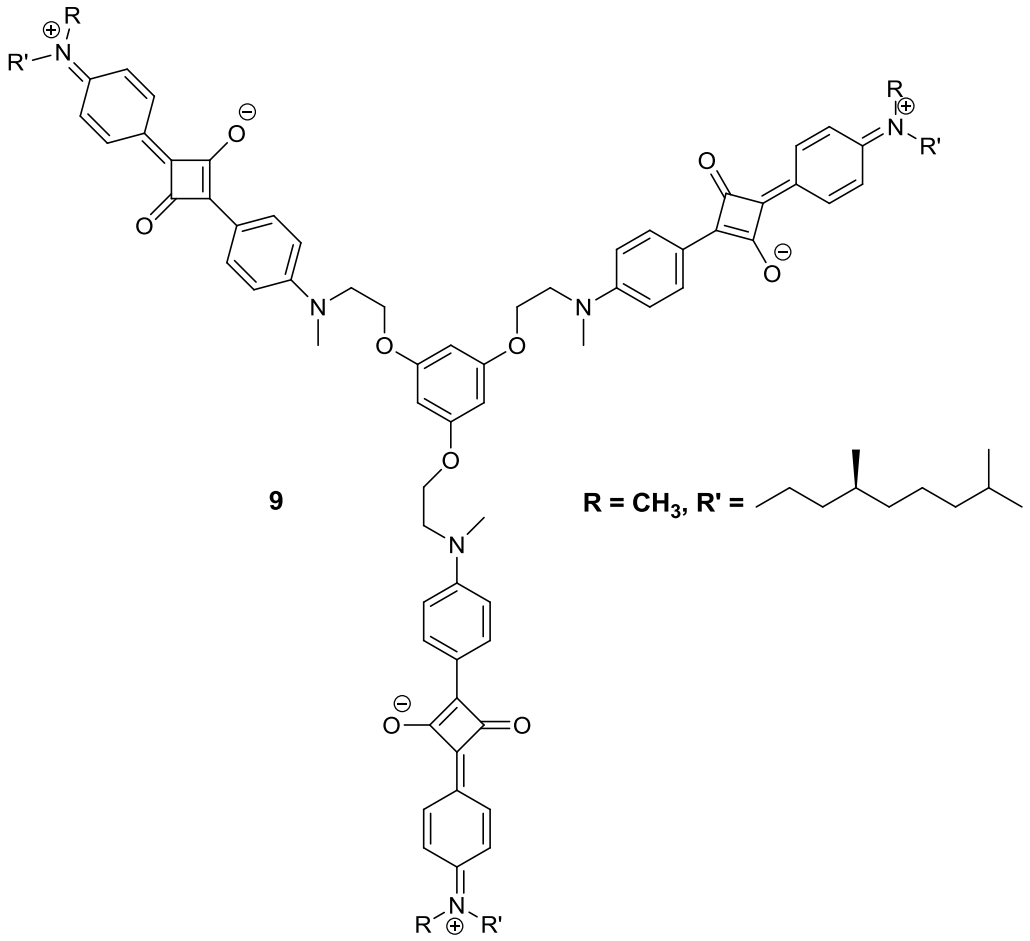

Figure 2.9. Molecular structure of tripodal squaraine, **9**

Our group also conducted a detailed investigation on the aggregation properties of the squaraine dyes.[27] Water soluble benzothiazole based squaraine dyes (**10**, **11**, Figure 2.10) were synthesized, their aggregation properties and the influence of external agents polyvinylpyrrolidine (PVP) and β-cyclodextrin were studied.[28] These squaraine dyes formed dimer in water with blue shift in the absorption spectra. Aggregate formation was high in D_2O than in water. Higher concentration of PVP and β-cylodextrin in water solution leads to the formation of a new species with a red shift in the absorption spectrum of squaraine dye (**10**) attributed to monomeric forms microencapsulated in hydrophobic environment of PVP while squaraine dye (**11**) showed less/low binding affinity toward PVP and β-cyclodextrin. The influence of

heavy atoms such as halogens on the aggregation behaviour of squaraine dyes was investigated with halogenated bis(2,4,5-trihydroxyphenyl)squaraine dyes **12-14** (Figure 2.10) in aprotic solvents.[29] These heavy atom substituted squaraine dyes formed J-type dimer aggregates in acetonitrile solutions at high concentrations of the dye. The J-type dimer is formed through hydrogen bonding interaction between adjacent molecules (Figure 2.11).

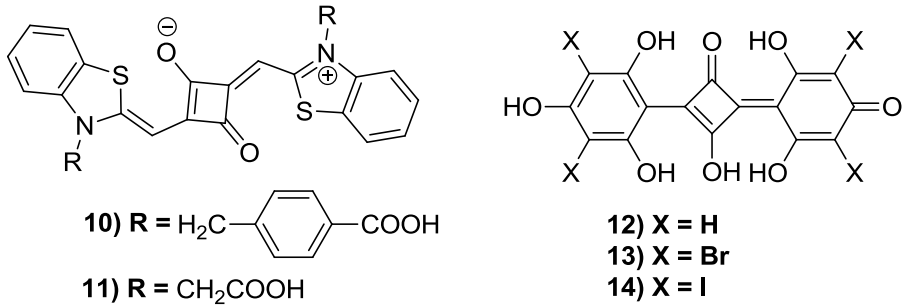

Figure 2.10. Molecular structure of squaraine dyes **10-14**.

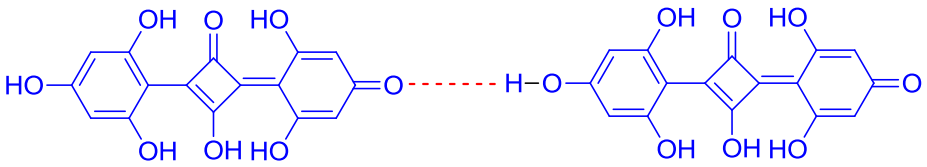

Figure 2.11. Proposed structure for the squaraine dimer formed from squaraine dyes **12-14**.

2.2. Statement of the problem

The earlier discussions point to the need of detailed study on the aggregation behavior of squaraine molecules, especially in water solvent. Squaraine dyes have proven to be excellent candidates for NIR imaging. But the aggregation caused quenching and the instability of squaraine dyes in the aqueous environment limits their application in bioimaging. Squaraine dyes have been extensively studied owing to their broad spectrum of applications, but there is dearth of the research focusing

squaraine molecules as building blocks for fashioning supramolecular architectures particularly chiral supramolecular architectures. As a continuation of our research interest in the field of squaraine chemistry, we undertook a detailed investigation of the aggregation properties of the carbohydrate appended squaraine dyes. Sugar moiety is selected due to its versatile functions, chirality and which contains hydroxyl groups as hydrogen bond donors. Thus sugar molecule can offer chirality as well as water solubility to the squaraine skeleton simultaneously. The significance of carbohydrates and applications of various fluorescent labeled glycans were discussed in Chapter 1. Additionally, sugar molecules being involved in most of the biological functions and are the primary energy source, which have been exploited as targeting ligands in the biomedical field. Our aim is to design a fluorogenic probe based on anilinium squaraine scaffold and study their aggregation properties using photophysical, chiroptical and microscopic techniques.

2.3. Results and Discussion

2.3.1. Design Strategy

Our strategy involved the design of glycoconjugated squaraine dyes, monosugar appended (**ASqβGl**) and bis-sugar appended (**SSqβGl**). Glucose moiety was conjugated to squaraine moiety *via* triazole linker through the β-glycosidic bond in order to improve the water solubility, and it also acts as a chiral ligand. 1,2,3-triazole is an isoster of the peptide bond and was chosen as linker because of its enhanced water solubility and cell permeability.[27] Unlike amides, triazoles are resistant to hydrolysis and are relatively stable to either oxidation or reduction. They can be easily introduced by Huisgen 1,3-dipolar cycloaddition reaction of an azide with an alkyne. The molecular structure of the target molecules are shown in Figure 2.12.

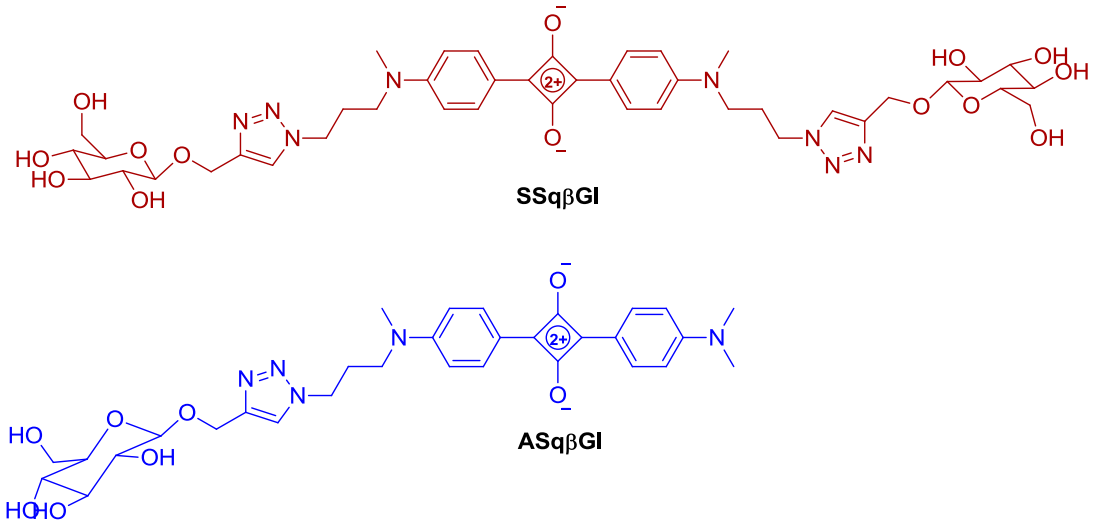

Figure 2.12. Molecular structure of target molecules, glycoconjugated squaraine dyes **SSqβGl** and **ASqβGl**

2.3.2. Synthesis

The synthetic strategy toward the target molecules is depicted in Scheme 2.1, Scheme 2.2 and Scheme 2.3. First step involves the synthesis of starting materials (azide and alkyne) for the Huisgen 1,3-dipolar cycloaddition toward the triazole functional group. Peracylated glucose upon glycosidation in the presence of Lewis acid, $BF_3.Et_2O$ and propargyl alcohol in dichloromethane solvent afforded β-propargylated glycoside **17** (Scheme 2.1). Azide derivative, *N*-(3-azidopropyl)-*N*-methylaniline (**20**) was obtained from *N*-methylaniline (**18**). Alkylation of *N*-methylaniline with 1,3-dibromopropane followed by condensation with sodium azide in dimethylformamide afforded compound **20** (Scheme 2.2). Coupling of compounds **17** and **20** in the presence of a copper catalyst followed by deprotection of acetyl group on carbohydrate moiety with sodium carbonate in methanol yielded the corresponding hydroxylated triazole **βGlTZLOH** (**21**) (Scheme 2.3). Finally, condensation of the hydroxylated triazole (**21**) with squaric acid (**22**) and 3-(4-dimethylamino)phenyl-4-hydroxycyclobut-3-ene-1,2-dione (**23**) yielded squaraine

dyes **SSqβGl** and **ASqβGl** respectively, following the traditional procedure for the squaraine synthesis (Scheme 2.4 and 2.5). The Bis-sugar appended squaraine dye, **SSqβGl** was synthesized by refluxing a mixture of squaric acid (**22**) and the triazole derivative, **βGlTZLOH** in *n*-butanol:benzene (2:1) solvent system for 20 h followed by azeotropic removal of water (Scheme 2.4). Condensation of the triazole derivative, **βGlTZLOH** with 3-(4-dimethylamino)phenyl-4-hydroxycyclobut-3-ene-1,2-dione (**23**) in *n*-butanol:benzene (2:1) solvent system for 8 h followed by azeotropic removal of water furnished the corresponding monosugar appended squaraine dye, **ASqβGl** (Scheme 2.5).

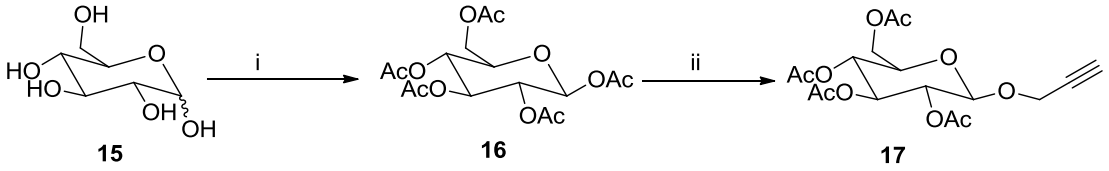

Scheme 2.1. (i) Ac_2O, NaOAc, Reflux, 9 h, 90; (ii) $BF_3.Et_2O$, CH_2Cl_2, Propargyl alcohol, 8 h, 0 °C-rt, 73 %.

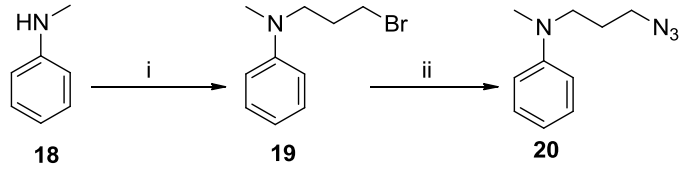

Scheme 2.2. (i) 1,3-Dibromopropane, K_2CO_3, TBAB, DMF, 80 °C, 12 h, 54 %; (ii) NaN_3, DMF, 80 °C, 6 h, 80 %.

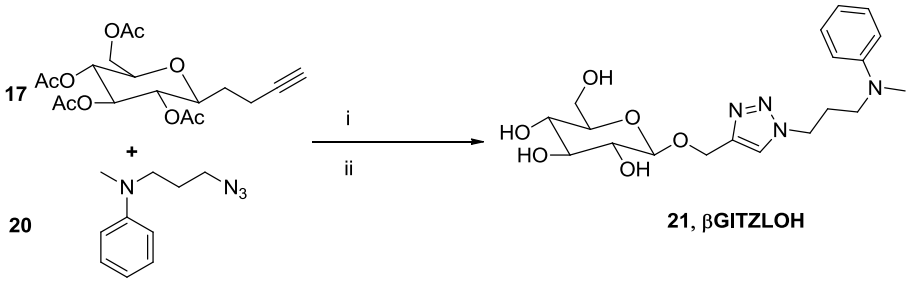

Scheme 2.3. (i) CuI, DIPEA, CH_3CN, 0 °C- rt, 2 h; (ii) Na_2CO_3, rt, 2 h, 54 %.

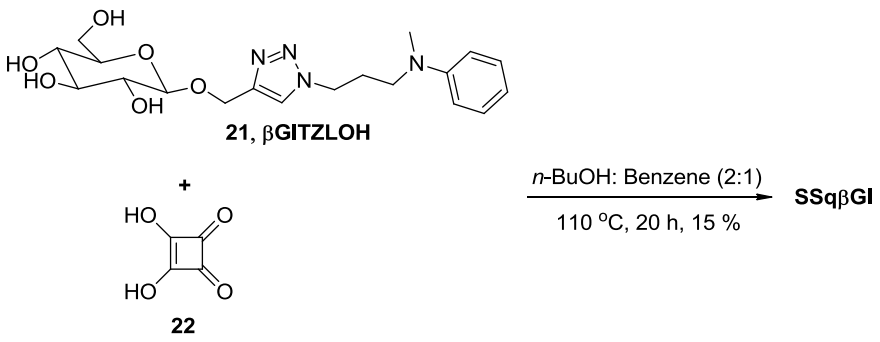

Scheme 2.4. (i) *n*-butanol/benzene azeotropic mixture (2:1), 110 °C, 20 h, 15 %.

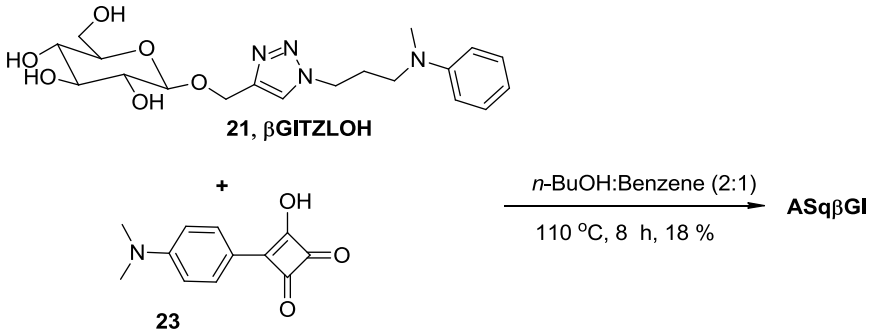

Scheme 2.5. (i) *n*-butanol/benzene azeotropic mixture (2:1), 110 °C, 8 h, 18 %.

2.3.3. Photophysical properties

The absorption and emission spectra of **SSqβGl** and **ASqβGl** were recorded in dimethyl sulfoxide (DMSO) and in water in which the dyes were easily solubilized, and the corresponding photophysical data are summarized in Table 2.1. The normalized absorption and emission spectra of squaraine dyes (**SSqβGl** and **ASqβGl**) are shown in Figure 2.13. In DMSO solvent, **SSqβGl** and **ASqβGl** exhibited a sharp band centered at 649 nm, a typical absorption feature of squaraine chromophores in polar solvents.[31] While in water, SSqβGl and ASqβGl exhibited a sharp band centred at 642 nm along with less intense shoulder band in the shorter wavelength region, indicating the formation of H-type aggregates (Figure 2.13a and 2.13c). Squaraine dyes are known to aggregate strongly in the presence of water.[32] In DMSO, both squaraine dyes-**SSqβGl** and **ASqβGl** exhibited good emission in the NIR region with

emission maxima centred on 668 nm (Figure 2.13b and 2.13d) and fluorescence quantum yields of 0.38 and 0.27 respectively. These dyes are practically non-fluorescent in the aqueous solutions, and this could be attributed to the combined effect of the interaction of excited state of the dyes with protons of water and aggregation of the dyes in aqueous solution.[33]

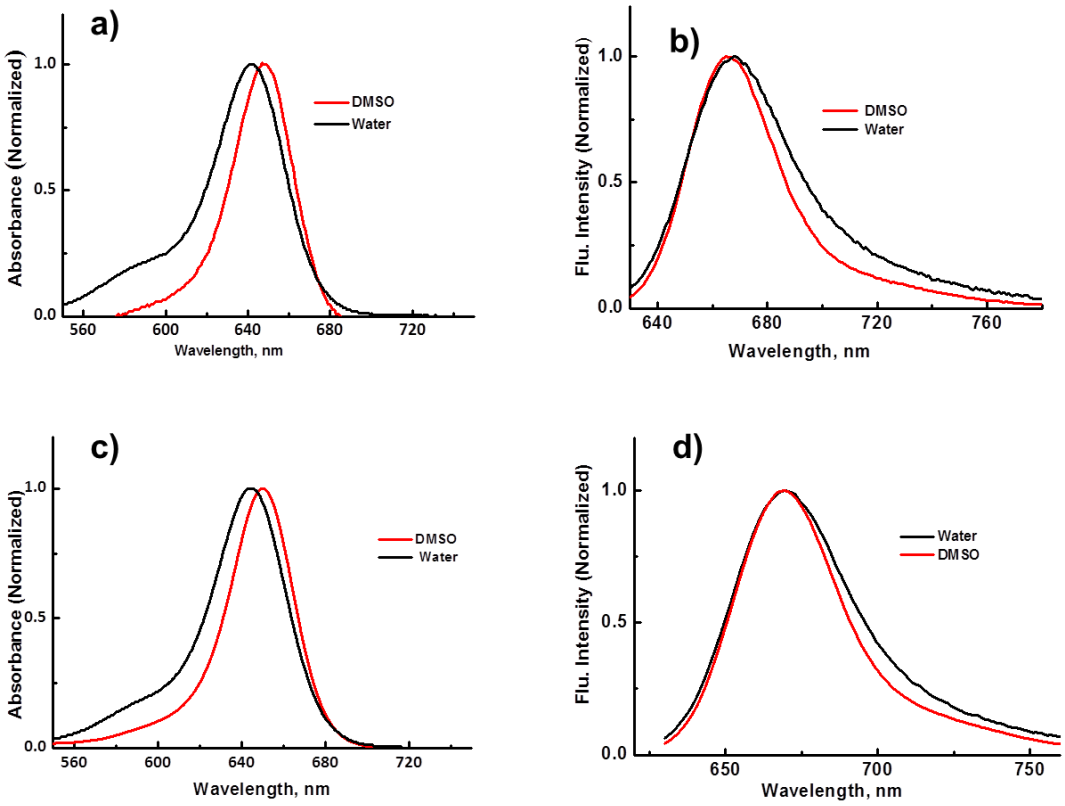

Figure 2.13. Normalized UV-Vis absorption spectra of **ASqβGl** (a), **SSqβGl** (c) and normalized emission spectra of **ASqβGl** (b), **SSqβGl** (d) in DMSO and water.

Table 2.1. Photophysical data of **ASqβGl** and **SSqβGl** dyes

	ASqβGl					**SSqβGl**				
Solvent	Abs. λ_{max} (nm)	Em. λ_{max} (nm)	Stokes shift (cm^{-1})	ε ($M^{-1}cm^{-1}$)	Φ_f	Abs. λ_{max} (nm)	Em. λ_{max} (nm)	Stokes shift (cm^{-1})	ε ($M^{-1}cm^{-1}$)	Φ_f
DMSO	649	665	347.02	1.7± 0.5x10^5	0.27	649	669	460.63	1.9± 0.4x10^5	0.38
Water	641	668	460.63	-	0.01	644	669	580.26	-	0.02

(Fluorescence quantum yields (Φ_f) were measured by relative method using squarylium III (Φ_f = 0.65 in dichloromethane) as standard, λ_{ex} = 630 nm, accuracy ± 0.04)

Since the squaraine dyes exhibited strong tendency to form aggregates in water, their absorption and emission properties as a function of concentration were studied (Figure 2.14 and 2.15). In aqueous solution with an increase in the concentration of the squaraine dyes, two new peaks appeared- one blue shifted, and the other red shifted along with the monomer peak which could be attributed to the formation of H- and J-type aggregates (Figure 2.14 and 2.15).[31] In the case of **SSqβGl**, relative intensity of the blue shifted band was high compared to both the monomer band and the newly formed red shifted band (Figure 2.14a). Whereas the relative intensity of the red shifted band was high for ASqβGl in aggregate solution (Figure 2.14b), indicating that the contribution of blue shifted H-aggregate formation was significantly higher for **SSqβGl** compared to that of **ASqβGl**. The unsymmetric squaraine dye, **ASqβGl** molecules prefer to undergo end-to-end orientation to form J-type aggregates which is evidenced by the relatively high intensity of red shifted band compared to that observed for the symmetric dye, **SSqβGl**.

The effect of temperature on the formation of aggregate from **SSqβGl** and **ASqβGl** in water was further studied. At 25 °C, the absorption spectra of both dyes

consist of structured peaks corresponding to monomer and aggregates. With the increase in temperature, reduction in the intensities of the bands attributable to aggregates was observed along with a concomitant increase in the intensity of the monomer band. At 50 °C, the absence of absorption band centred at 695 nm confirmed the break-up of the J-aggregates formed from **SSqβGl**, whereas a marginal decrease in intensity of blue shifted bands indicated that the H-aggregates formed are quite stable even at higher temperatures (Figure 2.15a). In the case of unsymmetric dye **ASqβGl** with the increase in temperature, blue shifted band vanished, and a slight decrease in intensity of the red shifted band was observed at 50 °C which indicates that for this dye the red shifted J-aggregate was much more stable than its H-aggregate (Figure 2.15b).

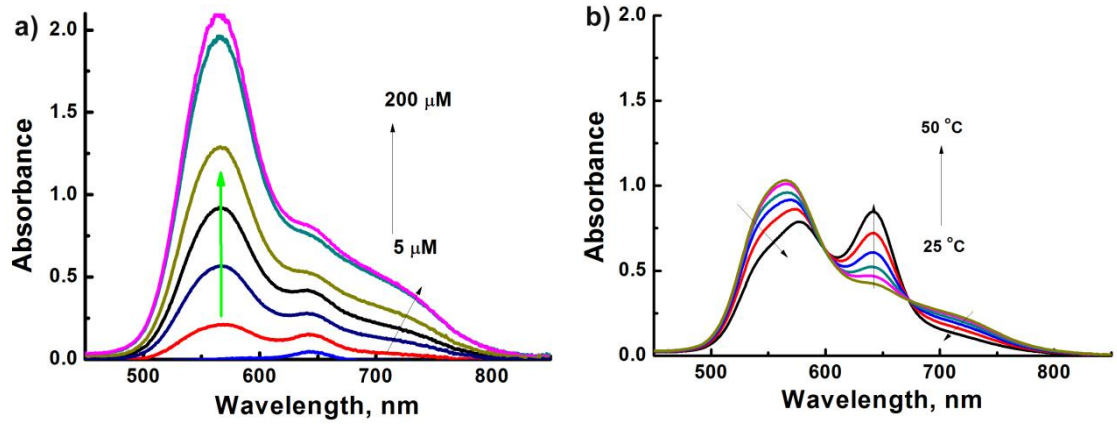

Figure 2.14. Absorption and emission spectral changes of (a) **SSqβGl** [5, 20, 40, 80, 100, 200 μM, pathlength 10 mm] in water with increase in concentration and (b) temperature dependent absorption spectral changes of **SSqβGl** (20 μM) with increase in temperature from 25, 30, 35, 40, 45 and 50 °C.

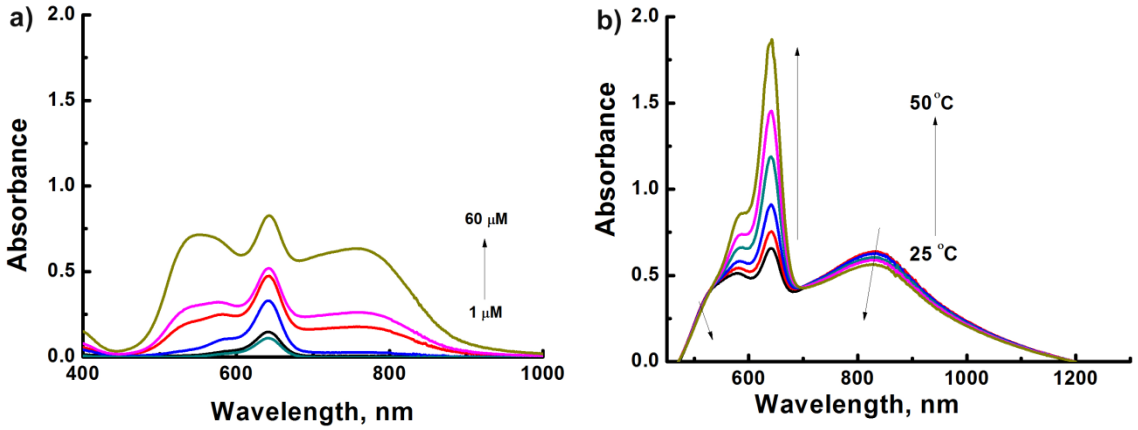

Figure 2.16. Absorption spectral changes of (a) **ASqβGl** [1, 5, 10, 20, 30 & 60 μM, Path length 1 mm] in water with increase in concentration and (b) temperature dependent absorption spectral changes of **ASqβGl** (30 μM) with increase in temperature from 25, 30, 35, 40, 45 and 50 °C.

The difference spectra resulted by subtracting the normalized absorption spectra (at 649 nm) of the aggregate from that of monomer (5 μM) of **SSqβGl** showed two peaks which correspond to H-aggregate (564 nm) and J-aggregate (700 nm, Figure 2.16a). Similarly, the difference spectra of **ASqβGl** showed two peaks at 570 nm (H-aggregate) and 830 nm (J-aggregate, Figure 2.16b). This spectral information revealed that both dyes have greater tendency to get aggregated in aqueous solutions. From the concentration dependent emission changes of both dyes, it was found that both dyes exhibited emission centred at 669 nm at lower concentration (Figure 2.16). With an increase in concentration, intensity of the emission band decreased gradually which again confirming that the aggregates formed contributed to the non-emissive route of energy loss from the excited state. Excitation spectra of **ASqβGl** and **SSqβGl** were measured and based on which, it could be concluded that emission arises only from the monomers and that the aggregates are non-emissive (Figure 2.17).

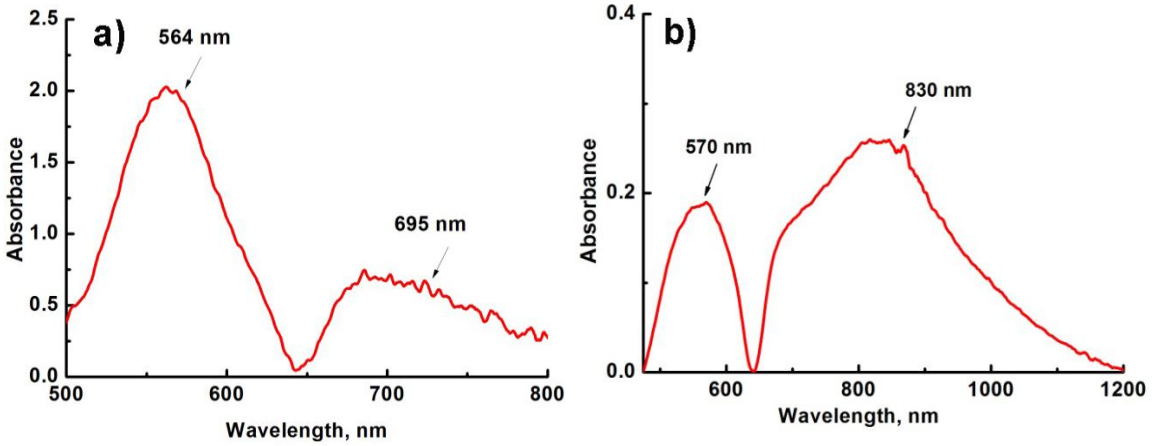

Figure 2.17. Difference spectra obtained by subtracting the normalised absorption spectra of the aggregate from that of monomer (at lower concentration) of (a) **SSqβGl** (b) **ASqβGl**.

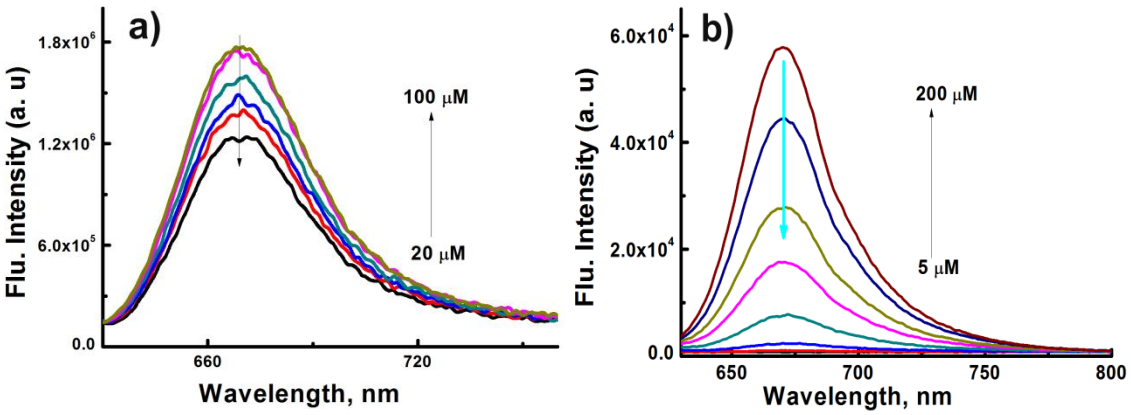

Figure 2.18. Changes in emission spectra of (a) **ASqβGl** [20, 30, 40, 60, 80 and 100 μM**]** and (b) **SSqβGl** [5, 10, 20, 40, 60, 80, 100 and 200 μM] in water solution.

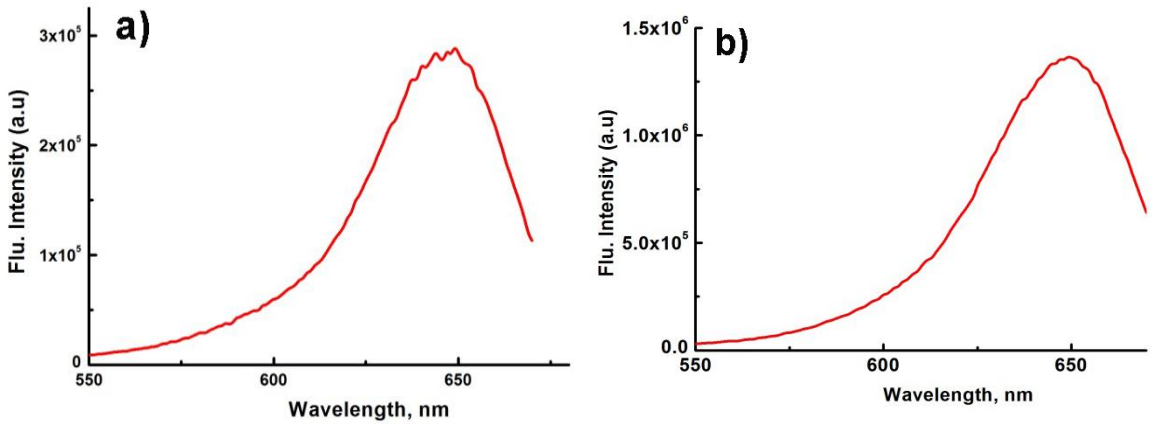

Figure 2.19. Excitation spectra of (a) **ASqβGl** [5.5x10^{-5} M concentration, emission collected at 670 nm] and (b) **SSqβGl** [5.5x10^{-5} M concentration, emission collected at 669 nm].

We then moved on to check the chirality of the synthesized squaraine dyes in solution (DMSO and water). Both the squaraine dyes exist as monomers in DMSO solvent and were found to be CD inactive. But in aqueous solution bis-sugar appended squaraine derivative, **SSqβGl** showed exciton coupled signal in CD spectra at higher concentration (Figure 2.19) and the wavelength coincides with that of the H-aggregate. While the monosugar appended squaraine dye, **ASqβGl** was CD inactive in the aqueous solvent also. This observation indicated that the chiral ligand conjugation to the squaraine dye did not induce any chirality to the chromophore instead, the supramolecular orientation of the symmetrical bis-sugar appended squaraine scaffold in water induce chirality to the aggregate. The slipped plane to plane orientation of the dye resulted from π-π stacking, and hydrogen bonding between the adjacent molecules lead to the helical self-assembly. At lower concentrations where monomer molecules predominate in solution, no CD signal was observed. While increasing the concentration of the dye CD signal was appeared with positive Cotton effect. Temperature sensitivity of the helical self-assemblies was also studied. With an increase in temperature decrease in the helicity was observed

attributed to the cleavage of the aggregates (Figure 2.20), which is evident from the corresponding aggregation spectrum. Reversibility of the chirality was checked by sudden cooling of that solution. Helicity did not retain upon sudden cooling, but the complete helicity was retained only after 24 h of cooling followed by sonication (Figure 2.21).

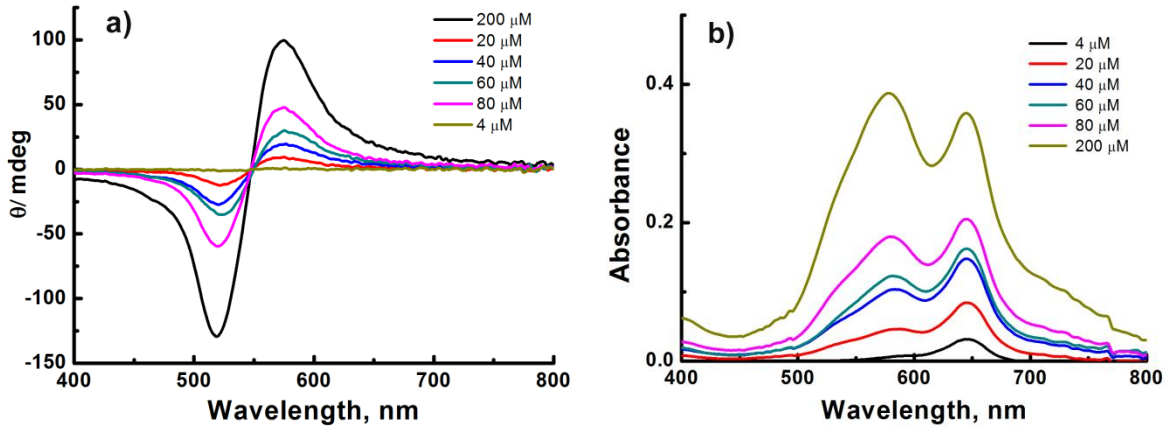

Figure 2.19. a) CD spectra and b) corresponding absorption of the dye **SSqβGl** recorded in water solvent with increasing concentration.

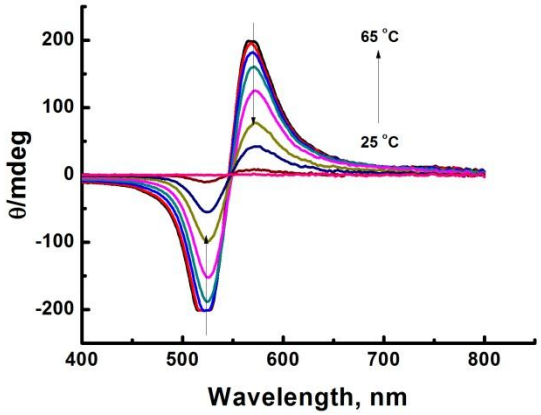

Figure 2.20. CD spectral changes with increase in temperature from 25 to 65 °C for **SSqβGl** in water ($2x10^{-4}$ M)

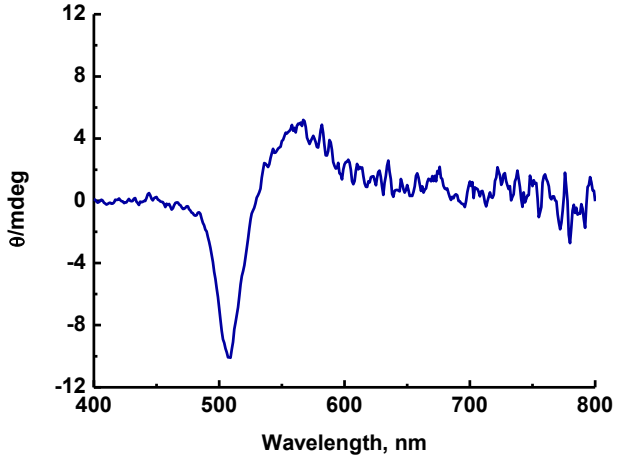

Figure 2.21. CD spectrum of the squaraine, **SSqβGl** solution ($2x10^{-4}$ M) after sudden cooling (after 35 min.)

2.3.4. Atomic force microscopic (AFM) studies of the dye aggregate

Morphological analysis was carried out using atomic force microscopy by drop casting the sonicated solution of **SSqβGl** on to freshly peeled mica sheets. AFM analysis of the symmetrical, bis-sugar appended squaraine dye **SSqβGl** ($2x10^{-4}$ M) showed the formation of fibrillar network (Figure 2.22). Helicity of the fibers was visible in the zoomed image. Clustered morphology was observed for aggregates derived from **ASqβGl** in water.

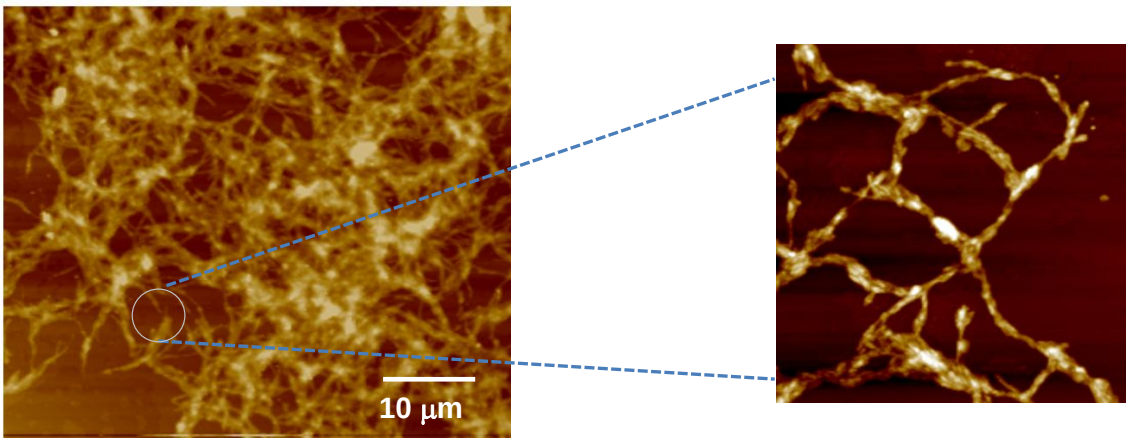

Figure 2.22. Tapping-mode AFM images of samples prepared by drop casting solutions of the dye **SSqβGl** ($2x10^{-4}$ M)

2.3.5. Fluorogenic response to β-glucosidase enzyme

Aggregation caused quenching of the squaraine dyes **SSqβGl** and **ASqβGl** in aqueous solution were confirmed from the aggregation studies. Finally, the potency of the squaraine dyes as a fluorogenic probe in the biological media was the monitored. To study this property, we have selected **SSqβGl** which has high water solubility. The enzyme β-glucosidase is a lysosomal lipid hydrolase, membrane-associated glycoprotein that facilitates the cleavage of the β-glycosidic linkage. β-Glucosidase plays vital role in the biological system and the mis-function of this enzyme lead to a number of diseases including Gaucher's disease.[34] In the case of squaraine dye, we anticipated the cleavage of reducing sugar from the squaraine skeleton in the presence of β-glucosidase enzyme. Change in the photophysical properties of the squaraine dye **SSqβGl** was monitored in the presence of the β-glucosidase enzyme. The addition of enzyme to the solution of the dye **SSqβGl** (10 μM) leads to the decrease in intensity of the absorption peak located in the blue region along with a concomitant increase in the intensity of the monomer band at 649 nm (Figure 2.23a). This observation indicates the cleavage of the H-aggregate formed in water associated with the cleavage of the glycosidic bond in the presence of β-glycosidase enzyme. The emission spectral changes in the presence of β-glucosidase enzyme were also monitored (Figure 2.23b), enhancement in the emission was observed upon addition of the enzyme by 10 μL. Additionally, it is interesting to notice the visible color change in the presence of β-glycosidase enzyme from violet to blue (Figure 2.23c).

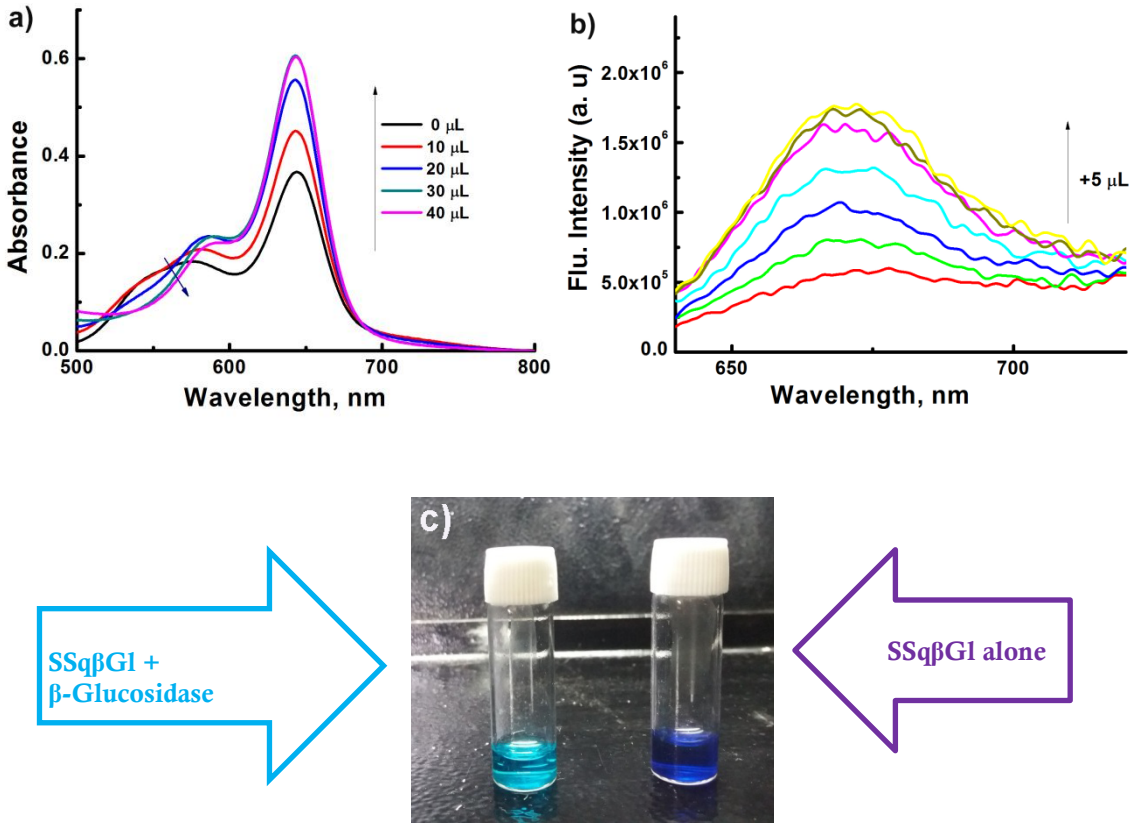

Figure 2.23. (a) Absorption spectral changes of the dye **SSqβGl** with addition of β-glucosidase enzyme in PBS solution. (b) Emission spectral changes with increase in concentration of β-glucosidase enzyme in **SSqβGl** solution in PBS and (c) Visible colour change from violet to blue upon addition of β-glucosidase enzyme.

2.4. Conclusion

We have designed and synthesized two novel carbohydrate appended squariane dyes-**SSqβGl** and **ASqβGl**. Squaraine dye, **SSqβGl** exhibited good solubility in water whereas **ASqβGl** showed moderate solubility. Both the squaraine dyes exhibited aggregation caused quenching in water while existed as monomers with intense emission in DMSO solution. **SSqβGl** prefers to orient in the plane to plane fashion to form H-aggregates while **ASqβGl** preferably formed J-aggregates in water. Additionally, bis-sugar appended squaraine dye **SSqβGl** formed helical supramolecular self-assemblies in water. Specifically, helical fibirillar morphology was observed in AFM images. Further, we have demonstrated the fluorogenic

sensing ability of the squaraine aggregates in PBS against a biologically relevant β-glucosidase enzyme. Visible as well as emission profile changes were displayed in the presence of β-glucosidase enzyme. These results support the utility of non-fluorescent aggregates as fluorogenic probes in aqueous solution to overcome the aggregation caused quenching that restricts the biological application of squaraine dyes.

2.5. Experimental section

2.5.1. Materials and methods

Chemicals used for the synthesis of squaraine dyes and their synthetic precursors were purchased from Sigma-Aldrich, Alfa Aesar, Merck and SDFCL and were used without further purification. ^{1}H and ^{13}C were recorded on Bruker 500 MHz spectrometer and tetramethylsilane (TMS) as the standard. IR spectra were recorded on Bruker FT-IR spectrometer. Mass spectra were recorded under EI/HRMS at 60,000 resolution using Thermo Scientific Exactive Mass Spectrometer and MALDI-TOF MS spectra were recorded using Shimadzu Axima CFR (Plus). Absorption spectra were measured on a Shimadzu UV-3101 PC NIR scanning spectrophotometer and emission recorded on SPEX Fluorolog F112X spectrofluorimeter. AFM images were recorded under ambient conditions using a NTEGRA (NT-MDT) operating with a tapping mode regime. Micro-fabricated TiN cantilever tips (NSG10) with a resonance frequency of 299 kHz and a spring constant of S8 20-80 Nm^{-1} was used. AFM section analysis was done offline. Temperature dependent studies were carried out with a thermostat directly attached to the wall of the cuvette holder. Fluorescence quantum yield (Φ_f) were measured by the relative method using squarylium III (Φ_f = 0.65 in dichloromethane) as standard.[35]

2.5.2 AFM sample preparation: Squaraine dye **SSqβGl** ($2x10^{-4}$ M) was dissolved in HPLC water and subjected to sonication. This sonicated solution was drop casted on freshly peeled mica sheets and the sample was dried under *vacuo* for 24 h.

2.5.3. Synthesis of *N*-(3-bromopropyl)-*N*-methylaniline (19): *N*-(3-bromopropyl)-*N*-methylaniline (**19**) was synthesized according to the conventional procedure. To a solution of *N*-methylaniline (5 g, 46.6 mmol) in dry DMF (20 mL), potassium carbonate (32 g, 233 mmol) was added and allowed to stir for 10 min. To this reaction mixture, 1,3-dibromopropane was added slowly and then reaction mixture was allowed to stir for 12 h at room temperature under argon atmosphere. After the completion of reaction, reaction mixture was filtered and compound was extracted with diethyl ether. Organic layer was washed with brine and solvent removed under reduced pressure. Residue was then subjected to column chromatography on silica gel, eluting with hexane to yield the title compound **19** as yellow liquid (5.3 g, 50 %). **^{1}H NMR** ($CDCl_3$, 500 MHz): δ 7.23 (t, *J* = 8.0 Hz, 2 H) 6.71 (m, 3 H), 3.48 (t, *J* = 7.0 Hz ,2 H,), 3.44 (t, *J* = 6.5 Hz, 2 H), 2.94 (s, 3 H), 2.150-2.09 (m, 2 H) ppm. **^{13}C NMR** ($CDCl_3$, 125 MHz): δ 149.2, 129.5, 127.2, 112.7, 50.9, 38.9, 31.9, 30.2 ppm. HRMS (ESI) *m/z* calcd for $C_{10}H_{15}BrN$: 228.0388; found: 228.04 $[M+H]^+$.

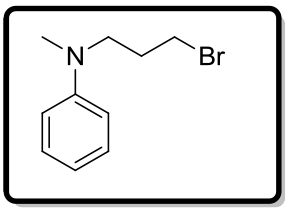

2.5.4. Synthesis of *N*-(3-azidopropyl)-*N*-methylaniline (20): Compound **19** (3 g, 23.3 mmol) and sodium azide (2.2 g, 35 mmol) was allowed to reflux in dry DMF for 8 h. Completion of reaction was monitored by thin layer chromatography (TLC). Reaction mixture was cooled to room temperature and diluted with diethyl ether (25 mL). Organic layer was washed with brine and dried over sodium sulphate. Solvent was evaporated under *vacuo*. Crude product obtained was subjected to silica gel column

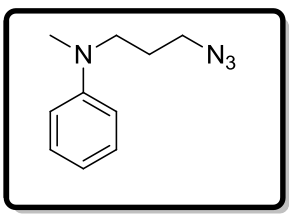

chromatography using hexane as eluent to afford the title compound **20** as yellow liquid (2 g, 80 %). **^{1}H NMR** ($CDCl_3$, 500 MHz): δ 7.20 (t, *J* = 7.0 Hz, 2 H,), 6.68 (bs, 3 H), 3.35 (d, *J* = 7.0 Hz, 2 H), 3.28 (t, *J* = 6.0 Hz, 2 H), 2.87 (s, 3 H), 1.79 (t, *J* = 6.5 Hz, 2 H) ppm. **^{13}C NMR** ($CDCl_3$, 125 MHz) δ 149.2, 129.4, 116.6, 112.4, 49.8. 49.2, 38.5, 26.3 ppm. HRMS (ESI) *m/z* calcd for $C_{10}H_{15}N_4$: 191.121; found: 191.129 $[M+H]^+$.

2.5.5. Synthesis of alkyne

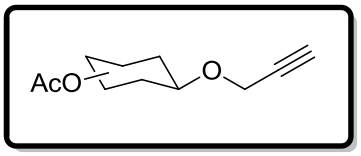

The alkyne derivative 2, 3, 4, 6-Tetra-O-acetyl-1-(2′-propargyl)- β-D-glucose was obtained by following the reported procedures.[36] Glucose was peracetylated in presence of sodium acetate and products formed were confirmed from HRMS analysis.

2.5.6. Synthesis of 1,2,3-triazole, βGlTZLOH (21): Propargylated glycoside (**17**), (2.5g, 0.011 mol) and azide (2.24g, 0.011 mol) were dissolved in acetonitrile. Copper iodide (2.37g, 0.165 mol) was added to this solution followed by the addition of *N*,*N*-diisopropylamine (5.74 mL, 0.33 mol) and the reaction mixture was allowed to stir for 2 h at room temperature. After the completion of reaction, reaction mixture was diluted with water and ammonium chloride. Extracted with ethyl acetate and the combined organic layer was washed with brine solution, dried over sodium sulphate. Solvent removed under reduced pressure and the residue obtained was directly used for next reaction. Crude product was dissolved in methanol and allowed to stir in presence of sodium carbonate (6.24 g, 0.058 mol) for 2 h at room temperature. After monitoring the

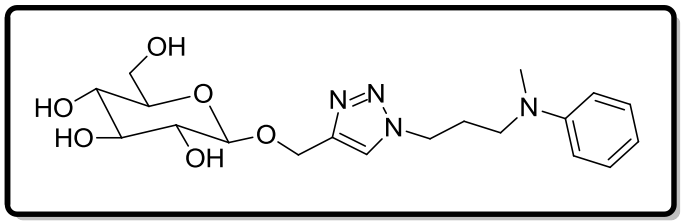

completion of reaction with TLC, reaction mixture was filtered and solvent removed under reduced pressure. Residue obtained was purified by silica gel column chromatography using $CHCl_3$/MeOH (9:1) solvent system to afford corresponding 1,2,3- triazole derivative (**21**) as yellow coloured highly viscous liquid in 56 % yield (2.6 g). **^{1}H NMR** (CD_3CN, 500 MHz): δ 7.82 (s, 1 H), 7.19-7.16 (m, 2 H), 6.67-6.64 (m, 3 H), 4.91 (d, *J* = 12.5 Hz, 1 H), 4.43 (d, *J* = 8.9 Hz, 1 H), 4.35 (t, *J* = 7.0 Hz, 2 H), 3.82 (d, *J* = 11.5Hz, 1 H), 3.68-3.66 (m, 1 H), 3.44-3.40 (m, 1 H), 3.36-3.3 (m, 2 H), 3.25 (t, *J* = 8.0 Hz,1 H), 2.85 (s, 3 H), 2.10 (t, *J* = 7.5 Hz, 2 H) ppm. **^{13}C NMR** (CD_3CN, 125 MHz): δ 154.5, 149.2, 134.5, 129.4, 122.8, 121.6, 117.7, 107.3, 101.3, 83.3, 81.8, 78.8, 75.4, 67.2, 66.8, 54.5, 53.3, 43.2, 32.4 ppm. HRMS (ESI) m/z calcd for $C_{19}H_{28}N_4O_6Na$: 431.1907; found: 431.1916 $[M+Na]^+$.

2.5.7. Synthesis of 3-(4-(dimethylamino)phenyl)-4-hydroxycyclobut-3-ene-1,2-dione (23): Compound **23** was synthesised according to the traditional procedure. 3,4-Dichlorocyclobutene-1,2-dione (1.5 g, 9.9 mmol), and N,N-dimethylaniline (1.2 g, 9.7 mmol), were dissolved in dry benzene (30 mL) and refluxed for 8 h. After cooling, the reaction mixture was poured into ice water (200 mL) and the two layers formed were separated. The organic layer was washed with water, and the crude product obtained was dissolved in a mixture of acetic acid (25 mL), water (25 mL) and 2N HCl was added (10 mL). The resulting mixture was then refluxed for 4 h at 120 °C. After cooling, this solution was added to crushed ice, the precipitated product was isolated by filtration, washed with diethylether, and dried to yield 2.0 g (50 %) of the pure product as a brown coloured powder. **^{1}H NMR (**500 MHz, DMSO-d_6): δ 7.86 (d, *J* = 9 Hz, 2H,), 6.88 (d, *J* = 9 Hz, 2H,), 3.03 (s, 6H) ppm.

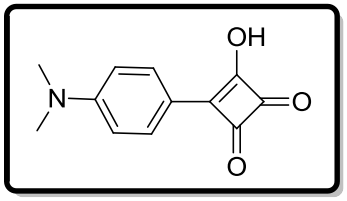

2.5.8. Synthesis of SSqβGl:

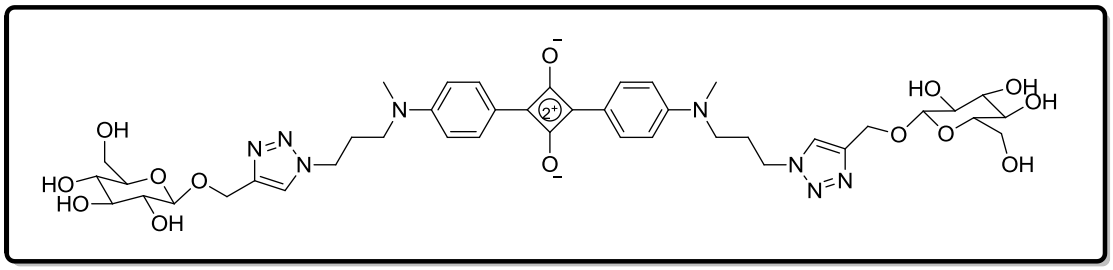

Symmetrical squaraine **SSqβGl** was synthesized by refluxing **βGlTZLOH**-(**21**) (500 mg, 1.22 mmol) and 3,4-dihydroxycyclobutene-1,2-dione (**22**) (70 mg, 0.6 mmol) in *n*-butanol/benzene (2:1) solvent mixture at 110 °C for 20 h accompanied by azeotropic removal of water using Dean Stark trap. After completion of the reaction, solvent was removed under reduced pressure. Residue obtained was purified by repeated precipitation from MeOH/EtOAc (1:9) solvent mixture and finally from methanol. The desired product was obtained as dark blue solid (160 mg, 15 %) m p:165-170 °C (decomposing). **^{1}H NMR** (DMSO-d_6, 500 MHz): δ 8.18 (s, 2 H), 8.14 (d, J = 8.5 Hz, 4 H), 6.96 (d, J = 9.0 Hz, 4 H), 5.04-5.03 (m, 2 H), 4.94-4.91 (m, 4 H), 4.75 (d, J = 12.5 Hz, 4 H), 4.57 (bs, 2 H), 4.46 (t, J = 7.0 Hz, 2 H), 4.26 (d, J = 7.5Hz, 2 H), 3.72-3.69 (m, 2 H), 3.61 (m, 4 H), 3.47-3.44 (m, 2 H), 3.15 (s, 6 H), 3.13-3.12 (m, 3 H), 3.07-3.06 (m, 2 H), 2.99-2.98 (m, 2 H), 2.17 (t, J = 6.5Hz, 2H) ppm. **^{13}C NMR** (DMSO-d_6, 125 MHz): δ 181.6, 154.0, 143.9, 131.7, 124.2, 118.8, 113.1, 102.1, 99.5, 76.9, 73.4, 61.5, 61.2, 46.9, 39.7, 39.6, 27.4 ppm; MALDI-TOF calculated for $C_{42}H_{54}N_8O_{14}$ 894.3770 found 894.00 $[M]^+$.

2.5.9. Synthesis of unsymmetrical squaraine, ASqβGl: Unsymmetrical squaraines were synthesised by the condensation of 3-(4-(dimethylamino)phenyl)-4-hydroxycyclobut-3-ene-1,2-dione (1 equiv.) and corresponding triazole substrate (1 equiv.) in 1-butanol/benzene (1:2) solvent mixture at 110 °C for 8 h. Where 3-(4-

(dimethylamino)phenyl)-4-hydroxycyclobut-3-ene-1,2-dione was

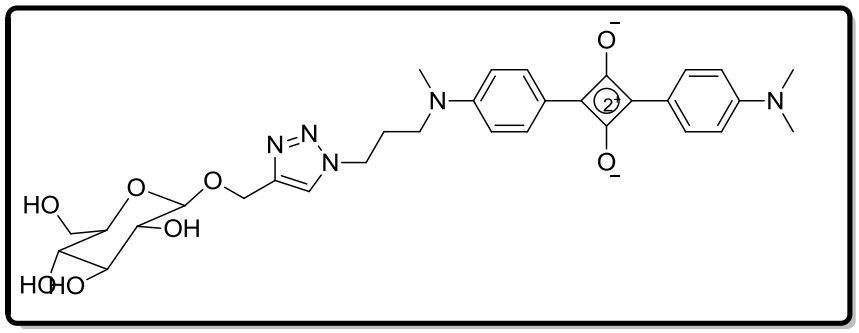

obtained from the conventional synthetic procedure.[4] After monitoring completion of the reaction using TLC, solvent was removed under reduced pressure. The residue obtained was purified by repeated precipitation from EtOAc/MeOH solvent mixture and finally from methanol solvent to yield the unsymmetrical squaraines as blue solid.(132 mg, 18 %) m p: 238-242 °C. **^{1}H NMR** (DMSO-d_6, 500 MHz): δ 8.81 (s, 1 H), 8.14 (t, *J* = 13.0 Hz, 4 H), 6.96 (t, *J* = 9.0 Hz, 4 H), 5.03-4.92 (m, 2 H), 4.26 (d, *J* = 8.0 Hz, 1 H), 4.85 (d, *J* = 12.5 Hz, 1 H), 4.66 (d, *J* = 12.0 Hz, 1 H), 4.45 (t, *J* = 7.0 Hz, 2 H), 4.26 (d, *J* = 8.0 Hz, 1 H), 3.65 (d, *J* = 11.5 Hz, 1 H), 3.60 (t, *J* = 7.0 Hz, 2 H), 3.47-3.44 (m, 1 H), 3.20 (s, 6 H), 3.14 (s, 3 H), 3.12 (bs, 2 H), 3.07-3.03 (m, 1 H), 2.99 (t, *J* = 8.0 Hz, 1 H), 2.17 (t, *J* = 7.0 Hz, 2 H). **^{13}C NMR** (DMSO-d_6, 125 MHz): δ 187.0, 182.2, 155.6, 144.4, 132.2, 132.0, 124.7, 119.4, 119.2, 113.7, 102.6, 77.5, 77.2, 73.9, 70.6, 62.0, 61.7, 49.7, 47.5, 40.8, 39.2, 27.9 ppm. HRMS (ESI): *m/z* calcd for $C_{31}H_{37}N_5O_8Na$: 630.2551; found: 630.2556 $[M+Na]^+$.

2.6. References

1. (a) H. J. Snaith, *Adv. Funct. Mater*. **2010**, *20*, 13-19.; (b) T. Geiger, S. Kuster, J.-H. Yum, S.-J. Moon, M. K. Nazeeruddin, M. Grätzel, F. Nüesch, *Adv. Funct. Mater.* **2009**, *19*, 2720-2727.
2. (a) C. W. Dirk, W. C. Herndon, F. Cervantes-Lee, H. Selnau, S. Martinez, P.Kalamegham, A. Tan, G. Campos, Velez, M. *J. Am. Chem. Soc.* **1995**, *117*, 2214-2225.; (b) H.-Y. Ahn, S. Yao, X. Wang, and K. D. Belfield, *ACS Appl. Mater. Interfaces* **2012,** *4*, 2847–2854.
3. K. T. Kamtekar, A. P. Monkman, and M. R. Bryce, *Adv. Mater.* **2010,** *22,* 572-582.
4. (a) J. J. Gassensmith, E. Arunkumar, L. Barr, J. M. Baumes, K. M. DiVittorio, J. R. Johnson B. C. Noll,and B. D. Smith, *J. Am. Chem. Soc.* **2007**, *129*, 15054-15059.; (b) J. M. Baumes, J. J. Gassensmith, J. Giblin, , J.-J. Lee, A. G. White, W. J. Culligan, W. M. Leevy, M. Kuno, and B. D. Smith, *Nat. Chem.* **2010**, *2*, 1025-1030.
5. Z. Yan, S. Guang, X. Su, and H. Xu, *J. Phys. Chem. C.* **2012***, 116*, 8894-8900.
6. K. D. Volkova, V. B. Kovalska, M. Y. Losytskyy, L. V. Reis, , P. F. Santos, P. Almeida, D. E. Lynch, S. M. Yarmoluk, *Dye. Pigm.* **2011**, *90*, 41-47.
7. (a) R. R. Avirah, D. T. Jayaram, N. Adarsh, D. Ramaiah, *Org. Biomol. Chem.* **2012**, *10*, 911-920.; (b) L. Beverina, M. Crippa, M. Landenna, R. Ruffo, P. Salice, F. Silvestri, S. Versari, A. Villa, L. Ciaffoni, E. Collini, C. Ferrante, S. Bradamante, C. M. Mari, R. Bozio, G. a. Pagani, *J. Am. Chem. Soc.* **2008**, *130*, 1894-1902.
8. V. S. Jisha, K. T. Arun, M. Hariharan, D. Ramaiah, *J. Am. Chem. Soc.* **2006**,*128*, 6024-6025.

9. (a) R. J. Stokes, A. Ingram, J. Gallagher, D. R. Armstrong, W. E. Smith, D. Graham, *Chem. Commun.* **2008**, 567-569.; (b) A. Ramya, A. Samanta, N. Nisha, Y.-T. Chang, K. K. Maiti, *Nanomedicine* **2015**, *10*, 561-571.; (c) N. Narayanan, V. Karunakaran, W. Paul, K. Venugopal, K. Sujathan, K. Kumar Maiti, *Biosens. Bioelectronics* **2015**, *70*, 145-152.
10. K. Y. Law, *Chem. Rev.* **1993**, *93*, 449-486.
11. S. Das, K. G. Thomas, M. V. George, P. V. Kamat, *J. Chem. Soc. Faraday Trans.* **1992**, *88*, 3419-3422.
12. (a) J. J. Gassensmith, J. M. Baumes, B. D. Smith, *Chem. Commun.* **2009**, *42*, 6329-6338.; (b) E. Arunkumar, C. C. Forbes, B. C. Noll, B. D. Smith, *J. Am. Chem. Soc.* **2005**, *127*, 3288-3289.; (c) S.-Y. Hsueh, C.-C. Lai, Y.-H. Liu, Y. Wang, S.-M. Peng, S.-H. Chiu, *Org. Lett.* **2007**, *9*, 4523-4526.
13. F.-P. Gao, Y.-X. Lin, L.-L. Li, Y. Liu, U. Mayerhoffer, P. Spenst, J.-G. Su, J.-Y. Li, F. Würthner, H. Wang, *Biomaterials* **2014**, *35*, 1004-1014.
14. Z. Yan, H. Xu, S. Guang, X. Zhao, W. Fan, X. Y. Liu, *Adv. Funct. Mater.* **2012**, *22*, 345-352.
15. S. Hotchandani, S. Das, K. G. Thomas, M. V. George, P. V. Kamat, *Res. Chem. Intermed.* **1994**, *20*, 927-938.; (b) J. J. McEwen, K. J. Wallace, *Chem. Commun.* **2009**, 6339-6351.; (c) H. Chen, K.-Y. Law, J. Perlstein, D. G. Whitten, *J. Am. Chem. Soc.* **1995**, *117*, 7257-7258.; (d) H. Chen, K.-Y. Law, D. G. Whitten, *J. Phys. Chem.* **1996**, *100*, 5949-5955.; (e) U. Santhosh, S. Das, *J. Phys. Chem. A* **2000**, *104*, 1842-1847.
16. F. J. M. Hoeben, P. Jonkheijm, E. W. Meijer, A. P. H. J. Schenning, *Chem. Rev.* **2005**, *105*, 1491-1546.; A. Lohr, M. Lysetska, F. Würthner, *Angew. Chem. Int. Ed*. **2005**, *44*, 5071-5074.

17. U. Mayerhoeffer, F. Wuerthner, *Chem. Sci.* **2012**, *3*, 1215-1220.

18. S. Yagi, Y. Hyodo, M. Hirose, H. Nakazumi, Y. Sakurai, A. Ajayaghosh, *Org. Lett.* **2007**, *9*, 1999-2002.

19. A. Ajayaghosh, P. Chithra, R. Varghese, K. P. Divya, *Chem. Commun.s* **2008**, 969-971.

20. Z. Yan, S. Guang, H. Xu, X. Su, X. Ji, X. Liu, *RSC Adv*. **2013**, *3*, 8021-8027.

21. A. Lohr, M. Lysetska, F. Würthner, *Angew. Chem. Int. Ed*. **2005**, *44*, 5071-5074.

22. (a) E. Yashima, K. Maeda, O. Sato, *J. Am. Chem. Soc.* **2001**, *123*, 8159-8160.; (b) E. Yashima, K. Maeda, Y. Okamoto, *Nature* **1999**, *399*, 449-451.; (c) T.-F. Lin, R.-M. Ho, C.-H. Sung, C.-S. Hsu, *Chem. Mater.* **2008**, *20*, 1404-1409.; (d) A. Ohira, M. Kunitake, M. Fujiki, M. Naito, A. Saxena, *Chem. Mater.* **2004**, *16*, 3919-3923.

23. R. S. Stoll, N. Severin, J. P. Rabe, S. Hecht, *Adv. Mater.* **2006**, *18*, 1271-1275.

24. H. Chen, K.-Y. Law, D. G. Whitten, *J. Phys. Chem.***1996**, *100*, 5949-5955.

25. K. Jyothish, M. Hariharan, D. Ramaiah, *Chem. Eur. J.* **2007**, *13*, 5944-5951.

26. A. Ajayaghosh, P. Chithra, R. Varghese, *Angew. Chem. Int. Ed.* **2007**, *46*, 230-233.

27. S. Das, K. G. Thomas, R. Ramanathan, M. V. George, P. V. Kamat, *J. Phys. Chem.* **1993**, *97*, 13625-13628.

28. K. G. Thomas, K. J. Thomas, V. Madhavan, S. Das, D. Liu, P. V. Kamat, M. V. George, *J. Phys. Chem.* **1996**, *100*, 17310-17315.

29. S. Alex, M. C. Basheer, K. T. Arun, D. Ramaiah, S. Das, *J. Phys. Chem. A* **2007**, *111*, 3226-3230.

30. (a) V. D. Bock, D. Speijer, H. Hiemstra, J. H. Van Maarseveen, *Org. Biomol. Chem.* **2007**, *5*, 971-975.; (b) H. C. Kolb, K. B. Sharpless, *Drug Discovery Today* **2003**, *8*, 1128-1137.
31. (a) S. Das, K. G. Thomas, K. J. Thomas, P. V. Kamat, M. V. George, *J. Phys. Chem.* **1994**, *98*, 9291-9296.; (b) S. Das, T. L. Thanulingam, K. G. Thomas, P. V. Kamat, M. V. George, *J. Phys. Chem.* **1993**, *97*, 13620-13624.
32. (a) K. G. Thomas, K. J. Thomas, V. Madhavan, S. Das, D. Liu, P. V. Kamat, M. V. George, *J. Phys. Chem.* **1996**, *100*, 17310-17315.; (b) S. Alex, M. C. Basheer, K. T. Arun, D. Ramaiah, S. Das, *J. Phys. Chem. A* **2007**, *111*, 3226-3230
33. H. Chen, M. S. Farahat, K.-Y. Law, D. G. Whitten, *J. Am. Chem. Soc.* **1996**, *118*, 2584-2594.
34. (a) I. Bendikov-Bar, M. Horowitz, *Hum. Mutat.* **2012**, *33*, 1398-1407.;(b) A. H. Futerman, F. M. Platt, *Mol. Genet. Metab.* **2016**, *120*, 22-26.
35. K. Y. Law, *J. Phys. Chem.* **1987**, *91*, 5184-5193.
36. (a) Q. Zhang, J. Collins, A. Anastasaki, R. Wallis, D. A. Mitchell C. R. Becer, D. M. Haddleton, *Angew. Chem. Int. Ed.* **2013,** *52*, 4435-4439.; (b) J. Zhao, Y. Liu, H.-J. Park, J. M. Boggs, A. Basu, *Bioconjug. Chem.* **2012**, *23*, 1166-1173.

CHAPTER 3

Glycoconjugated squaraine dyes for selective tumor optical imaging

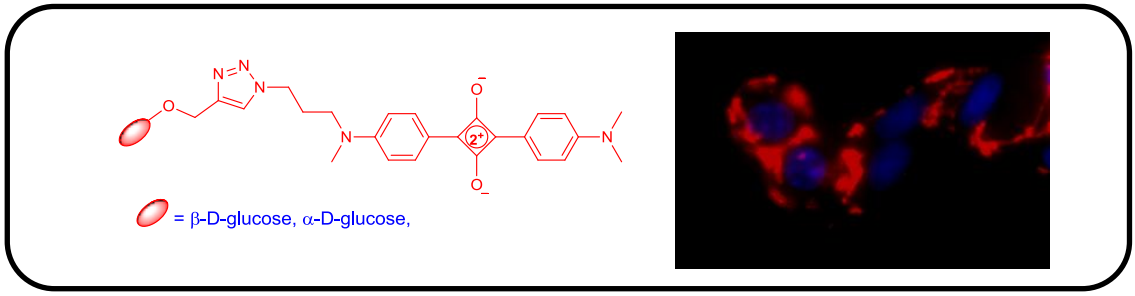

Abstract

Tumor is one of the life threatening diseases and second leading cause of death. The increased mortality rate reported for the cancer cases can be attributed to the failure of the early stage detection and diagnosis with the existing conventional tools. NIR-fluorescence imaging is a promising non-invasive tool for tumor detection which can provide better spatial and temporal resolution and allows cellular and molecular level monitoring with relatively high sensitivity. These factors lead to intense research in developing efficient target-specific fluorescent probes for imaging technology. An ideal fluorophore for specific and sensitive cancer detection requires a cancer cell targeting agent conjugated chemically or biologically to it. Warburg effect is one of the important features of tumor cells and has been widely explored as targeting element towards the design of therapeutic and diagnostic probes. Glycolytic enzymes and glucose transporters are overexpressed at the tumor cite to satisfy high energy demands and the glucose consumption rate will be high in tumor cells. This phenomenon is known as Warburg effect. Here we demonstrate the application of glycoconjugated squaraine dyes for selective tumor cell imaging.

3.1. Introduction

Cancer is one of the most threatening public health problems in the world around the globe with an estimated 8.8 million deaths reported in 2016 worldwide (World Health Organisation). The increased mortality rate is due to the failure of early detection and diagnosis of disease using the conventional clinical tools because of poor target specificity, sensitivity and image contrast.[1] Fluorescence imaging is a promising non-invasive tool for tumor detection which can provide better spatial and temporal resolution and allows cellular and molecular level monitoring with relatively high sensitivity.[2] Fluorescence detection in the optical window ranging from 650-900 nm (NIR region) offers several advantages over traditional methods such as decreased penetration, minimized photo damage to the biological samples, non-invasive nature and sensitivity.[3] In addition, optical imaging techniques are free from radioactive risks associated with the use of ionization radiation. Now a days, fluorescent labeled marker guided surgery has emerged as an excellent treatment modality.[4] All these factors led the way to rigorous research in imaging technology and there has been tremendous interest in the development of target-specific fluorescent probes.[5]

An ideal fluorophore for specific and sensitive cancer detection requires a cancer cell targeting agent conjugated chemically or biologically to it.[6] Targeting the Warburg effect, one of the important characteristic features of cancer cells has attracted great interest in recent years.[7] Otto Warburg first proposed the cancer cell metabolism that is different from normal cells.[8] Normal cells rely on mitochondrial oxidative phosphorylation for the energy production in the presence of O_2 (aerobic glycolysis) and the total energy production is 36 molecules of adenosine-5-triphosphate (ATP)/per glucose. In the absence of oxygen (anaerobic glycolysis),

normal cells direct the conversion of the glycolysis product to lactate without storing pyruvate in mitochondria. Energy production in the absence of oxygen is 2 molecules of ATP/glucose. Cancer cells do not keep an eye on whether oxygen is present or not; glycolysis will proceed through lactate production and only a few amount of pyruvate is stored in the mitochondria (5 %). Energy production is very less and rapidly growing cancer cells require more energy when compared to normal cells. To satisfy the high energy demand of cancer cells, more glucose is required and consequently, glycolytic enzymes and insulin-independent glucose transporters (GLUTs) are over expressed at the tumor site.[9] This phenomenon is known as Warburg effect. The rate of consumption of glucose, the primary source of energy, is significantly higher in cancer cells compared to normal cells and this phenomenon has been used to differentiate cancer cells from normal cells (Figure 3.1). This is possible by monitoring the glucose uptake in the cells specifically through the GLUTs.

Glucose transporters are the membrane proteins that facilitate the bidirectional and energy-independent process of glucose transport in most of the tissues and cells (Figure 3.2).[10] GLUT family constitute 13 members, GLUT 1-12 and HMIT. Each GLUT has distinct and regulatory functions that reflect their unique role in the cellular and whole body homeostasis.

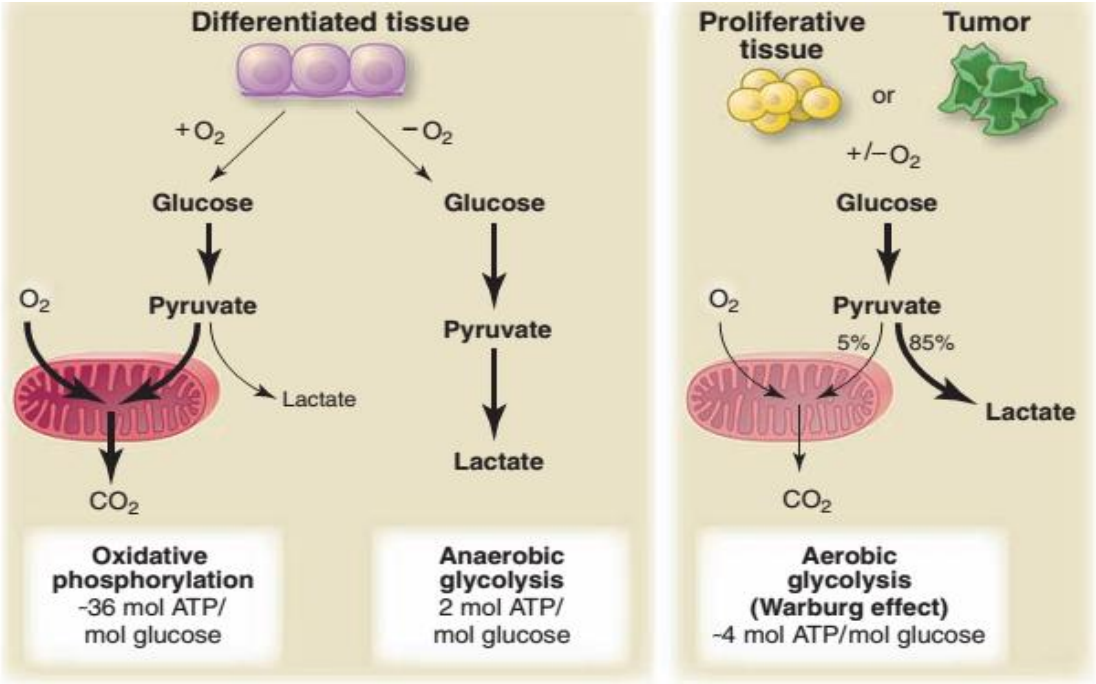

Figure 3.1. Schematic representation of aerobic and anaerobic glycolysis occurring in the normal cells as well as in cancer cells (Warburg effect).[9d]

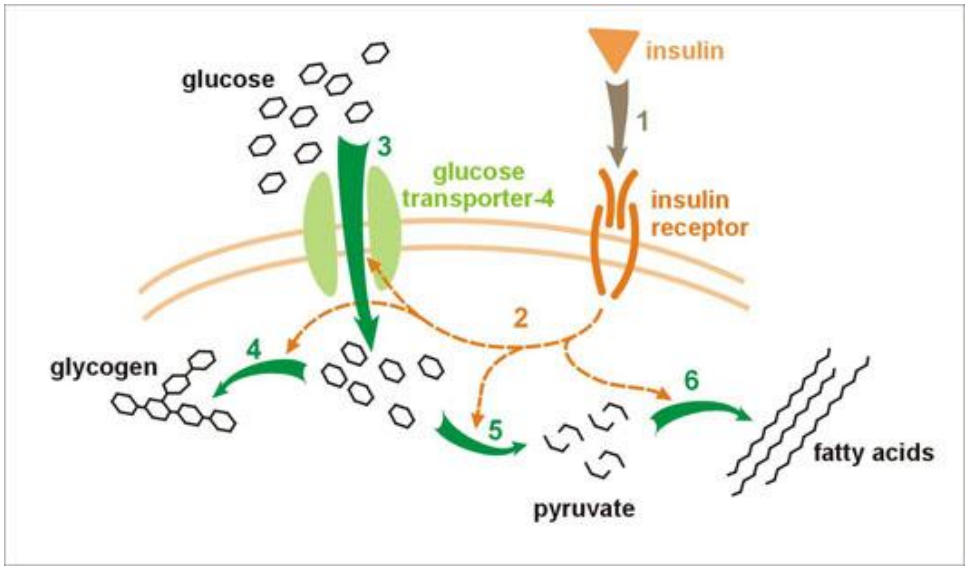

Figure 3.2. Graphical representation of the GLUT facilitated glucose uptake.

Radiolabeled glucose tracers, were widely used for monitoring glucose consumption prior to the development of fluorescent glucose analogues.[11] 18-F labeled 2-deoxy (FDG) glucose analogue has been widely used in the *in vivo* analysis of tumor diagnosis (Figure 3.3) with positron emission tomography (PET). The first

fluorescent glucose analogue introduced was 6-deoxy-*N*-(7-nitrobenz-2-oxa-1,3-diazol-4-yl)aminoglucose [6-NBDG] by Kutchai and co-workers.[12] A decade later, Matsuoka *et al*. introduced the C-2 analogue of NBDG (2-NBDG) and this has been widely used in various studies related to glucose monitoring.[13] Even though 2-NBDG has proven to be an excellent substrate of GLUTs, poor fluorescence and kinetic behaviour of NBDG analogues restricted its application in living cells. Since then, several glucose analogues labeled with various fluorophores have been developed to overcome these limitations.[3a,14]

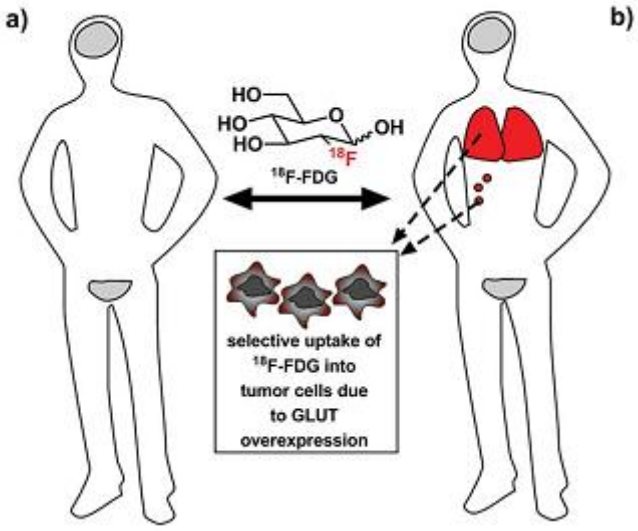

Figure 3.3. Positron emission tomography (PET) imaging using the radiolabeled glucose analogue,^{18}F-FDG. (a) In a healthy human being, ^{18}F-FDG will be concentrated in the brain and bladder (grey), the tissues that constitutively consume glucose, (b) In the patient, the tumor cells have preferentially taken up ^{18}F-FDG (red).[7]

A fluorescent glucose probe generally contains three parts, a fluorophore, the linker and a sugar unit. The linkers connecting the glucose and fluorophore will influence the uptake efficiency of the probe and has been a subject of study.[15] Generally stable, biocompatible polar linkers like triazole, amide and ester are

favoured for the biomolecule designing. Sometimes the linkers help to reduce the cytotoxicity of the fluorophore. NIR- emitting fluorophores are preferred for imaging applications owing to their advantages.[3a,16] Intensive research has been going on in this area of NIR fluorescent materials and labeling of biomolecules with these fluorescent materials. Despite of these great advances, lot of challenges still exist in the path of development of NIR fluorescent probes for biological imaging. Only few NIR- emitting fluorophores are FDA approved in this regard. The NIR emitting glucose analogues reported (Figure 3.4) include Pyro-2DG,[17] Cy 5.5-2DG,[18] IR dye 800 CW-2DG,[19] CyNE-2DG,[20] Cy3-α-gl and Cy3-β-gl.[21] Most of the dyes currently used for labeling of the glucose analogues contain one or more charges in their structure that will inversely affect their application in cell imaging. In addition, the difficulty in synthetic modification and water solubility are some of the problems encountered in the designing of NIR- emitting fluorophores. The glycosylation site on glucose plays a key role in the glucose uptake activity. Difference in the internalization efficiency was reported for α & β analogues of glucose.[21] Conjugation site of the fluorophore on glucose has great impact in the internalization mechanism. As soon as the glucose analogue enters the cell, it will undergo the glycolysis pathway. First step of glycosylation is the phosphorylation of glucose at the C-6 position by the enzymes, hexokinase/fructokinase. Therefore the phosphorylation site (C-6) and the hydroxyls at C-3 and C-4 on the glucose unit have critical roles in enzyme binding and should be left free for the effective binding with GLUTs.[19] Most of the glucose analogues developed were *N-2* amino derivatives, recently Park *et al.* introduced the *O-1* derivatives of glucose and are proven to be better candidates for imaging studies.[21] Some of the glucose analogues function as photodynamic therapeutic agents.[15]

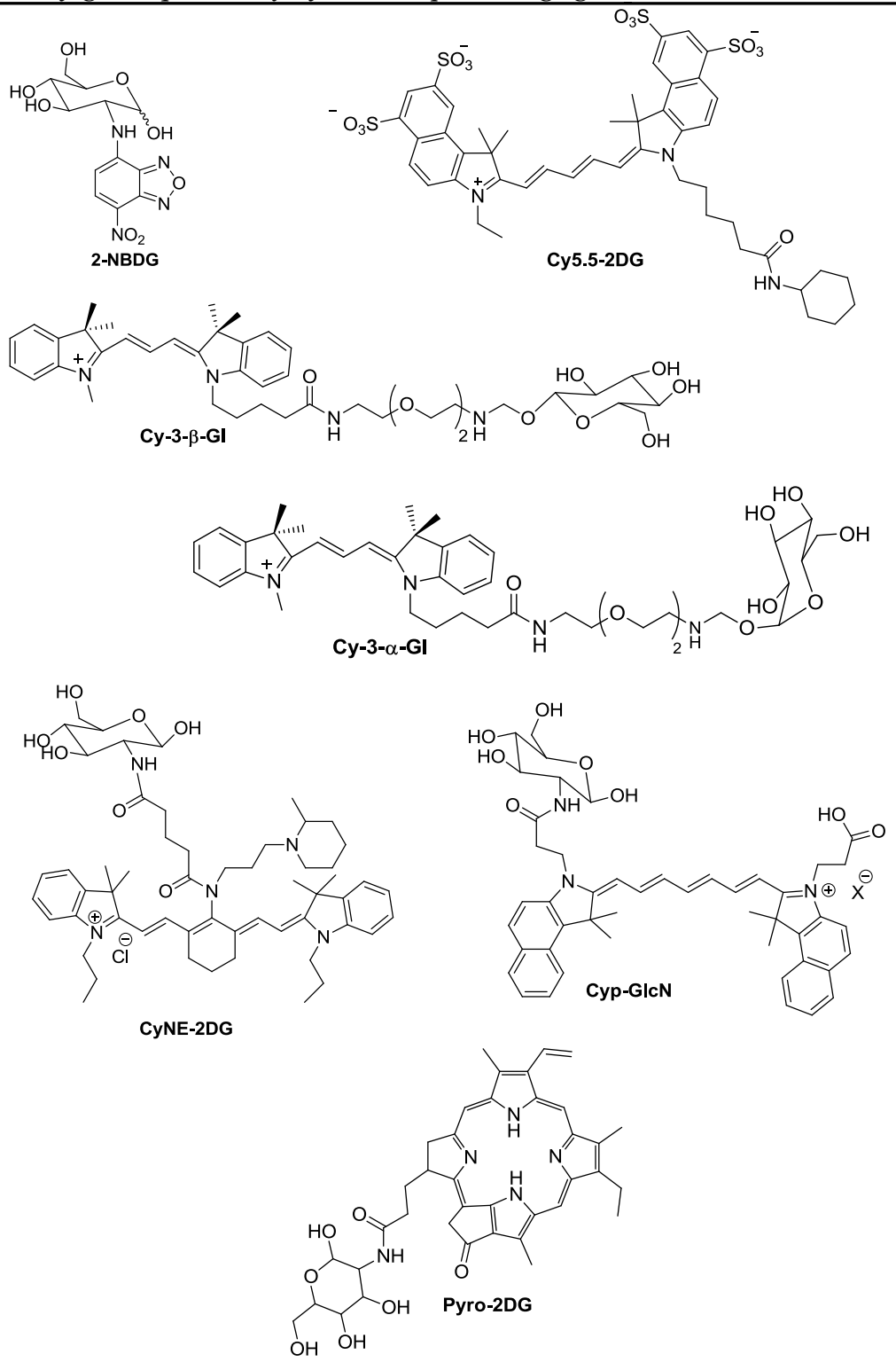

Figure 3.4. Molecular structure of fluorescent glucose anlaogues developed so far.

Squaraines are an important class of organic dyes with versatile applications due to their unique photophysical properties. Squaraines possess sharp and narrow absorption and emission in the NIR region. The ease of structural modification offers wide scope for squaraine dyes in the optical imaging field. However, the

photostability and aggregation of the squaraine dyes retards them in bioimaging applications. Enormous efforts have been put forward to overcome the aggregation. Supramolecular encapsulation, supramolecular squaraine adducts and squaraine rotaxanes are some of the successful attempts among them. The efforts in the direction to overcome this aggregation behaviour was discussed in detail in Chapter 2.

Recently, Würthner and co-workers demonstrated imaging and *in vivo* photothermal therapy of tumor cells with highly stable and biocompatible adducts of squaraine (**1**), with bovine serum albumin (BSA).[22] The squaraine dye (**1**) formed supramolecular adduct with natural carrier protein-BSA through hydrophobic and hydrogen bonding interactions and this adduct formation resulted in 80-fold enhancement of fluorescence in phosphate buffer solution. The targeting ligand, folic acid is covalently connected to the squaraine adduct. (Figure.3.5).

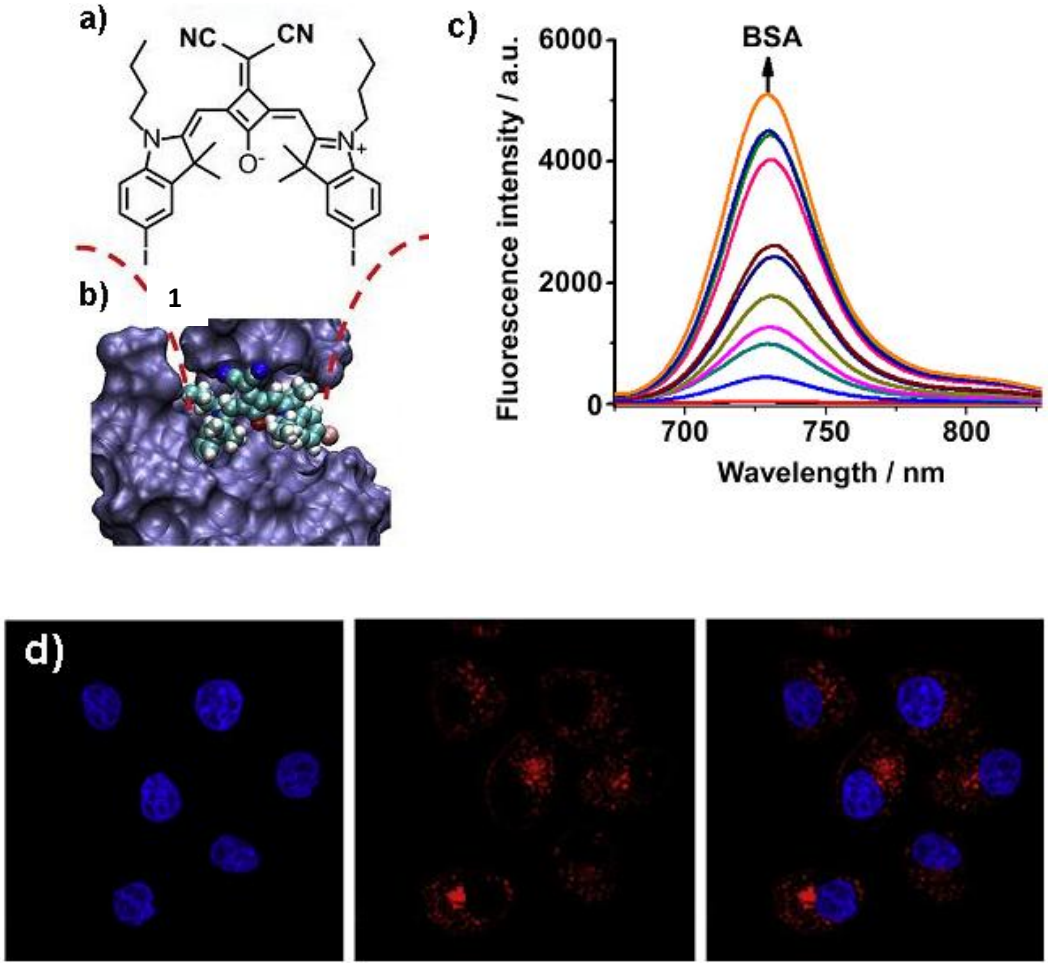

Figure 3.5. (a) Molecular structure of the squaraine dye, (b) schematic diagram of **1**-BSA adduct, (c) fluorescence enhacement upon addition of BSA and (d) the confocal fluorescence images of KB cells incorporated with squaraine-protein adduct.

3.2. Statement of the problem

Squaraine dyes are less explored in biological imaging due to their fluorescence quenching and unstability in biological media despite of their excellent photophysical properties. In the previous chapter, we have discussed the self assembly of glycoconjugated squaraine dyes in aqueous solution and their fluorogenic response with an analyte β-glycosidase enzyme. Herein we investigated the potency of glycoconjugated squaraine aggregates toward selective cancer cell optical imaging. Target specificity is achieved by exploring the "Warburg effect", one

of the characteristic feature of cancer cells. The simple glucose unit functions as the targeting ligand.

3.3. Results and discussion

3.3.1. Design strategy

The glycoconjugated squaraine chromophores, **ASqβGl** and **SSqβGl** (discussed in Chapter 2) synthesized were used as probes for the imaging studies in tumor cells. Glucose unit is attached to the squaraine dye through a biocompatible triazole linker through *O-1*, β-glycosidic bond. Glucose unit functions as targeting ligand as well as the hydrophillic group. Glucose unit together with triazole linker contributes to the increased water solubility and cell permeability of the probes. Synthetic strategy of the β-glucose analogues and the photophysical properties have been discussed in Chapter 2. Squaraine dye, **SSqβGl** was highly soluble and **ASqβGl** was moderately soluble in water. Both the squaraine dyes underwent aggregation in water which is associated with fluorescent quenching. For the detailed investigation of the mechanism of cellular uptake and imaging, we synthesized monosugar appended α-glucose (**ASqαGl**), α-galactose (**ASqαGa**), α-mannose (**ASqαM**) analogues of the squaraine dye. Molecular structure of the compounds used for imaging studies are listed below (Figure 3.6).

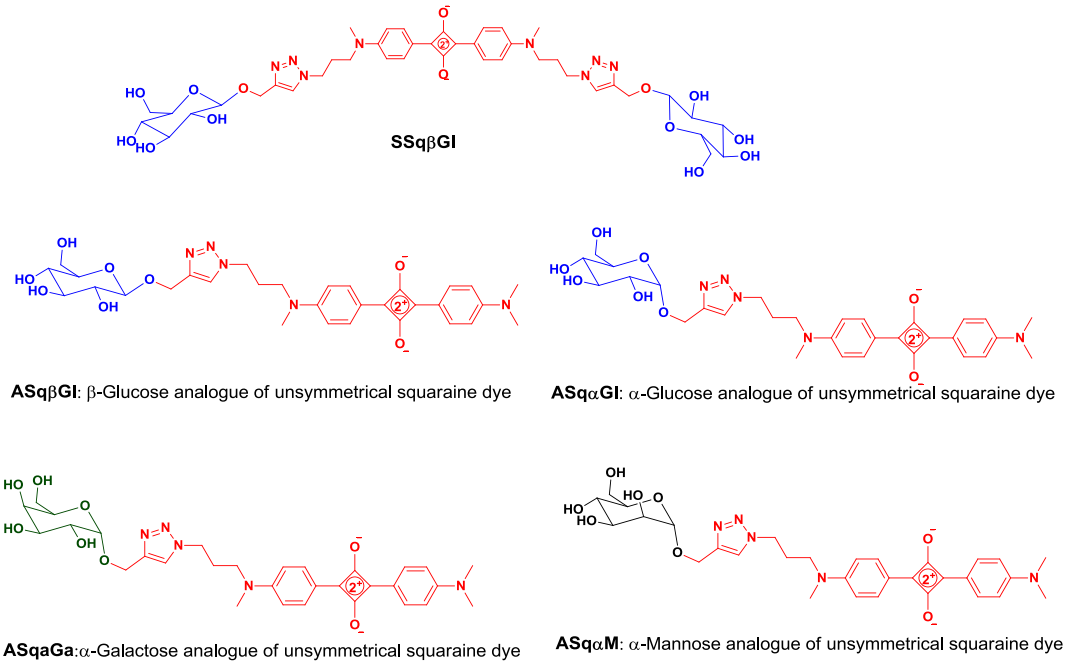

Figure 3.6. Molecular structure of the glycoconjugated squaraine dyes.

3.3.2. Synthesis

Synthetic strategy towards the target molecules **ASqαGl**, **ASqαGa**, **ASqαM** is described in Scheme 3.1, Scheme 3.2, Scheme 3.3, Scheme 3.4 and Scheme 3.5. In order to get α-glycoside selectively, we first treated the glucose unit with acidic ion exchange resin 50WX8-400 with excess amount of propargyl alcohol at 70 °C. The reaction afforded a mixture of both α and β-glycosides (**3**) in 2:1 ratio. Compound **3** was then subjected to protection with acetyl group using acetic anhydride in the presence of acetic acid affording the corresponding acetylated propargyl glycoside (**4**) (mix. of α & β isomers). Next, we synthesized the azide derivative (**7**) from *N*-methyl aniline (**5**). The propargyl glycoside (**4**) upon coupling with compound **7** in the presence of copper catalyst afforded the corresponding 1,4-disubstituted triazole in acylated form. This acylated triazole subjected to deprotection with sodium carbonate furnished the hydroxylated triazole and α-glycoside **8** was isolated

selectively. By following the same synthetic route, respective triazoles of mannose (**12**) and galactose (**13**) were also synthesized.

Condensation of the hydroxylated triazole of α-glycoside **8** with semisquaraine **11** yielded the squaraine dye **ASqαGl**. Semisquaraine (**11**) was prepared from squaryl chloride (**9**) and *N,N*-dimethylaniline (**10**) following the reported procedure.[23] By adapting the similar synthetic methodology, we synthesized other squaraine dyes **ASqαGl**, **ASqαGa**, **ASqαM**. All the starting materials and final products were characterised by using various spectroscpic techniques such as IR, ^{1}H, ^{13}C and MALDI-TOF analysis.

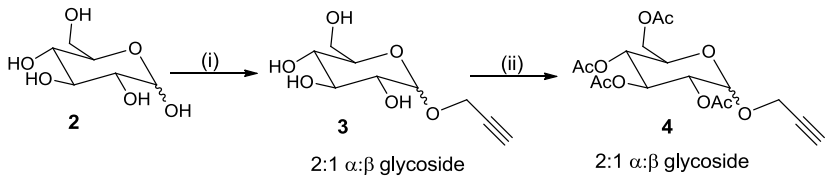

Scheme 3.1. (i) Dowex Resin, Propargyl alcohol, 70 °C, 64 %; (ii) Ac_2O, Sodium acetate, 120 °C, 83 %.

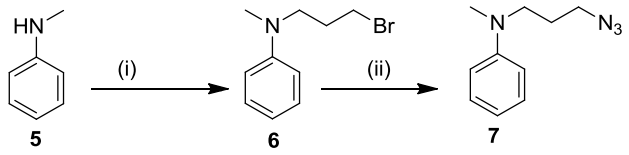

Scheme 3.2. (i) 1,3-dibromopropane, K_2CO_3, TBAB, DMF, 80 °C, 12 h, 54 %; (ii) NaN_3, DMF, 80 °C, 6 h, 82 %.

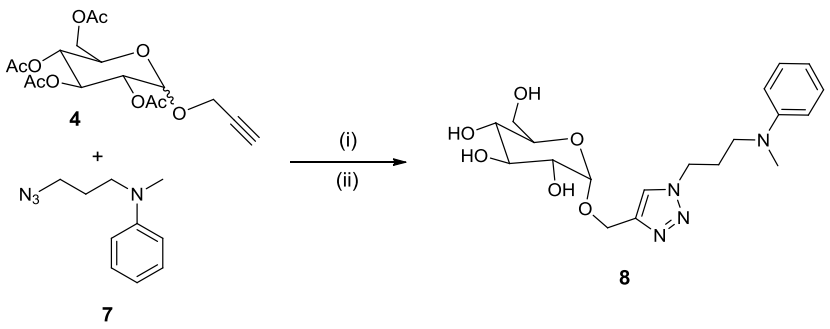

Scheme 3.3.(i) CuI, DIPEA, CH_3CN, 0 °C, rt, 2 h; (ii) Na_2CO_3, rt, 2 h, 55 %.

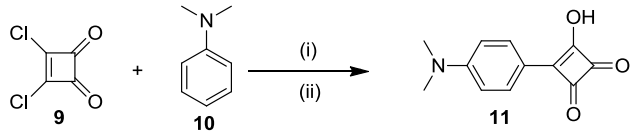

Scheme 3.4. (i) Benzene, reflux, 8 h; (ii) AcOH: H_2O (1:1), 2 N HCl, reflux, 4 h, 57 %.

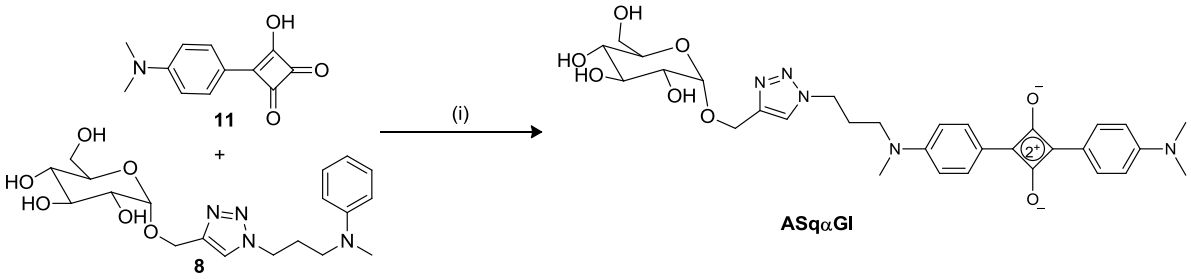

Scheme 3.5. (i) n-BuOH-Benzene (2:1), 110 °C, 8h, 17 %.

3.3.3. Photophysical properties

Photophysical properties of the newly synthesized squaraine dyes **ASqαGl**, **ASqαGa**, and **ASqαM** were measured in DMSO and water solvents and the results are summarized in Table 3.1. Absorption and emission characteristics of the squaraine dyes, **ASqαGl**, **ASqαGa**, **ASqαM** were similar to that of **ASqβGl** which we mentioned in Chapter 2.

Table 3.1. Photophysical characteristics of squaraine dyes **ASqαGl**, **ASqαGa** and **ASqαM**

Solvent	Abs. λ_{max} (nm)	Em. λ_{max} (nm)	Stokes shift (cm^{-1})	ε ($M^{-1}cm^{-1}$)	Φ_f (%)
ASqαGl					
DMSO	648	669	484.4	$1.8\pm0.1x10^5$	0.26
Water	642	667	583.8	-	0.01
ASqαGa					
DMSO	649	669	460.6	$1.7\pm0.2x10^5$	0.28
Water	642	667	583.8	-	0.03
ASqαM					
DMSO	648	668	462.0	$1.6\pm0.1x10^5$	0.25
Water	642	667	583.8	-	0.02

Fluorescence properties of the squaraine dyes, **ASqαGl**, **ASqαM**, **ASqαGa** in aqueous solution followed the same trend as that of **ASqβGl** (described in Chapter 2, Figure 3.7). Increase in concentration led to aggregate formation in aqueous solution that resulted in fluorescence quenching.

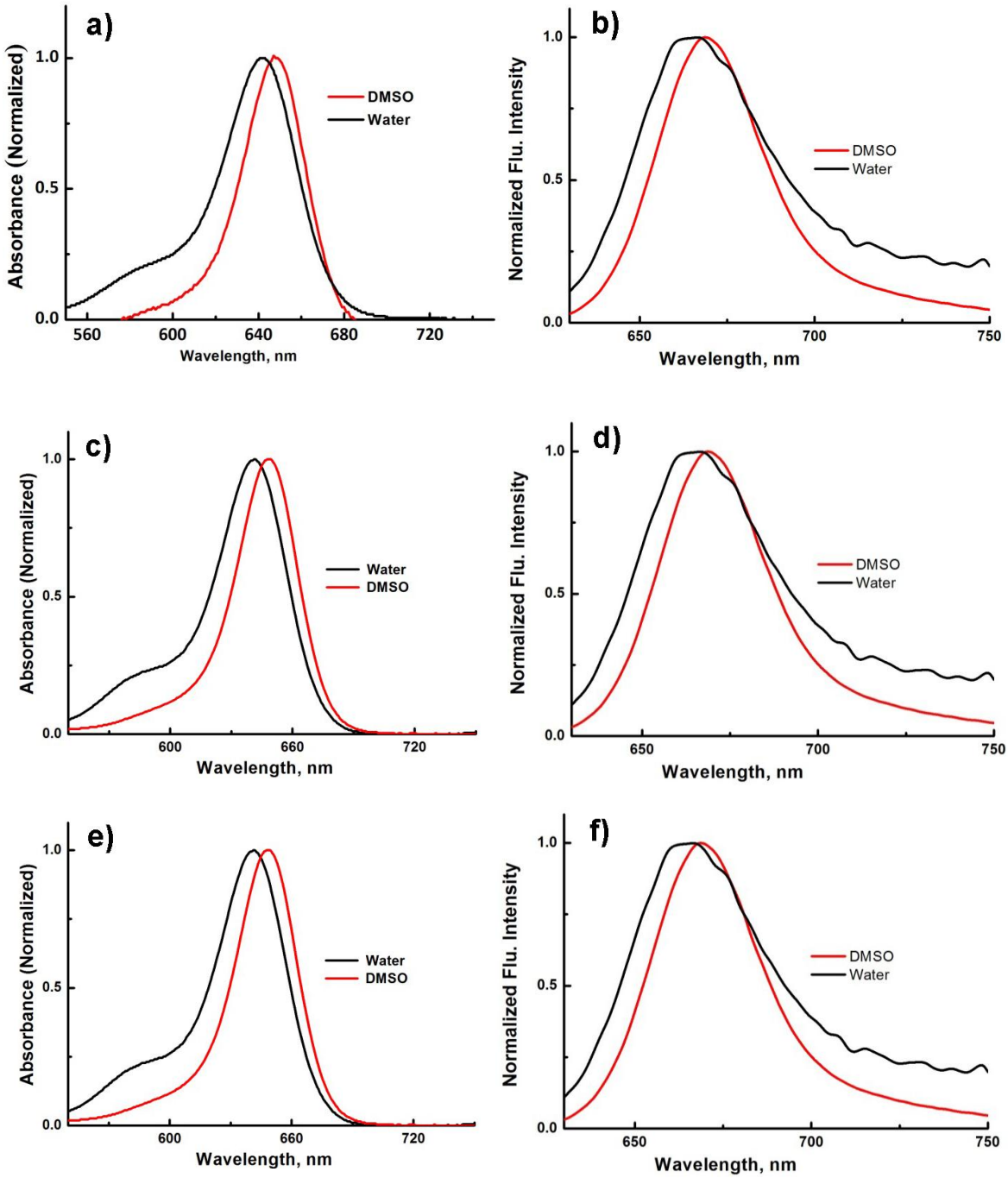

Figure 3.7. Normalized absorption spectra of (a) **ASqαGl** (b) **ASqαGa** (c) **ASqαM** and normalized emission spectra of (d) **ASqαGl** (e) **ASqαGa** (f) **ASqαM** in DMSO and water solvents.

3.3.4. pH Stability

For the fluorescent probes to be applied in biological media, they should be stable in the cellular environment. Stability of the squaraine dyes, **ASqαGl** and **ASqβGl** in phosphate buffer saline solution over a pH range of 4-8 have checked by monitoring the absorption and emission spectrum of the probe at varying pH levels. Optical properties of the squaraine dyes remain undisturbed with variation in fluorescence intensity that indicates the stability of the dyes over a pH range of 4-8 (Figure 3.8).

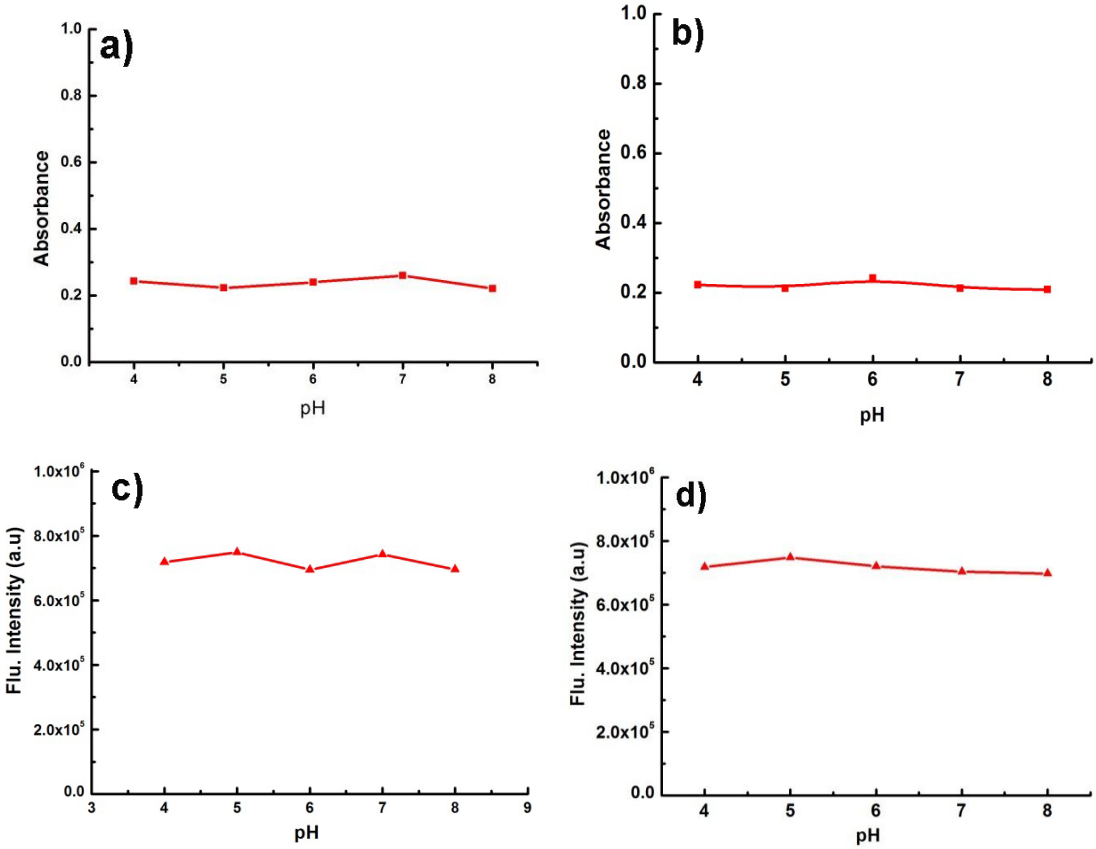

Figure 3.8. Changes in the absorption spectra with varying pH, (a) **ASqβGl** ($4.4x10^{-6}$ M) (b) **ASqαGl** ($4.4x10^{-6}$ M) and changes in the emission spectra with varying pH (c) **ASqβGl** [Emission max. 668 nm] and (d) **ASqαGl** [Emission max. 667 nm, λ_{ex} 630 nm.]

[Path length 10 mm. Absorbance monitored at 641 nm for ASqβGl and 642 nm for ASqαGl were plotted against pH].

3.3.5. Imaging studies

The potential of the synthesized squaraine dyes for tumor imaging was investigated in cervical cancer cell lines (HeLa), colon cancer cell lines (SW480) and normal (non-cancerous) cardiomyoblast cell lines (H9c2). For the applying these squaraine dyes in live cells, the cytotoxicity of the dyes was initially investigated.

3.3.5.1. Cytotoxicity assay

Cell viability after incubating the cells with different concentrations of squaraine dyes was determined by methyl thiazolyl tetrazolium (MTT) assay. It is a colorimetric assay based on the ability of live, but not dead cells to reduce MTT (yellow) to a purple formazan product. The cells were spread in 96-well plates at 10^4 cells/well. After 36 h of seeding, they were incubated with different concentrations of squaraine dyes individually for 24 h. Subsequently, the cells were exposed to MTT at a concentration of 50 µg/well for 2.5 to 3 h at 37 °C in CO_2 incubator. The working solution of MTT was prepared in Hanks balanced salt solution (HBSS). After viewing formazan crystals under the microscope, the crystals were solubilised by treating the cells with DMSO:isopropanol solvent mixture at a ratio of 1:1 for 20 min. at 37 °C. Plate was read at an absorbance of 570 nm. The relative cell viability in percent was calculated using the following equation and cell viability of control cells were kept as 100 %.

$$\text{Relative cell viability} = \frac{\text{Absorbance of treated}}{\text{Absorbance of control}} \times 100$$

From the *in vitro* cytotoxicity studies, it is found that all the squaraine dyes are non toxic up to 20 µM (Cell viability > 90 %, Figure 3.9).

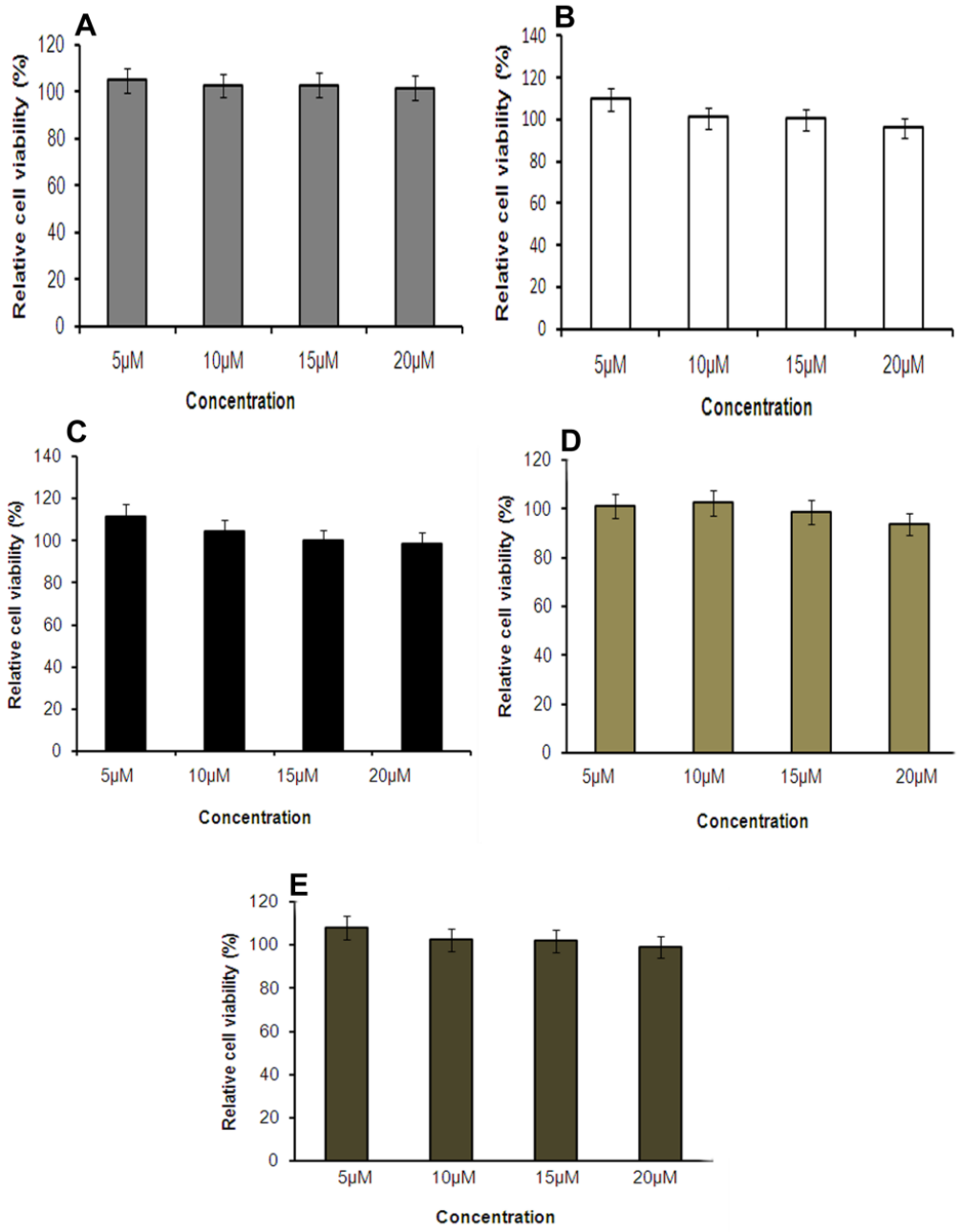

Figure 3.9. Relative cell viabilities of HeLa cells incubated with (**A**) **SSqβGl** (**B**) **ASqβGl** (**C**) **ASqαGl**, (**D**) **ASqαGa** and (**E**) **ASqαM** for a 24 h time period.

3.3.5.2. Cellular uptake studies of squaraine dyes by fluorescence imaging

Cellular uptake studies of squaraine dyes were executed by fluorescence imaging of adherent cells. The cells were seeded at a density of 10^4 cells/well of 96 well black plates *(BD Biosciences, USA)* for the purpose. After 36 h of seeding, the cells were incubated with different concentrations of squaraine dyes in serum deprived low glucose medium (5.5 mM glucose) for 30 min. Subsequently, the cells were washed twice with PBS solution. Nuclear staining was done by Hoechst. Images of the cells were collected by high-content spinning disk facility *(BD Pathway 855; BD Biosciences)* using *AttoVision 1.5.3 software.* For imaging cellular uptake of squaraine dyes, B635/20 excitation filter was used. Solution of the squaraine dye used for imaging studies contains 1% DMSO in PBS solution.

We commenced the internalization studies with two squaraine dyes, **SSqβGl** and **ASqβGl**, β-glucoside derivatives containing two and one glucose moieties respectively. Both **SSqβGl** and **ASqβGl** exhibited good cell permeability and internalization in the HeLa cell lines. Squaraine dyes generated red fluorescence inside the cells. Blue fluorescence indicates Hoescht staining of the nuclei. Figure 3.10 shows the merged images of red and blue fluorescence and they clearly indicate the localization of **SSqβGl** and **ASqβGl** inside the cancer cells. But the fluorescence intensities from the cells incubated with **SSqβGl** was significantly less when compared to **ASqβGl** (Figure 3.11).

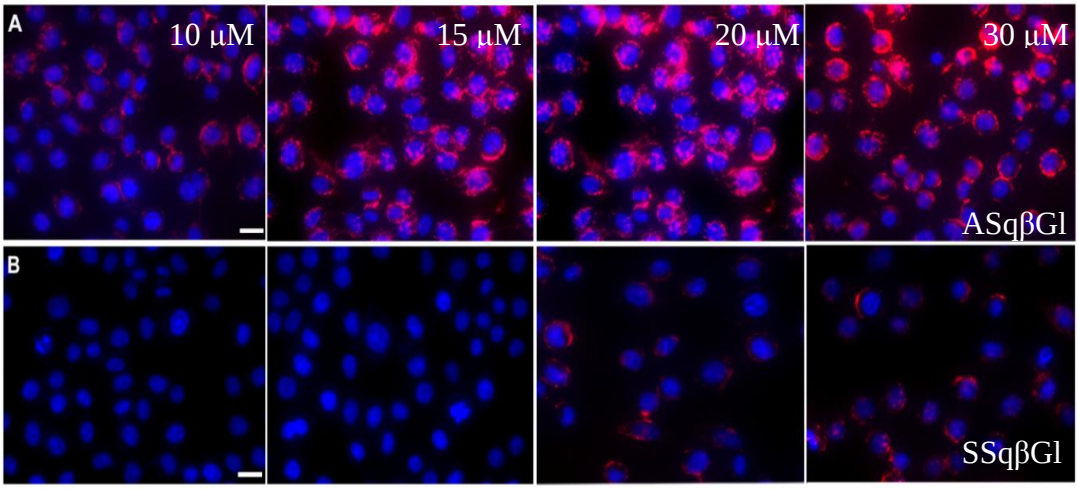

Figure 3.10. Fluorescence images of HeLa cells incubated with 10, 15, 20 & 30 µM concentrations of A) **ASqβGl** B) **SSqβGl**. Nuclear staining using Hoechst dye. (Incubation time: 30 min., Scale bar 20 µm).

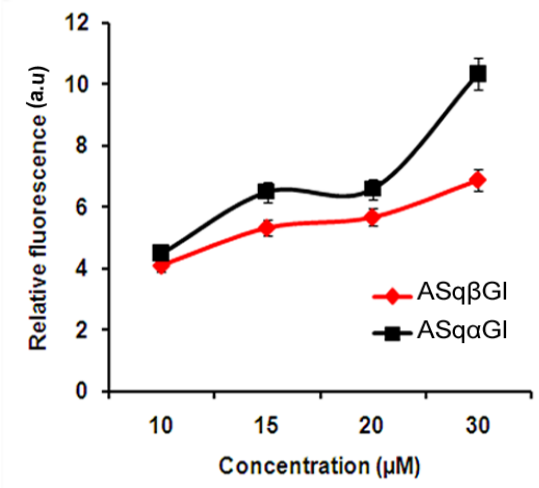

Figure 3.11. Chart representing the fluorescence intensity from the cells incubated with **ASqβGl** and **SSqβGl**. (Values represent mean ±SD).

Next step was to validate the internalization efficiency of other unsymmetrical squaraine dyes, **ASqαGl**, **ASqαGa** and **ASqαM** (Figure 3.12). All the squaraine dyes were internalized successfully, even though there exist difference in the fluorescence intensity from the cells incubated with different dyes. Comparing the fluorescence intensity from the cells incorporated with unsymmetrical squaraine

dyes, **ASqβGl**, **ASqαGl**, **ASqαGa** and **ASqαM**, internalization was interestingly high for α-glucoside derivative of the unsymmetrical squaraine dye, **ASqαGl** (Figure 3.12).

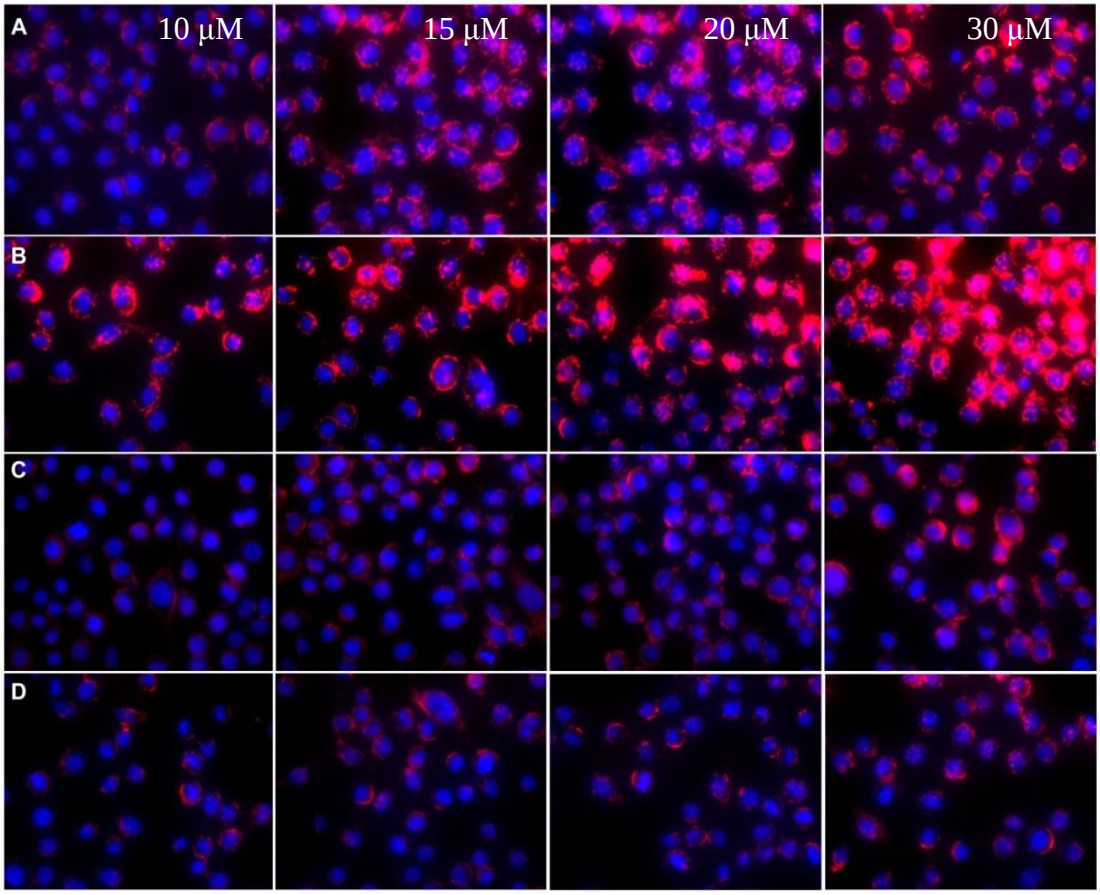

Figure 3.12. Cellular uptake of carbohydrate-appended squaraine dyes in HeLa cells demonstrated by fluorescence imaging of the cells after incorporating 10, 15, 20 & 30 μM concentrations of A. **ASqβGl** B. **ASqαGl** C. **ASqαGa** D. **ASqαM**. Nuclear staining using Hoechst dye. (Incubation time: 30 min., Scale bar: 20 μm).

3.3.5.3. Optimum concentration

To obtain the optimum concentration of **ASqαGl**, **ASqβGl** and **SSqβGl**, fluorescent images were collected after incorporation of the HeLa cells with different concentrations (5, 10, 20, 30 μM) of the dyes (Incubation time was 30 min.). Based on the fluorescent intensity of the images obtained from repeated trials, the minimum concentrations which yield clear images was chosen as the optimum concentration.

Accordingly, 20, 15 and 10 μM were the optimum concentration for **SSqβGl**, **ASqβGl** and **ASqαGl** respectively.

3.3.5.4. Competitive Assay

After the successful internalization of the squaraine dyes visualised by fluorescent microscopy, the mechanism of dye uptake in cancer cells and the role of GLUTs in the cellular uptake were investigated. For this, a competitive experiment was conducted by varying the glucose concentration in the extracellular medium [Dulbeccos Modified Eagle's Medium (DMEM) which is the cell growth and maintenance medium used]. GLUTs are a group of membrane proteins that facilitate the transport of glucose consistent with the gradient of glucose existing in the cellular environment. Direct competitive analysis with D-glucose was performed using a procedure reported earlier[24] to understand the cellular pathway of glucose analogue. The presence of excess amount of glucose in the extracellular medium generates a competition between glucose and the glucose analogue for cellular uptake. GLUTs allow the transport of glucose molecules which are exact substrates of GLUTs. This competition will cause a decrease in the glucose analogue uptake. A decrease in fluorescence intensity from the cells incorporated with **ASqβGl** and **ASqαGl** was observed upon increasing the concentration of D-glucose in the medium (Figure 3.13b and 3.13c). In contrast, no significant change in the fluorescence intensity was observed in the cells incorporated with **SSqβGl**, **ASqαGa**, **ASqαM** (Figure 3.13a, 3.13d and 3.13e) up to a glucose concentration of 50 mM. Variation in the fluorescence intensity observed in the case of cells incorporated with **ASqβGl** and **ASqαGl** could be ascribed to the inhibition of the respective dye uptake in competition with D-glucose. This

observation revealed the GLUT mediated internalization of squaraine-glucose analogues, **ASqβGl** and **ASqαGl**, thereby making them suitable candidates for tumor imaging.

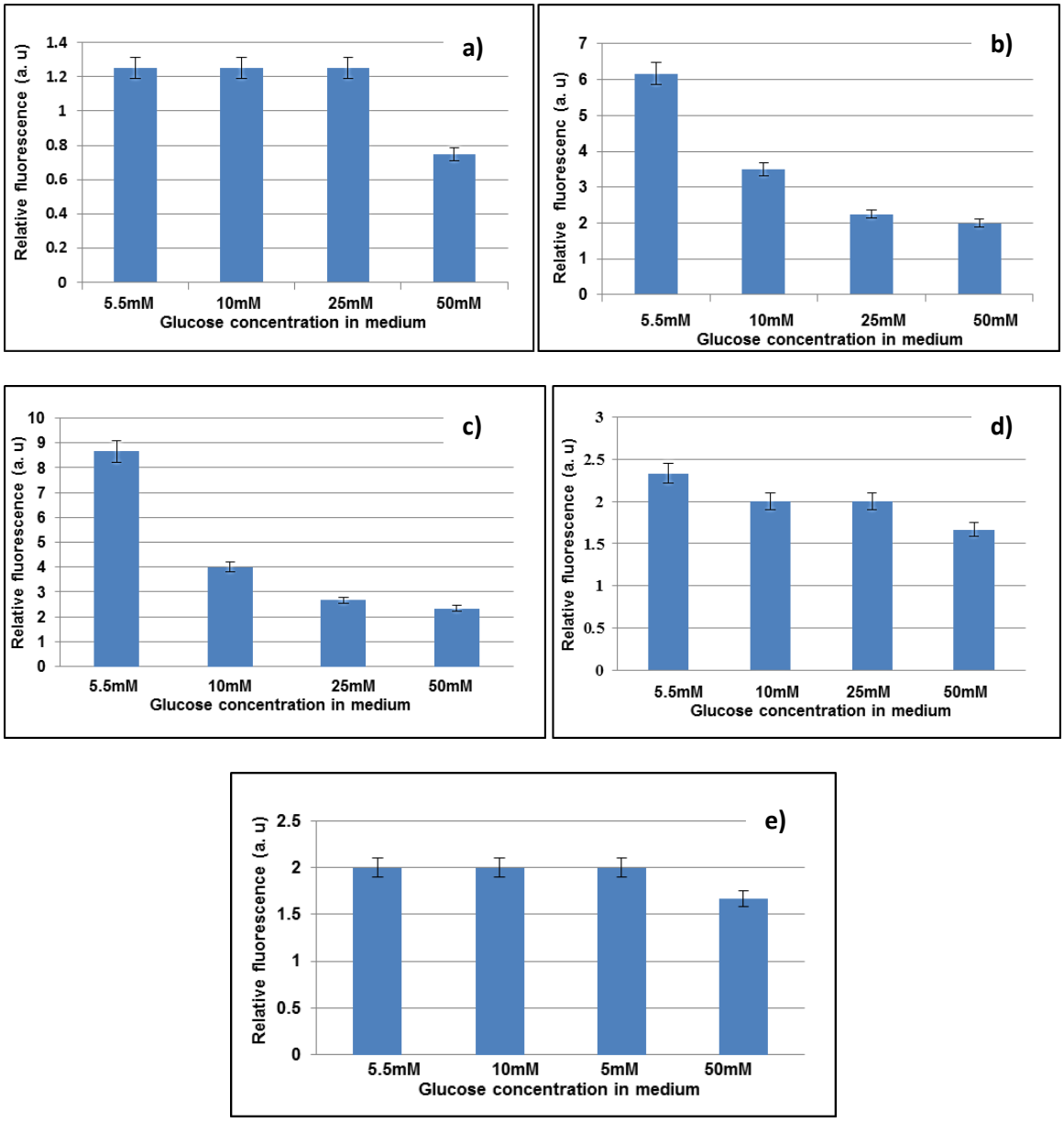

Figure 3.13. Inhibition of dye uptake in tumor cells with increasing glucose concentrations in the extracellular media: Statistical graph of competitive assay showing the mean relative fluorescence obtained from three independent trials (Values represent mean ± SD); (a) **SSqβGl**, (b) **ASqβGl** (c) **ASqαGl** (d) **ASqαGa** and (e) **ASqαM**.

Stereoselective recognition of substrates by GLUTs was further established by a competitive assay experiment with L-glucose. L-glucose is not a GLUT substrate; the changes in L-glucose concentration in the extracellular medium will not interfere with the dye internalization pathway of the glucose analogues and hence one cannot expect a variation in fluorescence intensity in a competitive assay. Competitive assay experiments of **ASqβGl** and **ASqαGl** (15 μM each) performed with L-glucose did not display any fluorescence intensity variation (Figure 3.14) and confirms the stereoselective uptake by GLUTs.

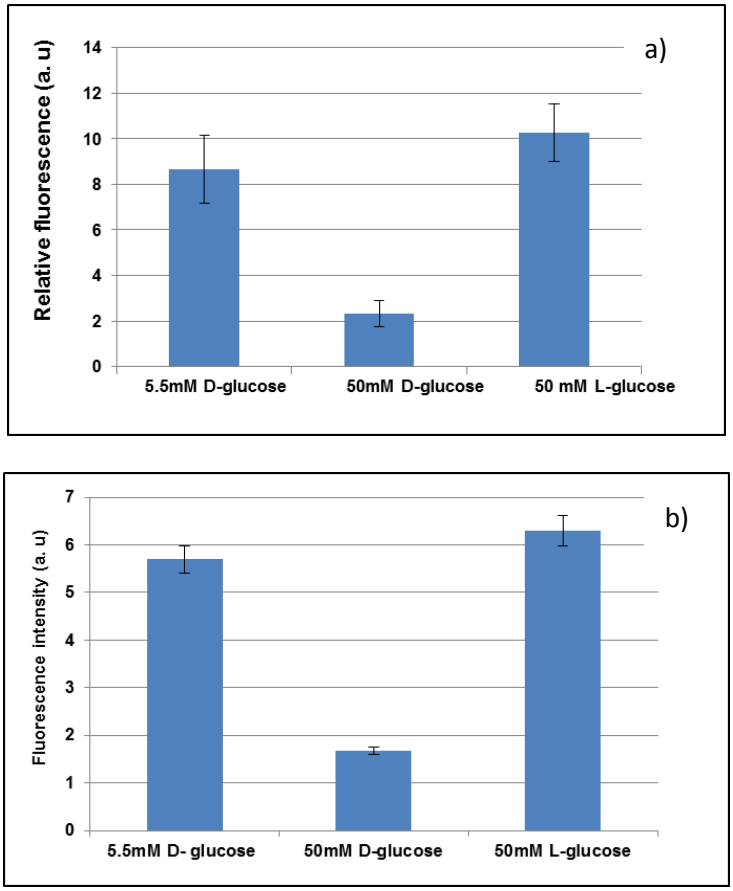

Figure 3.14. Dye uptake behaviour in tumor cells with increasing glucose concentrations in cellular media: Statistical graph of competitive assay with L-glucose and comparison with D-glucose; Mean relative fluorescence obtained from three independent trials (Values represent mean ± SD); (a) **ASqαGl** (b) **ASqβGl**.

3.3.5.5. Selective uptake of tumor cells

Preferential uptake of **ASqβGl** and **ASqαGl** in cancer cells was established by comparing the mean fluorescence intensity values for cancer cells (HeLa) and normal cells (H9c2, Figure 3.15). Observed fluorescence intensity from the cancer cells was found to be higher than that of the normal cells. Selective uptake in cancer cells was again confirmed by flow cytometry analysis (Figure 3.16) Imaging study was also conducted in colon cancer cell lines (SW480, Figure 3.17).

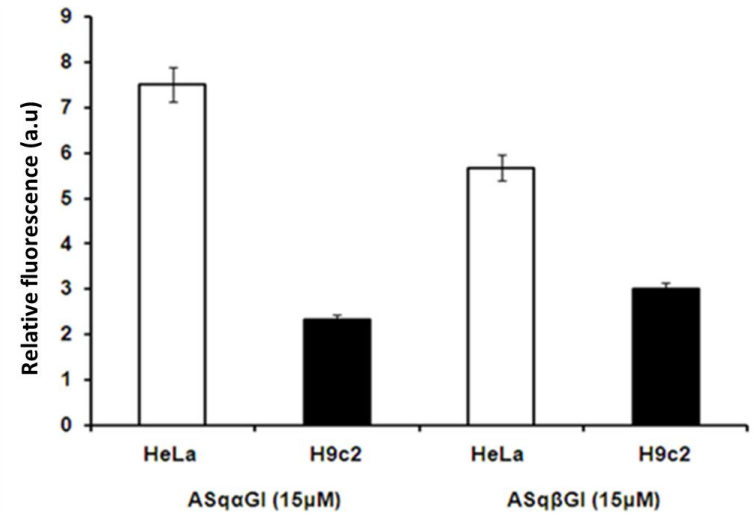

Figure 3.15. Preferential uptake of **ASqαGl** and **ASqβGl** in tumor cells (HeLa) compared to normal cells (H9c2). Statistical graph showing the mean relative fluorescence obtained from three independent trials (Values represent mean ± SD).

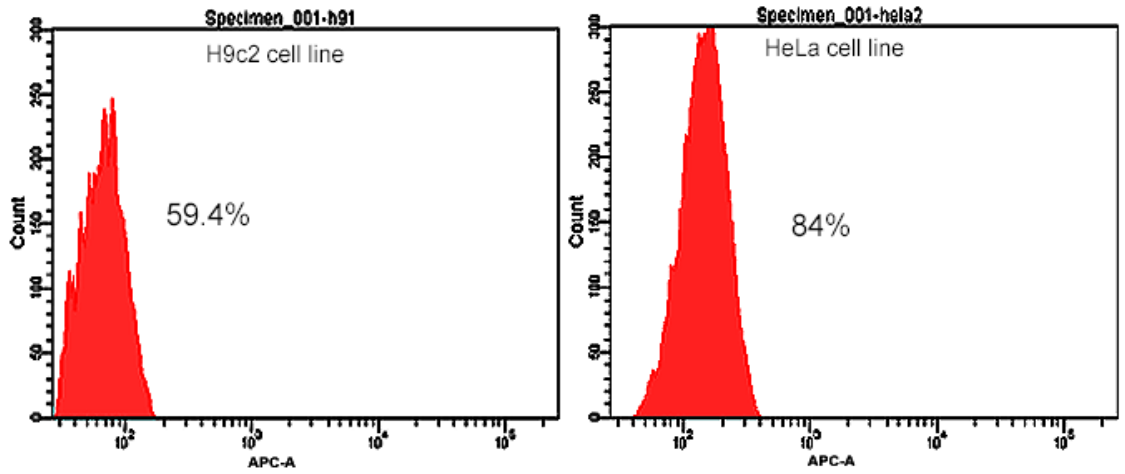

Figure 3.16. Representative histograms showing cellular uptake of **ASqαGl** demonstrated by mean cell fluorescence levels in APC-A histograms**.**

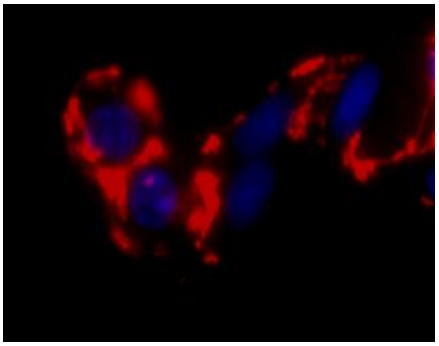

Figure 3.17. Colon cancer cell lines (SW480) incubated with **ASqαGl** (10 μM). Hoeschst staining done for nuclei.

3.3.6. Mechanism of cellular uptake

All the above experiments points to the GLUT mediated selective uptake of **ASqβGl** and **ASqαGl** in cancer cells. In aqueous solution, the fluorescence of the squaraine dyes remain quenched. But after their internalization into the cells, an intense red fluorescence could be observed from the cells incorporated with squaraine dyes. A fluorescence "turn-on" occurs inside the cells to bring about the cellular fluorescence. The mechanism of "turn-on" fluorescence observed for squaraine bio-probes can be proposed on the basis of previous literature reports as shown in Figure 3.18.[25,26] The

mechanism involves a rapid uptake of glucose analogues due to high energy demand of cancer cells. Later, the internalized glucose analogues undergo phosphorylation by the hexokinase enzyme at the C-6 position of the glucose attached to the squaraine dye yielding the corresponding glucose-6-phosphate derivative of the dye. Since the glucose-6-phosphate derivative is not being a substrate for GLUTs, it gets trapped inside the cell. Both the less hydrophilicity of the intracellular media and phosphorylation of the squaraine dyes contributed to their increased solubility inside the cells leading to their disaggregation inside the cells. This disaggregation occurring within the cell gives way to bright fluorescent images of the cells. Formation of glucose-6-phosphate derivative (molecular mass = 685.2171) was concluded from the MALDI-TOF mass spectral analysis. The mass spectral analysis produced a peak corresponding to $[M+Na]^+$: 708.250 (Figure 3.19) which supported the generation of an intermediate phosphate derivative. Symmetrical squaraine (**SSqβGl**) was also accumulated in the cells, but intracellular concentration was found to be very low. The low cellular fluorescence from the cells incubated with **SSqβGl** may be due to the passive transport of dyes across the cell membrane. The large size and high molecular mass of **SSqβGl** compared to that of unsymmetrical squaraines and glucose may make it an unsuitable substrate for GLUTs.

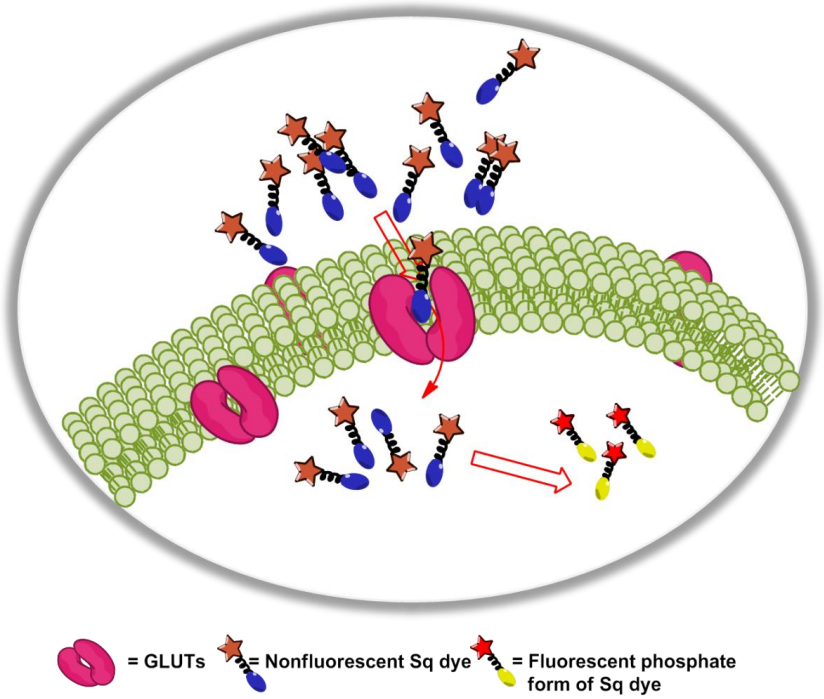

Figure 3.18. Mechanism of disassembly driven fluorescence "turn-on" inside the cancer cells.

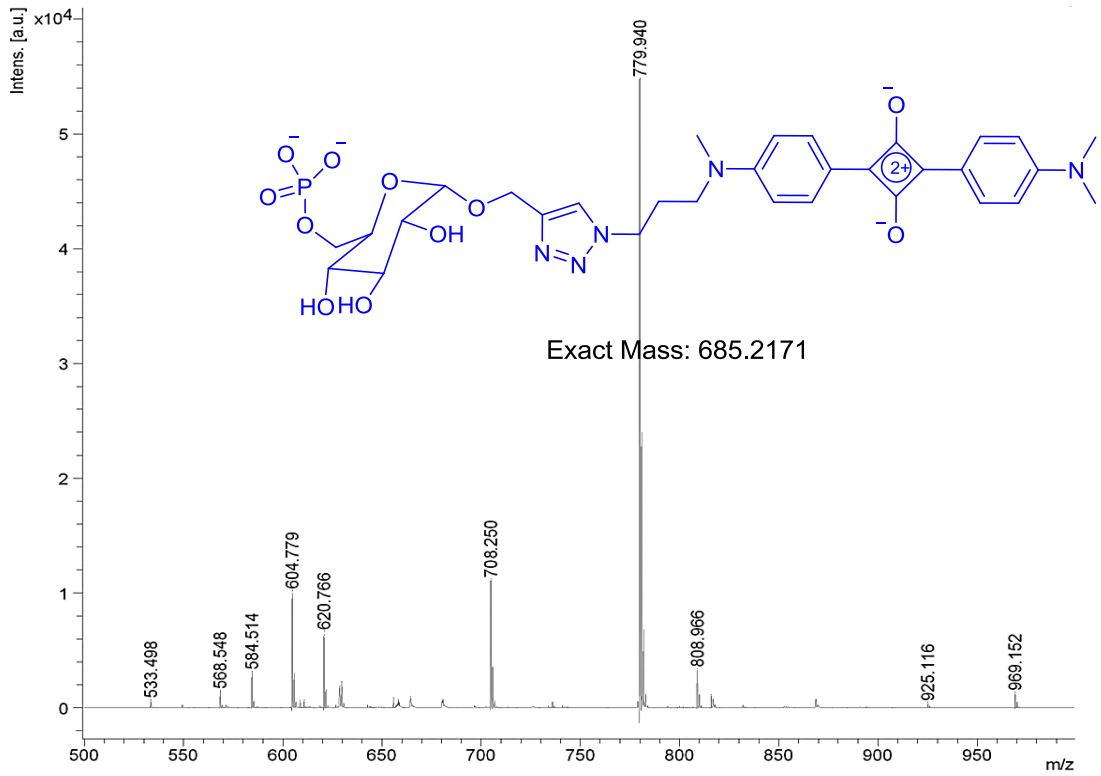

Figure 3.19. MALDI-TOF spectrum of glucose-6-phosphate derivative of **ASqαGl**

3.3.7. Comparison with a glucose analogue-2-NBDG

The efficiency of the glucose-squaraine analogue for bioimaging was also analyzed from a comparative study with a commercially available glucose bioprobe, 2-NBDG. 2-NBDG is being widely used in glucose uptake measurements. Cellular uptake of **ASqαGl** by GLUTs was compared with that of glucose tracer, 2-NBDG under similar experimental conditions. Fluorescent images obtained after incorporation of HeLa cells with 10 μM concentrations of **ASqαGl** and 2-NBDG are shown in Figure 3.20 and 3.21. It was observed that bright fluorescence was visible from the cells incorporated with **ASqαGl** (10 μM), whereas no fluorescence was obtained from the cells incubated with 2-NBDG of 10 μM concentration under similar experimental conditions. This inference suggests a higher uptake of **ASqαGl** when compared to 2-NBDG in the cancer cells.

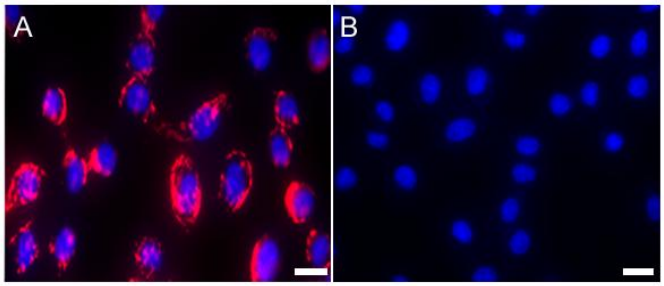

Figure 3.20. Fluorescence images of HeLa cells incorporated with A. ASqαGl and B. 2-NBDG at 10 μM concentration. Fluorescence of 2-NBDG is not visible under similar experimental conditions and exposure time (0.5 sec exposure). Nuclei stained with Hoechst dye. B635/20 and A488/10 nm excitation filters have been used to record the images of **ASqαGl** and 2-NBDG respectively. (Incubation time: 30 min., Scale bar: 20 μm).

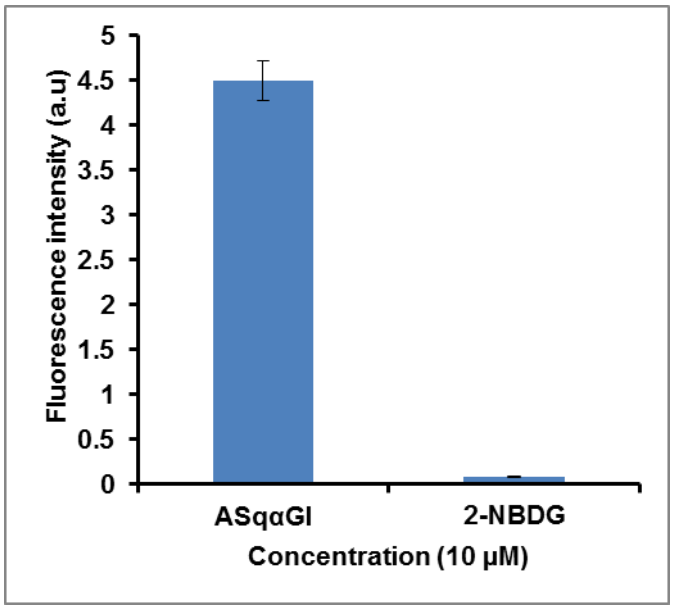

Figure 3. 21. Fluorescent intensity **ASqαGl** (10 μM) in HeLa cells compared with the commercially available glucose conjugtae 2-NBDG (10 μM) under similar experimental conditions.

3.4. Conclusions

We have demonstrated the selective imaging of cancer cells with glucose analogues of squaraine dyes utilizing "*Warburg effect*". Internalization efficiency of symmetrical (**SSqβGl**) and unsymmetrical (**ASqβGl**) squaraine dyes were compared. Even though both **SSqβGl** and **ASqβGl** were internalized, the intracellular concentration of **ASqβGl** was high as evident from the intracellular fluorescence. The internalization of **ASqβGl** was found out to be occurring through the GLUTs. Inferior uptake of **SSqβGl** may be attributed to its higher molecular weight. Cellular uptake was very high for α-glucose analogue, **ASQαGl** compared to **ASqβGl**. Stereoselective binding of GLUTs was confirmed by direct competitive experiments (both D- and L-glucose). The "turn-on" fluorescence of squaraine dyes internalized in the cells was exploited to obtain wash free imaging of the tumor cells. **ASQαGl** was

also shown to have superior imaging properties compared to the well-known glucose tracer 2-NBDG.

3.5. Experimental section

3.5.1. Materials and methods

All the chemicals were purchased from Sigma-Aldrich, Alfa Aesar, Merck and SDFCL were used without further purification. ^{1}H and ^{13}C were recorded on Bruker 500 MHz spectrometer and tetramethylsilane (TMS) used as the standard. IR spectra were recorded on Bruker FT-IR spectrometer. Mass spectra were recorded under EI/HRMS at 60,000 resolution using Thermo Scientific Exactive Mass Spectrometer and MALDI-TOF MS spectra were recorded using Shimadzu Axima CFR (Plus). Absorption spectra were measured on a Shimadzu UV-3101 PC NIR scanning spectrophotometer and emission recorded on SPEX Fluorolog F112X spectrofluorimeter. Fluorescence quantum yield (Φ_f) were measured by relative method using squarylium III (Φ_f = 0.65 in dichloromethane) as standard.[27]

3.5.2. Cell line maintenance

HeLa, H9c2 and SW480 cell lines were obtained from National Centre for Cell Science, Pune, India. For maintenance of cell lines, Dulbeccos Modified Eagle's Medium (DMEM) *(Sigma)* containing 10 % fetal bovine serum (FBS) *(Gibco),* antibiotics (100 U/mL Penicillin and 100 µg/mL streptomycin) and amphotericin (0.25 µg/mL) *(HiMedia)* were employed. The cells were maintained in CO_2 incubators at 37 °C with 5 % CO_2 in the air and 99 % humidity. Passaging of cells when confluent was carried out using 0.25 % trypsin and 0.02 % EDTA *(HiMedia)* in phosphate buffered saline (PBS). Experiments were carried out after 36 h of seeding the cells at appropriate density in suitable well plates.

3.5.3. MALDI-TOF experiment.

HeLa cells were incubated with **ASqαGl** (30 μM) for 1 h in low glucose medium. The cells were then washed twice with PBS, trypsinized using 0.25 % trypsin and 0.02 % EDTA in PBS to detach the cells from the substratum, trypsin-inactivated using 10 % serum-containing PBS, and centrifuged at 1500 rpm for 3 min. to pellet the cells. The supernatant was removed and the pelleted cells were resuspended in PBS and centrifuged at 1200 rpm for 1 min. The supernatant was removed and the cell pellet was resuspended in deionized water and again subjected to centrifugation at 1200 rpm for 1 min. The supernatant was removed and to the pellet, 1 ml of DMSO was added that gave a light blue colour. This solution was subjected to MALDI-TOF experiment.

3.5.4. General procedure for the synthesis of alkyne

1-(2'-propargyl)-D-glucoside was prepared according to the reported procedure.[19] A suspension solution of D-glucose (3g, 16.6 mmol) in excess propargyl alcohol and dowex resin was stirred at 70 °C for 8 h. After the completion of reaction, reaction mixture was cooled to ambient temperature and filtered. The residue was transferred to silica gel column and eluted with $CHCl_3$:MeOH (8:1) to remove excess propargyl alcohol. Thus obtained 1-(2'-propargyl)-D-glucose was acetylated by refluxing at 120 °C with acetic anhydride in the presence of sodium acetate. The reaction mixture was cooled to ambient temperature and washed with saturated sodium bicarbonate solution. Organic layer was extracted with dichloromethane solvent (15 mL x 3). Compound was purified by silica gel column chromatography using hexane:ethyl acetate solvent system.

2, 3, 4, 6-Tetra-O-acetyl-1-(2′-propargyl)- α-D-glucose (14): Compound **14** was prepared following the general procedure and obtained as mixture of anomers (α & β) in 2:1 ratio as viscous liquid. Formation of the product was confirmed by HRMS (ESI) analysis,*m/z* calcd for $C_{17}H_{22}O_{10}Na$: 409.1111, found 409. 1103 $[M+Na]^+$.

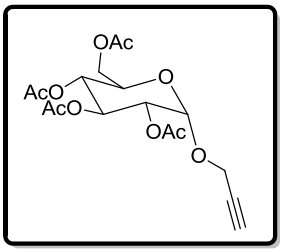

2, 3, 4, 6-Tetra-O-acetyl-1-(2′-propargyl)- α-D-galactose (15): Compound **15** was prepared following the general procedure and obtained as mixture of anomers (α & β) in 2:1 ratio as viscous liquid. Formation of the product was confirmed by HRMS (ESI) analysis, *m/z* calcd for $C_{17}H_{22}O_{10}Na$: 409.1111, found 409. 1103 $[M+Na]^+$.

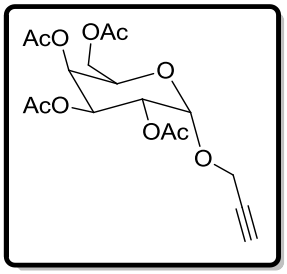

2, 3, 4, 6-Tetra-O-acetyl-1-(2′-propargyl)- α-D-Mannose (16): Compound **16** was prepared following the general procedure and upon purification the compound was isolated as α-anomer (viscous liquid). Formation of the product was confirmed by HRMS (ESI) analysis, *m/z* calcd for $C_{17}H_{22}O_{10}Na$: 409.1111, found 409. 1103 $[M+Na]^+$.

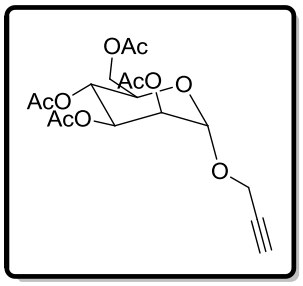

3.5.5. General procedure for the synthesis of triazole derivatives

Alkyne (1 equiv.) and azide (1 equiv.) were dissolved in acetonitrile. Copper iodide (1.5 equiv.) was added to this solution followed by the addition of *N,N*-diisopropylamine (3 equiv.) and the reaction mixture was allowed to stir for 2 h at room temperature. After the completion of reaction, reaction mixture was diluted with water and ammonium chloride. Extracted with ethyl acetate and the combined organic layer was washed with brine solution, dried over sodium sulphate. Solvent removed under reduced pressure and the residue obtained was directly used for next

reaction. Crude product dissolved in methanol and allowed to stir in the presence of sodium carbonate (5 equiv.) for 2 h at room temperature. After monitoring the completion of reaction with TLC, reaction mixture was filtered and solvent removed under reduced pressure. Residue obtained was purified by silica gel column chromatography using $CHCl_3$:MeOH (10:1) solvent system to afford corresponding 1,2,3-triazole derivatives.

2-(hydroxymethyl)6((1(3(methyl(phenyl)amino)propyl)-1-H-1,2,3-triazol-4-yl)methoxy)tetrahydro-2H-pyran-3,4,5-triol (αGlTZLOH, 8): Compound **8** was synthesized by reacting 2,3,4,6-Tetra-*O*-acetyl-1-(2′-propargyl)-α-D-glucose (**4**) and compound **7** to obtain acetylated derivative. Which then upon reaction with sodium carbonate yielded compound **8** as colourless viscous liquid (1.2 g, 56 %). **^{1}H NMR** (Methanol-d_4, 500 MHz): δ 8.01 (s, 1 H), 7.19-7.16 (m, 2 H), 6.71-6.64 (m, 3 H), 4.93 (d, *J* = 4.0 Hz, 1 H), 4.83 (bs, 1 H), 4.68 (d, *J* = 12.5 Hz, 1 H), 4.44 (t, *J* = 7.0 Hz, 2 H), 3.83 (d, *J* = 11.0 Hz, 1 H), 3.72-3.61 (m, 3 H), 3.45- 3.42 (m, 2 H), 3.38 (s, 1 H), 3.35-3.31 (m, 2 H), 2.89 (s, 3 H), 2.19-2.14 (m, 2 H) ppm. ^{13}C NMR (MeOH-d_4, 125 MHz): δ 148.8, 128.3, 123.6, 116.1, 112.1, 97.6, 76.1, 73.1, 72.1, 71.6, 71.5, 69.9, 59.5, 53.6, 48.8, 36.9, 26.4 ppm. HRMS (ESI) *m/z* calcd for $C_{19}H_{28}N_4O_6Na$: 431.1907; found: 431.1916 $[M+Na]^+$.

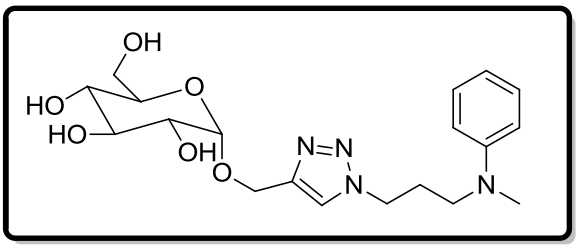

2-(hydroxymethyl)-6-((1-(3-(methyl(phenyl)amino)propyl)-1-H-1,2,3-triazol-4-yl)methoxy)tetrahydro-2H-pyran-3,4,5-triol (αMTZLOH, 12): Compound **12** was synthesized by reacting 2,3,4,6-Tetra-*O*-acetyl-1-(2′-propargyl)-α-D-mannose (**16**) and compound **7** to obtain acetylated derivative. Which then upon reaction with sodium

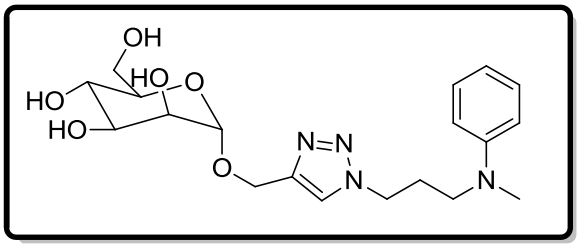

carbonate yielded compound **12** as colourless viscous liquid (1.3 g, 60 %). **^{1}H NMR** (Methanol-d_4, 500 MHz): δ 8.00 (s, 1 H), 7.19-7.16 (m, 2 H), 6.71-6.65 (m, 3 H), 4.87 (bs, 1 H), 4.81 (d, *J* = 12.0 Hz, 1 H), 4.66 (d, *J* = 12.0 Hz, 1 H), 4.46 (t, *J* = 7.0 Hz, 2 H), 3.88-3.86 (bs, 1 H), 3.86 (bs, 1 H), 3.75-3.87 (m, 2 H), 3.65 (d, 1 H), 3.59-3.57 (m, 1 H), 3.38 (t, *J* = 7.5 Hz, 2 H), 2.22-2.16 (m, 2 H) ppm. **^{13}C NMR** (Methanol-d_4, 125 MHz): δ 149.3, 143.9, 128.7,124.1, 116.5, 112.6, 99.4, 73.6, 70.6, 67.2, 61.6, 59.3, 49.2, 37.3, 26.9 ppm. HRMS (ESI) *m/z* calcd for $C_{19}H_{28}N_4O_6Na$: 431.1907; found: 431.1907 $[M+Na]^+$.

2-(hydroxymethyl)-6-((1-(3-(methyl(phenyl)amino)propyl)-1-H-1,2,3-triazol-4-yl)methoxy)tetrahydro-2H-pyran-3,4,5-triol (αGaTZLOH, 13): Compound **13** was synthesized by reacting 2,3,4,6-Tetra-*O*-acetyl-1-(2′-propargyl)-α-D-galactose (**13**) and compound **7** to obtain acetylated derivative. Which then reaction with sodium carbonate yielded compound **13** as colourless viscous liquid (1.4 g, 58 %). **^{1}H NMR** (CD_3CN, 500 MHz): δ 7.78 (s, 1 H), 7.21-7.09 (m, 2 H), 6.69-6.64 (m, 3 H), 5.01 (bs, 1 H), 4.75 (d, *J* = 12.5 Hz, 1 H), 4.61 (d, *J* = 12.5 Hz, 1 H), 4.38 (t, *J* = 7.0 Hz, 2 H), 3.99-3.98 (m, 3 H), 3.94 (s, 1 H), 3.75 (bs, 1 H), 3.60 (d, *J* = 6.0 Hz, 2 H), 3.34 (t, *J* = 7.0 Hz, 2 H), 2.13 (t, *J* = 7.0 Hz, 2 H) ppm. **^{13}C NMR** (CD_3CN, 125 MHz): δ 149.2, 144.2, 129.1, 123.7, 117.3, 116.3, 112.4, 107.4, 84.5, 81.3, 78.1, 63.3, 59.8, 49.2, 47.8, 37.7, 27.0 ppm. HRMS (ESI) *m/z* calcd for $C_{19}H_{28}N_4O_6Na$: 431.1907; found: 431.1910 $[M+Na]^+$.

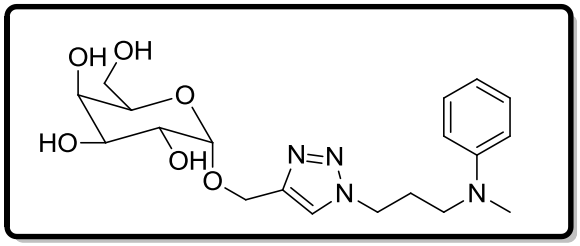

3.5.6. Synthesis of 3-(4-(dimethylamino)phenyl)-4-hydroxycyclobut-3-ene-1,2-dione (11): Compound **11** was synthesised according to the conventional procedure.[23] 3,4-dichlorocyclobutene-1,2-dione (**9**) (1.5 g, 9.9 mmol), and *N,N*-

dimethylaniline (**10**) (1.2 g, 9.7 mmol), were dissolved in dry benzene (30 mL) and refluxed for 8 h. After cooling, the reaction mixture was poured into ice water (200 mL) and the two layers formed were separated. The organic layer was washed with water, and the crude product obtained was dissolved in a mixture of acetic acid (25 mL), water (25 mL) and 2N HCl was added (10 mL). The resulting mixture was then refluxed for 4 h at 120 °C. After cooling, this solution was added to crushed ice, the precipitated product was isolated by filtration, washed with diethyl ether, and dried to yield 2.0 g (50 %) of the pure product as a brown coloured powder. **^{1}H NMR (**500 MHz, DMSO-d_6): δ 7.86 (d, J = 9 Hz, 2H,), 6.88 (d, J = 9 Hz, 2H,), 3.03 (s, 6H) ppm.

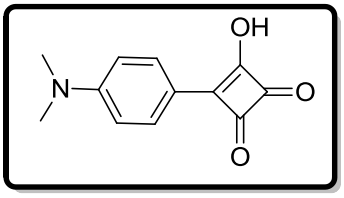

3.5.7. General procedure for synthesis of unsymmetrical squaraines

Unsymmetrical squaraines were synthesised by the condensation of 3-(4-(dimethylamino)phenyl)-4-hydroxycyclobut-3-ene-1,2-dione (**11**) (1 equiv.) and corresponding triazole substrate (1 equiv.) in n-butanol/benzene (1:2) solvent mixture at 110 °C for 8 h. After monitoring completion of the reaction using TLC, solvent was removed under reduced pressure. The residue obtained was purified by repeated precipitation from EtOAc/MeOH solvent mixture and finally from methanol solvent to yield the unsymmetrical squaraines as blue solids.

ASqαGl (124 mg, 17 %). m p: 220-224 °C. **^{1}H NMR** (DMSO-d_6, 500 MHz): δ 8.17 (s, 1 H) 8.15-8.12 (m, 4 H), 6.98-6.95 (m, 4 H), 4.78 (d, J = 3.5 Hz, 1

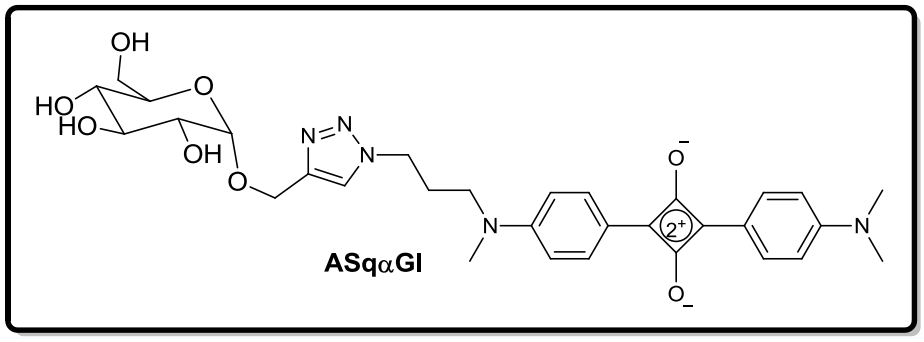

H), 4.71 (d, *J* = 12.5 Hz, 1 H), 4.53 (d, *J* = 12.5 Hz, 1 H), 4.46 (t, *J* = 7.0 Hz, 2 H), 3.65 (bs, 1 H), 3.63 (m, 4 H), 3.20 (s, 6 H), 3.17 (s, 3 H), 3.15 (bs, 4 H), 2.21 (m, 2 H) ppm. **^{13}C NMR** (DMSO-d_6, 125 MHz):δ 187.6, 181.6, 173.6, 155.0, 153.6, 143.9, 131.5, 124.1, 124.1, 119.0, 113.1, 113.0, 97.9, 73.7, 71.8, 70.3, 60.9, 39.7, 25.3 ppm. HRMS (ESI): *m/z* calcd for $C_{31}H_{37}N_5O_8Na$: 630.2551; found: 630.2555 $[M+Na]^+$.

ASqαGa (122 mg, 16 %). m p: 165-170 °C (decomposing). **^{1}H NMR** (DMSO-d_6, 500 MHz): δ 8.15-8.12 (m, 5 H), 6.98-6.95 (m, 4 H), 4.84 (bs, 1 H), 4.66 (d, *J* = 12.0 Hz, 1 H), 4.52 (d, *J* = 12Hz , 1H), 4.45 (t, *J* = 7.0 Hz, 2 H), 3.86-3.83 (m, 1 H), 3.79-3.78 (m, 2 H), 3.61-3.58 (m, 2 H), 3.51-3.50 (m, 3 H), 3.36 (s, 6 H), 3.20 (s, 3 H), 2.17 (t, *J* = 7.0Hz, 2H) ppm. **^{13}C NMR** (DMSO-d_6, 125 MHz):δ 186.3, 185.4, 154.8, 143.9, 131.6, 124.0, 118.8, 118.5, 113.1, 106.9, 94.5, 82.1, 76.7, 70.2, 62.6, 59.9, 49.1, 46.9, 38.9, 27.3. HRMS (ESI) *m/z* calcd for $C_{31}H_{37}N_5O_8Na$:630.2551; found: 630.2549 $[M+Na]^+$.

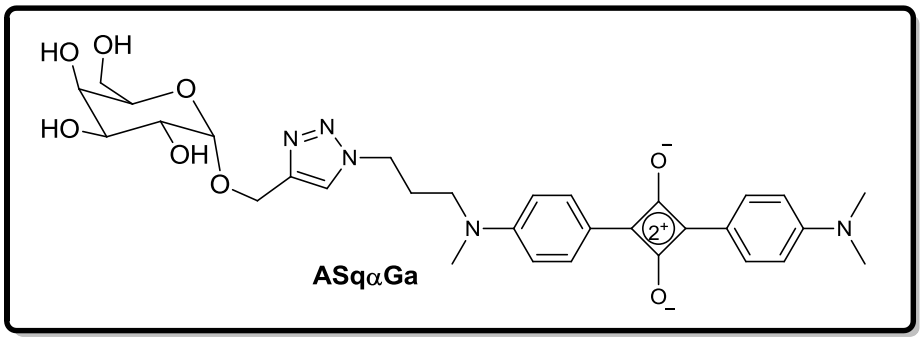

ASqαM (112mg, 14 %).m p:228-232 °C.^{1}**H NMR** (DMSO-d_6, 500 MHz): δ 8.01 (s, 1H), 7.19-7.1 (m, 2H), 6.71-6.65 (m, 3H), 4.87 (bs, 1H), 4.81 (d, J = 12.0 Hz, 1 H), 4.66 (d, J = 12.0 Hz, 1 H), 4.46 (t, J = 7.0 Hz, 2H), 3.88 (bs, 1 H), 3.86 (bs, 1 H), 3.75-3.69 (m, 2 H), 3.65 (d, 1 H), 3.59-3.57 (m, 1 H), 3.38 (t, J = 7.5 Hz, 2 H), 2.22-2.17 (m, 2 H) ppm. ^{13}**C NMR** (DMSO-d_6, 125 MHz): δ 149.3, 143.9, 128.7, 124.1, 116.5, 112.6, 99.3, 73.5, 71.1, 70.6, 67.2, 61.6, 59.3, 49.2, 37.3, 26.9 ppm. HRMS (ESI): m/z calcd for $C_{31}H_{37}N_5O_8Na$: 630.2551; found: 630.2555 $[M+Na]^+$.

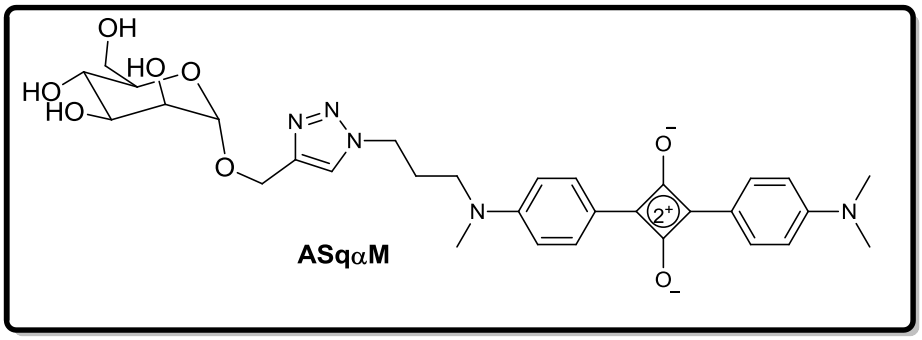

3.6. References

1. (a) S. Luo, E. Zhang, Y. Su, T. Cheng, C. Shi, *Biomaterials* **2011**, *32*, 7127-7138.; (b) A. Yuan, J. Wu, X. Tang, L. Zhao, F. Xu, Y. Hu, *J. Pharm. Sci.* **2013**, *102*, 6-28.
2. (a) R. Weissleder, M. J. Pittet, *Nature* **2008**, *452*, 580-589.; (b) E. M. Sevick-Muraca, *Annu. Rev. Med.* **2012**, *63*, 217-231.
3. W. H. Kim, J. Lee, D.-W. Jung, D. R. Williams, *Sensors* **2012**, *12*, 5005-5027.; (b) Weissleder, R. *Nat. Biotechnol.* **2001**, *19*, 316-317.; (c) Z. Guo, S. Park, J. Yoon, I. Shin, *Chem. Soc. Rev.* **2014**, *43*, 16-29.; (d) S. A. Hilderbrand, R. Weissleder, *Curr. Opin. Chem. Biol.* **2010**, *14*, 71-79.
4. J. O. Escobedo, O. Rusin, S. Lim, R. M. Strongin, *Curr. Opin. Chem. Biol.* **2010**, *14*, 64-70.
5. (a) R. Y. Tsien, Q. T. Nguyen, *Nat. Rev. Cancer* **2013**, *13*, 653-662.; (b) J. Yin, Y. Hu, J. Yoon, *Chem. Soc. Rev*. **2015**, *44*, 4619-4644.; (c) H. Kobayashi, M. Ogawa, R. Alford, P. L. Choyke, Y. Urano, *Chem. Rev*. **2010**, *110*, 2620-2640.; K. Umezawa, D. Citterio, K. Suzuki, *Anal. Sci.* **2014**, *30*, 327-349.
6. (a) S. Koga, Y. Oshima, N. Honkura, T. Iimura, K. Kameda, K. Sato, M. Yoshida, Y. Yamamoto, Y. Watanabe, A. Hikita, *et al. Cancer Sci.* **2014**, *105*, 1299-1306.; (b) S. Gao, D. Chen, Q. Li, J. Ye, H. Jiang, C. Amatore, X. Wang, *Sci. Rep*. **2014**, *4*, 4384/1-4384/6.; (c) X. Zhao, Y. Li, D. Jin, Y. Xing, X. Yan, L. Chen, *Chem. Commun.* **2015**, *51*, 11721-11724.; (d) S. G. König, S. Öz, R. Krämer, *Chem. Commun.* **2015**, *51*, 7360-7363.
7. E. C. Calvaresi, P. J. Hergenrother, *Chem. Sci.* **2013**, *4*, 2319-2333.

8. (a) O. Warburg, K. Posener, E. Negelein, *Biochem. Z.* **1924**, *152*, 309-344.; (b) O. Warburg, *Science* **1956**, *123*, 309-314.
9. a) H. Tanisaka, S. Kizaka-Kondoh, A. Makino, S. Tanaka, M. Hiraoka, S. Kimura, *Bioconjug. Chem.* **2008**, *19*, 109-117.; (b) R. A. Medina, G. I. Owen, *Biol. Res.* **2002**, *35*, 9-26.; (c) M. G. Vander Heiden, L. C. Cantley, C. B. Thompson, *Science* **2009**, *324*, 1029-1033.; (d) M. G. Vander Heiden, L. C. Cantley, C. B. Thompson, *Science* **2009**, *324*, 1029-1033.
10. (a) S. N. Vijayakumar, S. Sethuraman, U. M. Krishnan, *RSC Adv.* **2015**, *5*, 41751-41762; (b) B. Thorens, M. Mueckler, *Am. J. Physiol. Endocrinol. Metab.* **2010**, *298*, E141-145.; (c) F.-Q. Zhao, A. F. Keating, *Curr. Genomics* **2007**, *8*, 113-128.
11. (a) E. K. J. Pauwels, M. J. Ribeiro, J. H. M. B. Stoot, V. R. McCready, M. Bourguignon, B. Maziere, *Nucl. Med. Biol.* **1998**, *25*, 317-322.; (b) L. Sokoloff, M. Reivich, C. Kennedy, M. H. Des Rosiers, C. S. Patlak, K. D. Pettigrew, O. Sakurada, M. Shinohara, *J. Neurochem.* **1977**, *28*, 897-916.; (c) P. Som, H. L. Atkins, D. Bandoypadhyay, J. S. Fowler, R. R. MacGregor, K. Matsui, Z. H. Oster, D. F. Sacker, C. Y. Shiue, *et al.*, *J. Nucl. Med.* **1980**, *21*, 670-675.; (d) J. Segal, S. H. Ingbab, *J. Clin. Invest.* **1981**, *68*, 103-110.; (e) C. W. Keevil, A. S. McDermid, P. D. Marsh, D. C. Ellwood, *Arch. Microbiol.* **1986**, *146*, 118-124.
12. L. Speizer, R. Haugland, H. Kutchai, *Biochim. Biophys. Acta* **1985,** *815*, 75-84.
13. (a) K. Yoshioka, H. Takahashi, T. Homma, M. Saito, K.-B. Oh, Y. Nemoto, H. Matsuoka, *Biochim. Biophys. Acta,* **1996**, *1289*, 5-9.; (b) R. G. O'Neil, L. Wu, N. Mullani, *Mol. Imaging Biol.* **2005**, *7*, 388-392.; (c) T. Yamamoto, S.-i. Tanaka, S. Suga, S. Watanabe, K. Nagatomo, A. Sasaki, Y. Nishiuchi, T.

Teshima, K. Yamada, *Bioorg. Med. Chem. Lett.* **2011**, *21*, 4088-4096.; (d) K. Yamada, M. Saito, H. Matsuoka, N. Inagaki, *Nat. Protoc.* **2007**, *2*, 753-762.

14. M. Vendrell, A. Samanta, S.-W. Yun, Y.-T. Chang, *Org. Biomol. Chem.* **2011**, *9*, 4760-4762.
15. H. Y. Lee, J. J. Lee, J. Park, S. B. Park, *Chem. Eur. J.* **2011**, *17*, 143-150.
16. C. L. Amiot, S. Xu, S. Liang, L. Pan, J. X. Zhao, *Sensors* **2008**, *8*, 3082-3105.
17. M. Zhang, Z. Zhang, D. Blessington, H. Li, T. M. Busch, V. Madrak, J. Miles, B. Chance, J. D. Glickson, G. Zheng, *Bioconjug. Chem.* **2003**, *14*, 709-714.
18. Z. Cheng, J. Levi, Z. Xiong, O. Gheysens, S. Keren, X. Chen, S. S. Gambhir, *Bioconjug. Chem.* **2006**, *17*, 662-669.
19. J. L. Kovar, W. Volcheck, E. Sevick-Muraca, M. A. Simpson, D. M. Olive, *Anal. Biochem.* **2009**, *384*, 254-262.
20. J. Park, H. Y. Lee, M.-H. Cho, S. B. Park, *Angew. Chem. Int. Ed.* **2007**, *46*, 2018-2022.
21. H. K. Chenault, R. F. Mandes, K. R. Hornberger, *J. Org. Chem.* **1997**, *62*, 331-336.
22. F.-P. Gao, Y.-X. Lin, L.-L. Li, Y. Liu, U. Mayerhoffer, P. Spenst, J.-G. Su, J.-Y. Li, F. Wurthner, H. Wang, *Biomaterials* **2014**, *35*, 1004-1014.
23. K. M. Shafeekh, M. K. Rahim, M. C. Basheer, C. H. Suresh, S. Das, S. *Dyes. Pigm.* **2013,** *96*, 714–721.
24. J. Park, J. I. Um, A. Jo, J. Lee, D.-W. Jung, D. R. Williams, S. B. Park, C*hem. Commun.* **2014**. *50*, 9251-9254.
25. R. G. O'Neil, L. Wu, N. Mullani, *Mol. Imaging Biol.* **2005,** *7*, 388-392.

26. K. Yoshioka, M. Saito, K. B. Oh, Y. Nemoto, H. Matsuoka, M. Natsume, H. Abe, *Biosci. Biotech. Biochem.* **1996,** *60*, 1899-1901.

27. K.-Y. Law, *J. Phys. Chem.* **1987**, *91*, 5184-5193.

CHAPTER 4

pH Responsive fluorescent organogels derived from pyrene-sugar orthoesters

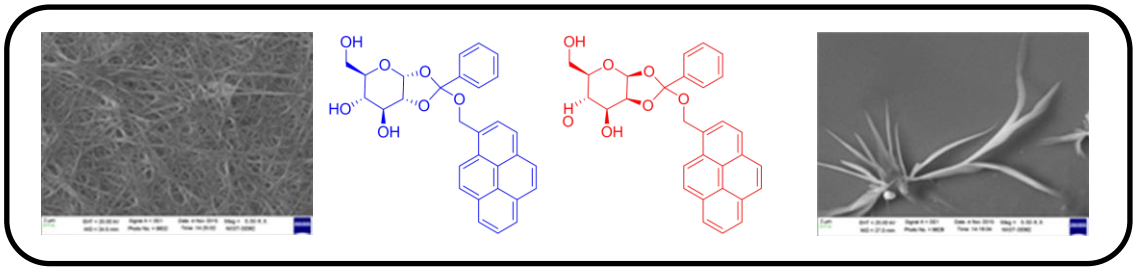

Abstract

Biologically active functional materials provide an excellent mode for understanding cellular events. Supramolecular chemistry stands out as the most adequate and suitable means for designing functional materials and nano-bio devices. Over the past few decades, science has witnessed a tremendous growth in supramolecular chemistry as an intensive destination to mimic nature, which is enriched with complex and excellent supramolecular architectures. Among these, fluorescent stimuli-responsive organogels received great interest due to their distinctive advantages such as diversity, flexibility and their promising applications in optoelectronics, erasable thermal imaging, tissue engineering, cosmetics and drug delivery. Considerable efforts have been devoted to the development of stimuli-responsive organogels, particularly pH responsive organogels owing to their biological applications. Carbohydrate molecules are excellent hydrogen bond donors and are biocompatible to yield functional materials with significant application in biology. This chapter deals with the design and synthesis of pyrene-sugar orthoester conjugates and their application as pH responsive gelator.

Orthoesters are important intermediates in the carbohydrate chemistry which are highly sensitive to acid whereas well stable in basic medium and function as an acid labile ligand in the target molecule.

4.1. Introduction

Over the past few decades, science has witnessed a tremendous growth in supramolecular chemistry[1] as an intensive destination to mimic nature, which is enriched with complex and excellent supramolecular architectures.[2] These supramolecular architectures include smart soft materials particularly, low molecular weight organogels which attracted a great deal of interest among both material chemists as well as the biologist ascribed to their unique supramolecular structures and potent applications in template synthesis, tissue engineering, cosmetics, drug delivery, and biomimetic systems.[1d] Organogels constitute the organized orientation of gelator molecules to generate three dimensional supramolecular network. Large amount of solvent molecules are trapped in the void spaces created during the hierarchical self-assembly process of gelators. This supramolecular self-assembly was built using the weak non-covalent interactions like π-π stacking, hydrogen-bonding, hydrophobic interactions, electrostatic interactions, and Van der Waals interactions.[3]

4.1.1. pH Responsive fluorescent organogelators

Fluorescent organogels represent an important class of organogels with promising applications in optoelectronics, tissue engineering, erasable thermal imaging and drug delivery. The emission profile variation accompanied by the sol to gel, gel to sol phase transition can provide crucial information at the molecular level. Thus, the incorporation of chromophores make it easy to predict the gelation phenomenon and hence to explain the structure-property relationship. Consequently, enormous number of fluorescent organogels based on various aromatic building

blocks including porphyrins,[4] pyrenyl,[5] perylene bisimides,[6] oligo-(*p*-phenylenevinylene)[7] and naphthalimides[8] have been developed by different research groups. Additionally, stimuli responsive organogels played a leading role in the development of sensor devices and found applications in the area of drug delivery, controlled release *etc*.[9] Stimuli responsive organogels respond to various stimuli and these stimuli trigger the gel-sol transition. These materials can be categorised based on the nature of the external stimuli like, light responsive,[10] thermoresponsive,[11] pH,[12] or chemoresponsive.[13] These stimuli responsive organogelators are generally constructed by incorporating appropriate functional groups into the chromophore. For successful results, there should be an effective coupling between the stimuli and the receptor unit and also the receptor unit should participate in self-assembly formation. Although great efforts have been devoted to the development of stimuli responsive organogels, only limited reports exist in the relative field. Therefore, the development of stimuli responsive fluorescent organogels is still remaining as a challenging area.

Intracellular pH (pH_i) plays a vital role in the live cells and thus the stringent regulation of pH_i is necessary for controlling various metabolic pathways.[14] Weakly acidic conditions were found in some pathological sites such as inflammation, cancer endosomal and lysosomal compartments.[15] Nowadays, pH responsive molecular systems have been identified as excellent molecular carriers for the targeted drug delivery, specifically for the treatment of diseases like cancer. In this therapeutic method, the acidic intracellular pH trigger the gel-sol transition thus facilitate the release of drug at the targeted site, which helps to reduce the "*off-target*" toxicity and the side effects reported.[16] Considerable endeavours have also been devoted to the development of pH responsive materials including low molecular weight

organogelators (LMWOGs)[17] and hydrogelators.[18] Acid sensitive organogelators can be engineered by tethering acid sensitive functional groups to the fluorophore. And the functional groups that are widely used comprise hydrazones[19] (Figure 4.1) acetals[20] (Figure 4.2) *etc.* Among these, orthoesters are more sensitve to acidolysis. Recently, Wagner and co-workers explored spiro di-orthoester as an acid labile ligand and a FRET based probe (**8**) was developed for the pH sensitive lysosomal release (Figure 4.3).

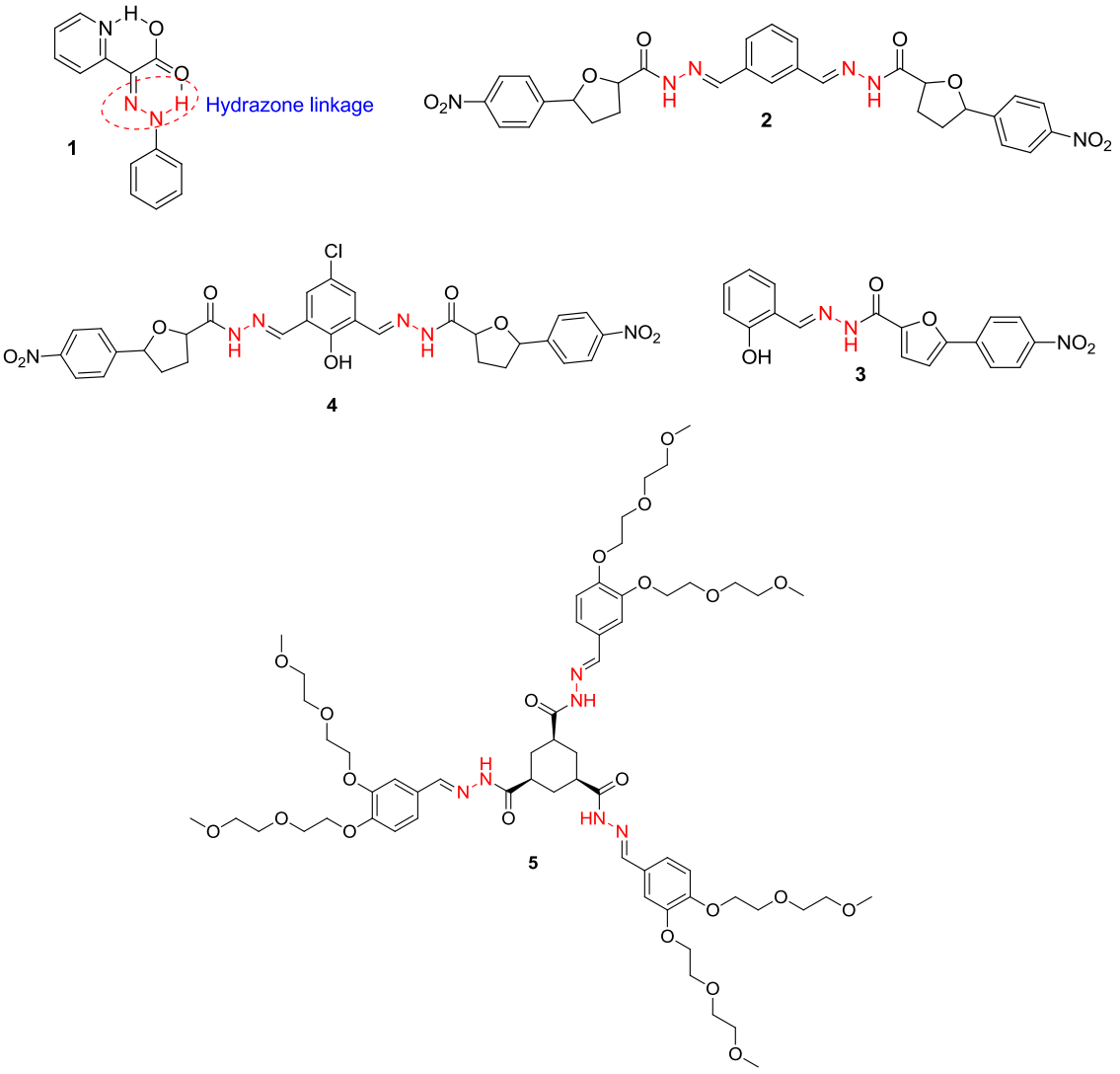

Figure 4.1. Hydrazone containing pH responsive organogelators.

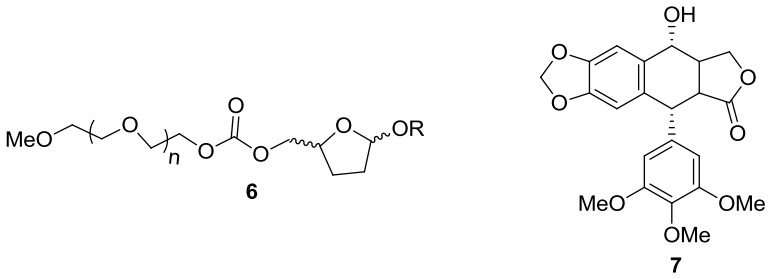

Figuret 4.2. Acetal containing pH responsive organogelators.

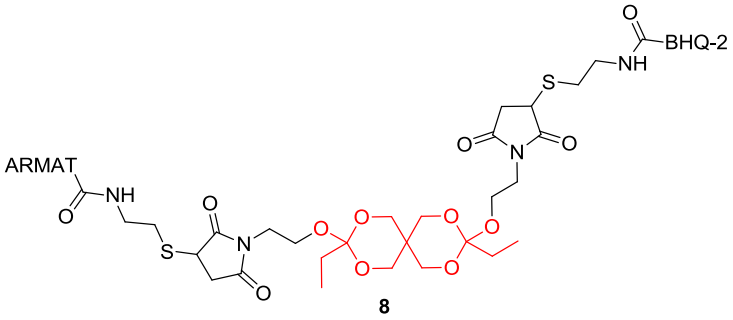

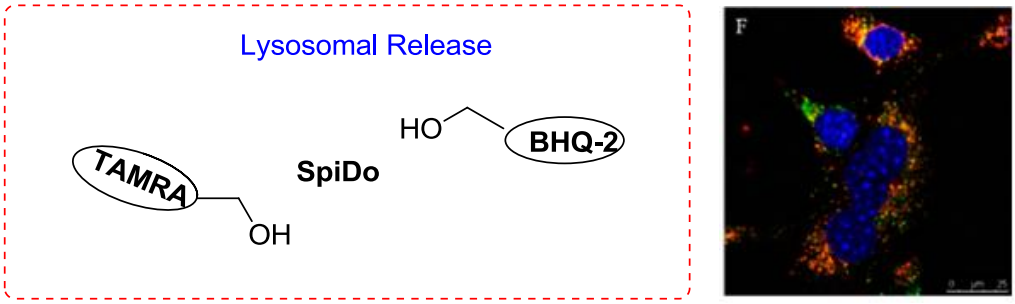

Figure 4.3. Structure of the spiro di-orthoester probe-**8,** lysosomal targeted fluorescence imaging using **8** and the scheme for lysosomal release of the fluorescent probe.

Pozzo and co-workers demonstrated the acid sensitive gelation ability of 2,3-di-*n*-alkoxyphenazines **9** and **10** (Figure 4.4) at ambient temperature in acetonitrile. Aggregation property was significantly increased upon protonation and this protonation/deprotonation process was reported to be reversible.[21]

A series of alkaline/acidic stimuli responsive LMWOGs based on amino acid derivatives of cholesterol (**11**,**11'** cholesteryl glycinate, cholesteryl L-alaninate, cholesteryl D-alaninate, cholesteryl L-phenyl alaninate, and cholesteryl D-phenyl

alaninate) were introduced by Fang *et al.*[12a] Bubbling HCl gas through the solution improves the gelation ability of the molecular system. The hydrochloric acid salts (**12**) produced are excellent gelators (Scheme 4.1), and exhibited gelation tendency in 18 solvents tested [benzene, formic acid, carbon tetrachloride, trichloromethane, acetic acid, propionic acid, water, methanol, ethanol, 1-propanol, 1-butanol, 1-pentanol, 1-hexanol, 1-heptanol, 1-octanol, 1-nonanol, 1-decanol and glycol]. The gel state was disturbed by the addition of bases like diethylamine, triethylamine, NH_3, *etc.* This alkaline/acid responsive phase transition was found to be reversible.

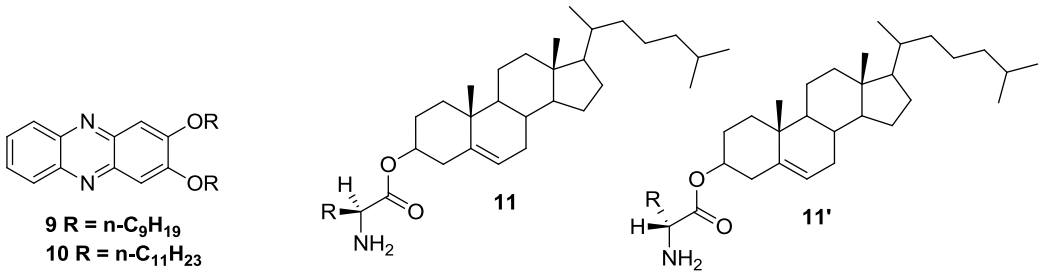

Figure 4.4. Structure of 2,3-di-*n*-alkoxyphenazines (**9,10**) and D, L aminoacid derivatives of cholesterol (**11,11**').

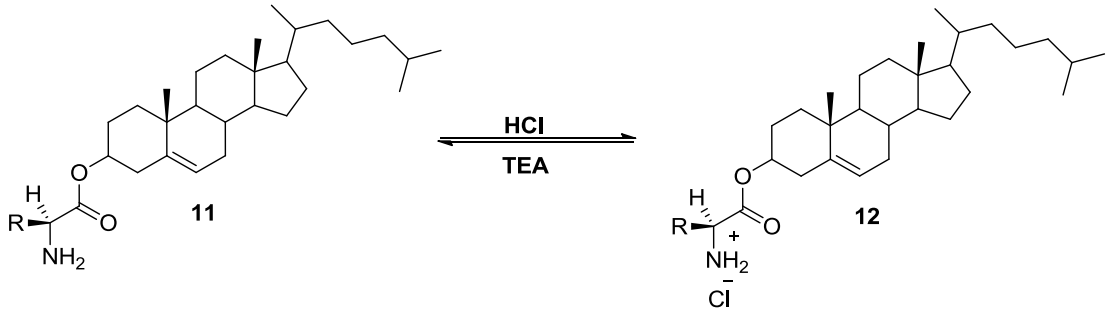

Scheme 4.1. Hydrochloric acid salt formation of aminoacid derivatives of cholesterol-**11.**

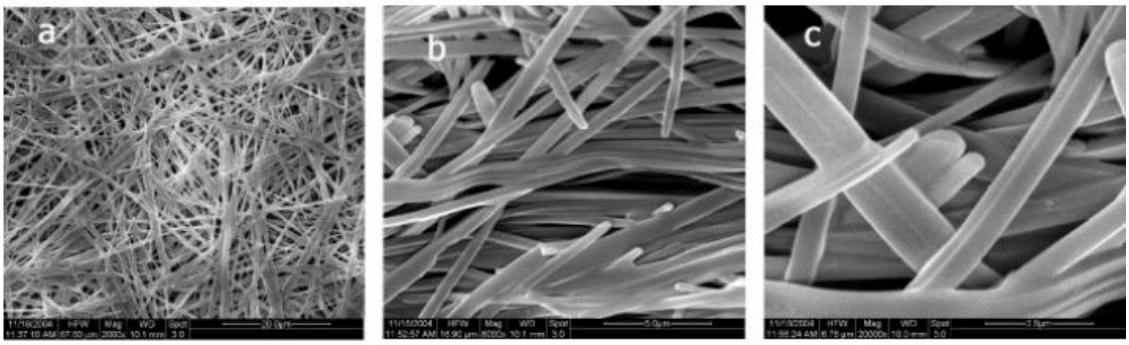

Figure 4.5. SEM micrographs of the xerogel of **12** from 1-octanol (transparent gel) (20 μm, 5.0 mm, and 2.0 μm for a, b, and c, respectively).

Recently, Wu and co-workers introduced a glucose/pH responsive LMWOGs based on phenyl boronic acid **13**. In this case hydrogen bonding, as well as the π-π stacking interactions, acts as the driving force toward gelation. Gels were formed in several solvents, and the organogel formed in cyclohexane showed high sensitivity (Scheme 4.2) at high pH [pH 11 and 13].[22]

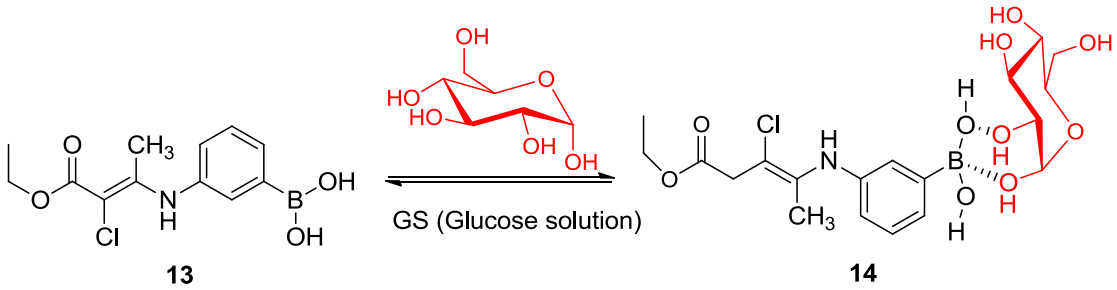

Scheme 4.2. Boronic acid-diol group coupling for compound **13**.

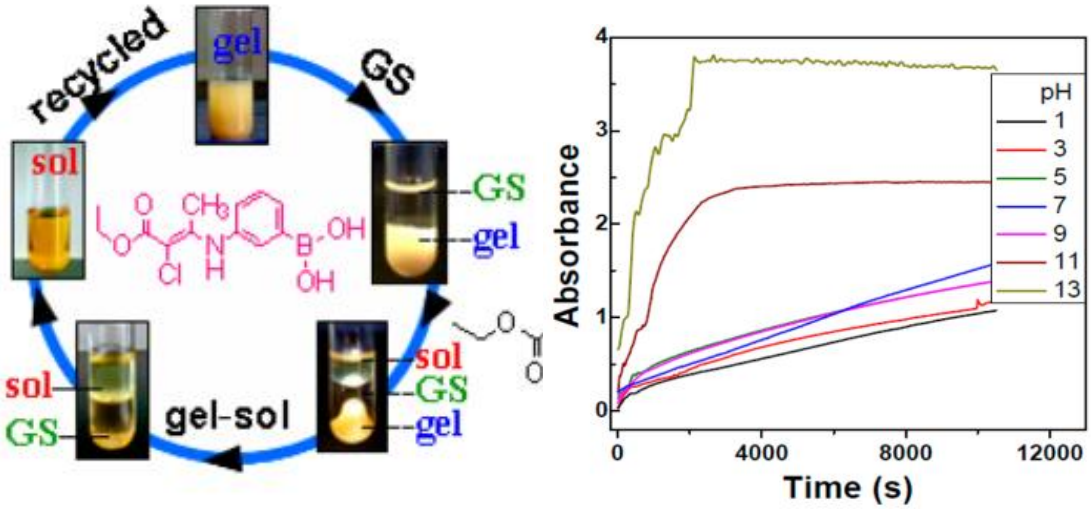

Figure 4.6. Cyclic diagram of glucose response and recycling use of the organogel and pH-response dynamic curve for gel in 3 mL solutions with different pH values (1, 3, 5, 7, 9, 11, 13) (Results from online UV spectroscopic study).

Poly (aryl ether) dendron based LWMOGs containing glucose moiety was introduced by Prasad *et al.*[23] Transparent pH responsive hydrogel was formed from the compound **15**. The gel was highly stable in the neutral condition, while at higher pH (under basic condition) the gel was converted to solution (Figure 4.7). This gel-sol transition was accompanied by morphological changes from nanofibres to spherical aggregates under basic pH, attributed to the disturbance in hydrogen bonding network and this process was found to be reversible. Moreover, dispersion of graphene oxide effectively reduces the critical gelation concentration up to 0.08 % and causes an increase in the mechanical strength compared to the native gel.

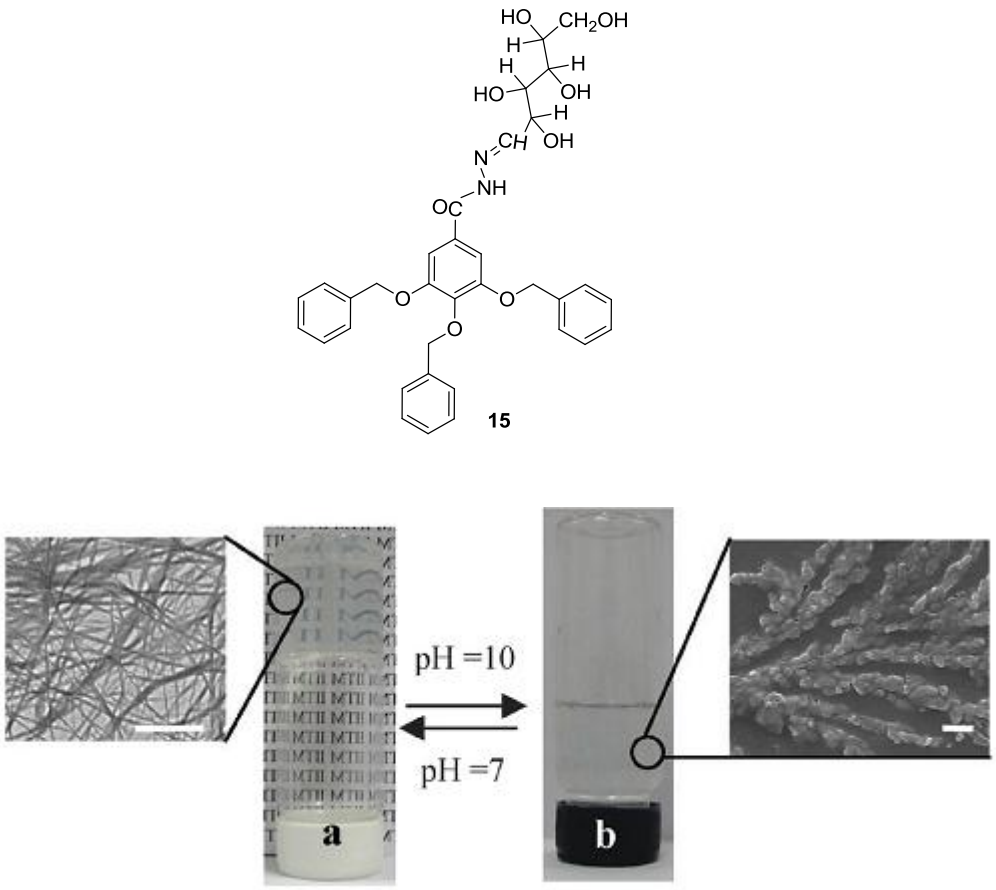

Figure 4.7. Structure of the compound **15** and the photograph of the gel formed from the compound **15** before and after addition of KOH and corresponding TEM (left) and SEM (right) images.

4.1.2. Sugar based low molecular weight organogelators

The fundamental requirement for a pH responsive biomaterial is that it should be biocompatible and have biodegradable core. Carbohydrates/sugars are naturally abundant, eco-friendly and biocompatible renewable materials, which are commercially available (Figure 4.8). The multiple hydroxyl groups (-OH) present in the sugar moiety can act as hydrogen bond source and hence provide driving force for the gelation. Also, the functionalization of these hydroxyl groups, protection and deprotection, anomeric configuration, interconversion of the conformers and variation in linkage points leads to the production of diverse LMWOGs with variable

and interesting properties.[24] And these sugar derived LMWOGs (S-LMWOGs) have applications in tissue engineering, sensors and cell encapsulation biology and functional materials.

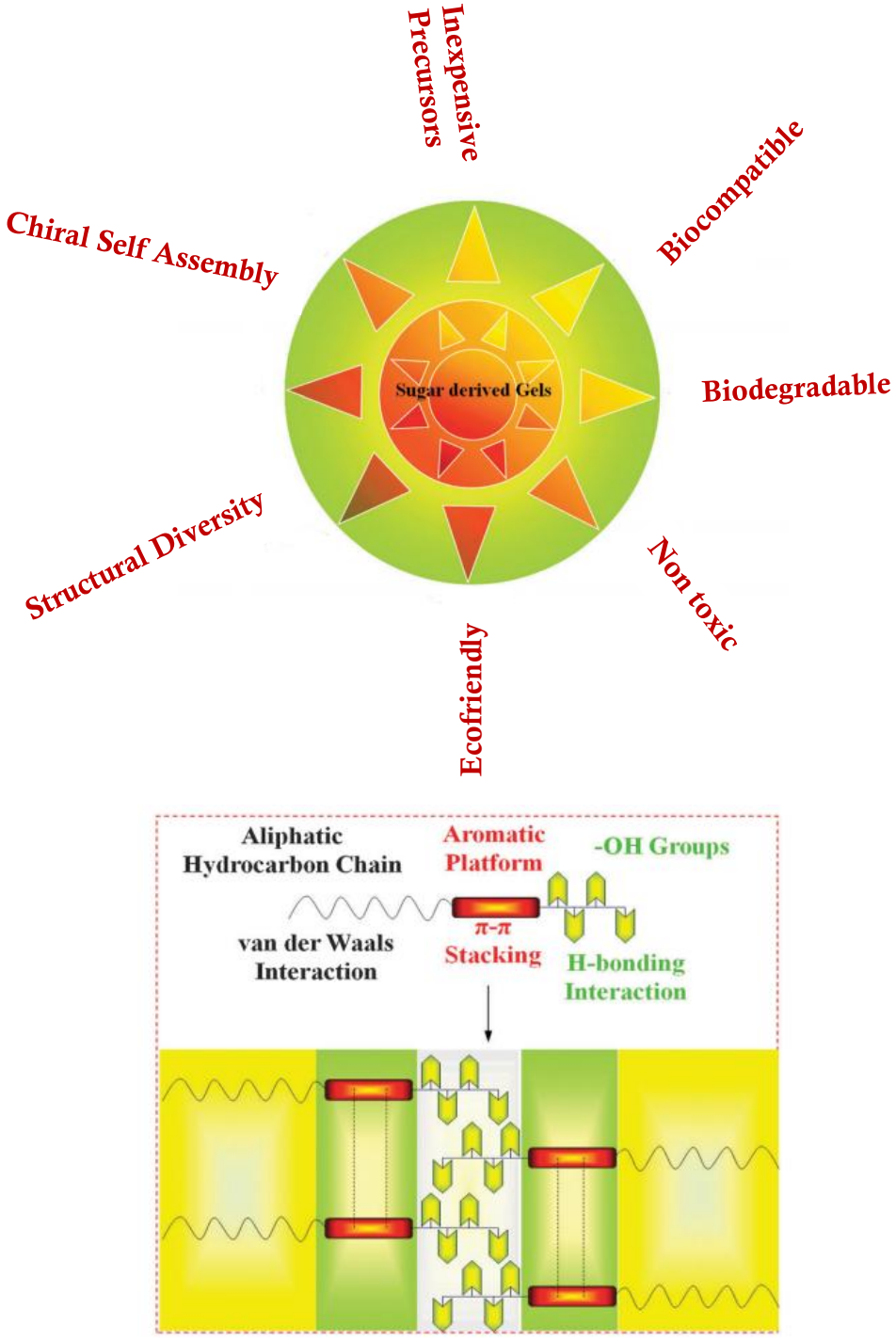

Figure 4.8. Advantages of sugar derived gels and schematic representation of non-covalent interaction mediated self-assembly of sugar derived LMWOGs (reproduced from reference 27).

Fuhrhop and co-workers studied the self-assembly and morphology of the sugar based LMWOGs for the first time.[25] They synthesized eight S-LMWOGs, aldonamides (**16-19**, Figure 4.9) from aldonic acids (D-glucose, D-gulose, D-mannose and L-mannose) and amines (octyl and octadecyl). Among these, octadecylmannonamide (**19a**) formed a helical fibrillar network (Figure 4.9) in the presence of detergents with a critical gelation concentration of 0.85 %. Later, Shinkai *et al.*,[26] Shimizu *et al.*[27] and Bhattacharya *et al.*[28] contributed to a great extent in the advancement of S-LMOGs. Plethora of hydrogen bond gelators have been synthesized from different carbohydrate molecules.[24,29]

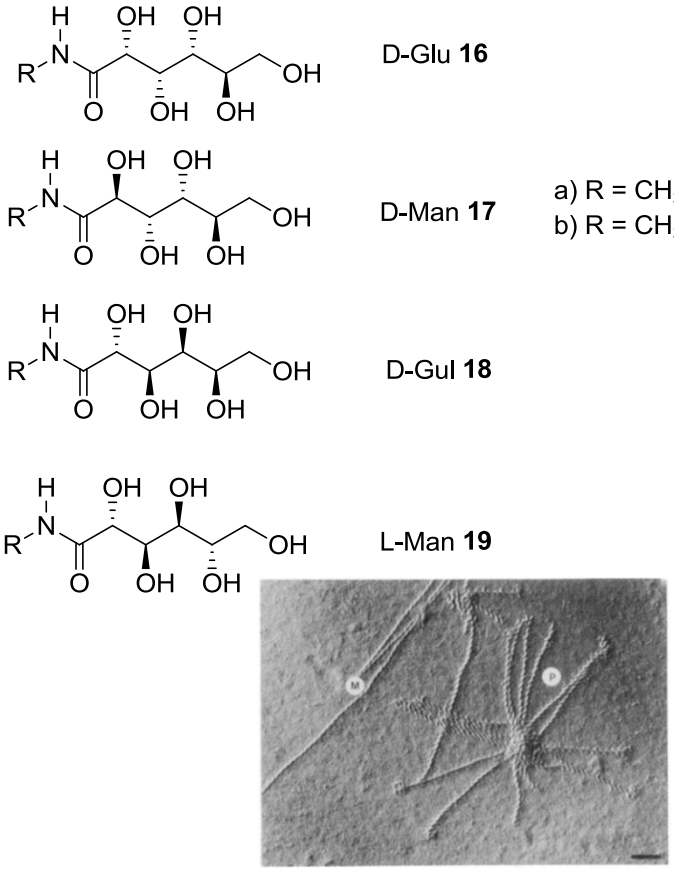

Figure 4.9. Structure of the aldonamides (**16-19**), *P* and *M* helices formed from **19a** in the presence of SDS.

Orthoesters can be viewed as acetals of esters or as the triesters of the unknown 'orthoacids'-the hydrates of carboxylic acids. Carbohydrate 1,2-orthoesters are extensively utilized intermediates in the synthesis of 1,2-trans glycosides.[30] Sugar 1,2-orthoesters (**23**) can be converted to corresponding 1,2-trans glycosides in the presence of protic or Lewis acids (Scheme 4.5),[31] they can be hydrolysed by water or, catalyzed by acid, to an ester and two alcohols. Another interesting characteristic feature of orthoester functional group is the stability in basic pH and high sensitivity towards acidic pH.

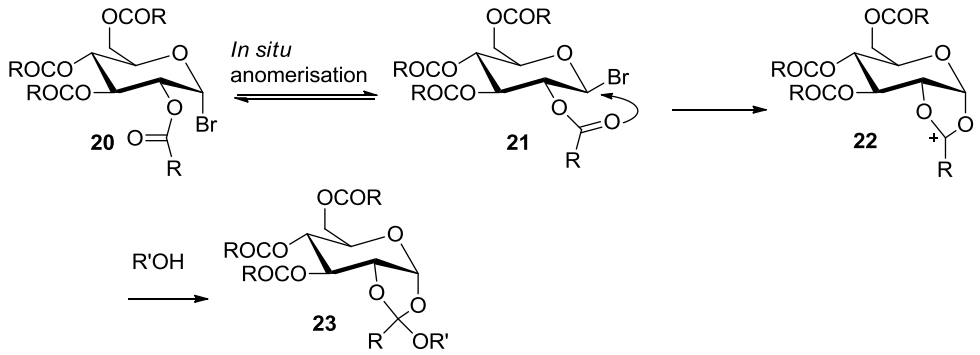

Scheme 4.4. Proposed mechanism for the formation of sugar 1,2-orthoester (**23**) from peracylated glucopyranosyl bromide (**20**).

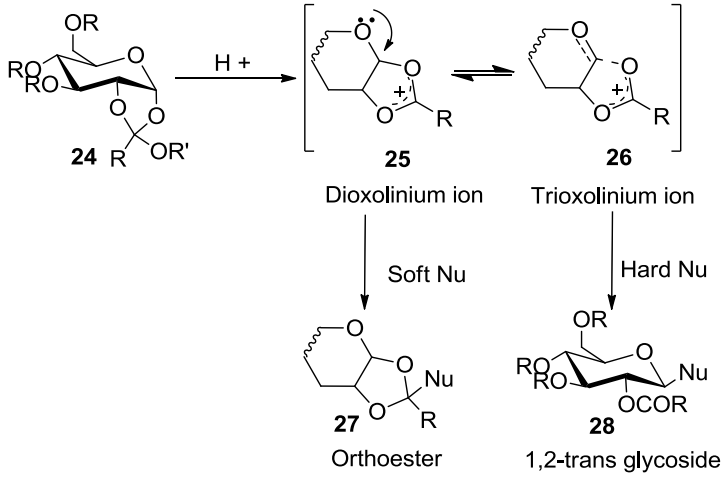

Scheme 4.5. Acid catalysed rearrangement of sugar 1,2-orthoester.

π-Conjugated back bone provides an excellent source for π-π stacking and thus improvise the self-assembly. Pyrene is a standard fluorophore with extensive π-conjugated skeleton because of its distinctive fluorescent parameters like, Ham effect, long fluorescence lifetime, excimer formation etc.[32] It is also amenable to various structural modifcations[33] and are widely explored as luminescent materials.[2a] Pyrene core have been widely employed in constructing LMWOGs.[2a] Some of the pyrene based LMWOGs[33,34,5b] are listed below (**29-34**, Figure 4.10).

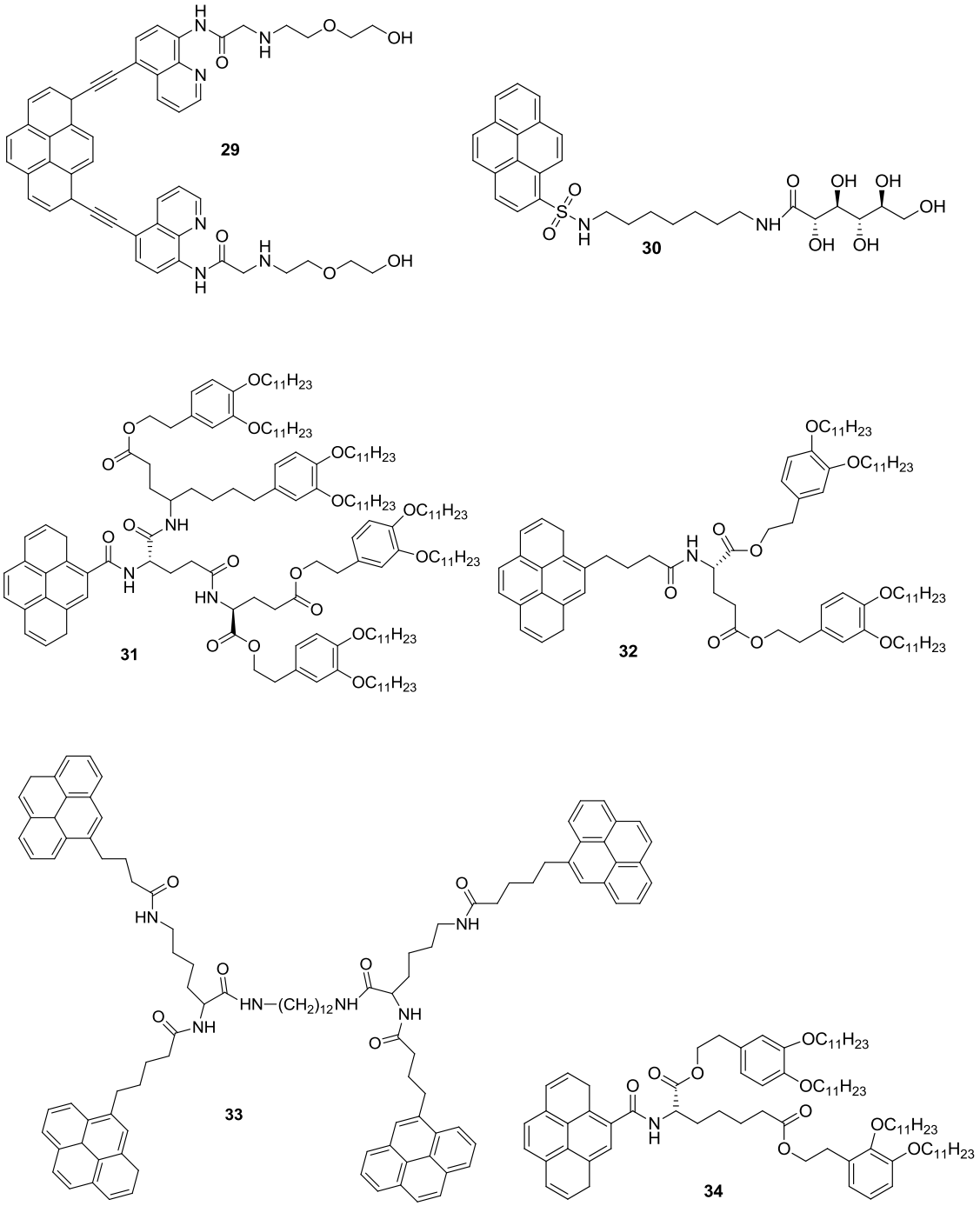

Figure 4.10. Structure of pyrene cored LMWOGs.

4.2. Statement of the problem

The significance of a pH responsive biomaterial is apparent from the above discussion. Among them, fluorescent pH responsive LMWOGs attracted particular interest owing to their sensitivity, flexibility and their application in the biomedical field. Carbohydrates are known economic, biocompatible building materials for the construction of LMWOGs. π-Extended chromophores also play a major role in gelation phenomena and pyrenes are extensively explored chromophores in the designing of LMWOGs. The present chapter deals with the design and synthesis of pyrene-carbohydrate-1,2-orthoester based pH responsive organogelator. Carbohydrate 1,2-orthoester is the acid labile functional group present in the gelator.

4.3. Results and discussion

4.3.1. Synthesis

Pyrene conjugated 1,2-orthoester based LMWOGs were synthesized. Two diastereomeric derivatives **PMO** and **PGO** were synthesized from the anomers mannose and glucose respectively. Orthoester linkage is formed in between pyrene methanol and sugar units by the condensation reaction of pyrenemethanol and bromoglycoside in the presence of bulky base 2,6-lutidine, tetrabutyl ammonium bromide in DCM solvent (Scheme 4.7).[31d] Molecular structures of the target molecules are listed in Figure 4.11. Synthetic strategy followed to obtain the pyrene-glucose orthoester-**PGO** derivative is shown below (Scheme 4.7 and 4.8), **PMO** was also synthesized by adapting the similar strategy starting from mannose. The structure of the orthoester derivative was unambiguously confirmed from the X-ray crystal analysis of **PMO** (Figure. 4.12).

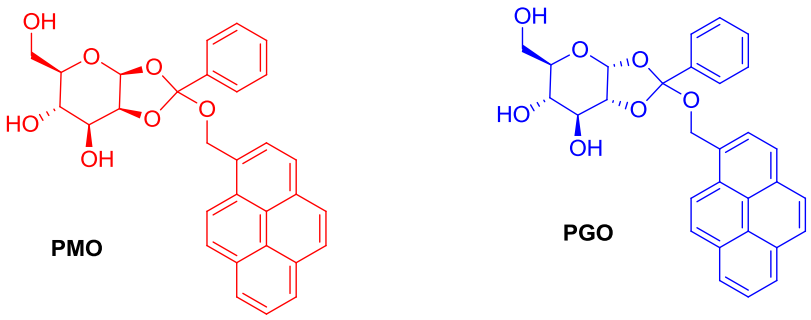

Figure 4.11. Molecular structure of target molecules **PMO** and **PGO**.

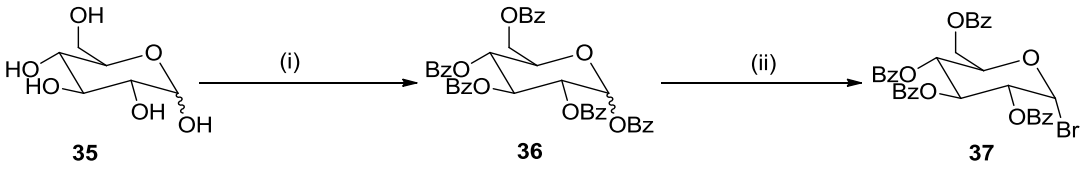

Scheme 4.7. (i) BzCl, Py, DMAP, DCM, 0 °C-rt, 12 h, 85 %; (ii) HBr in AcOH, DCM, 0 °C, 2 h, 60 %.

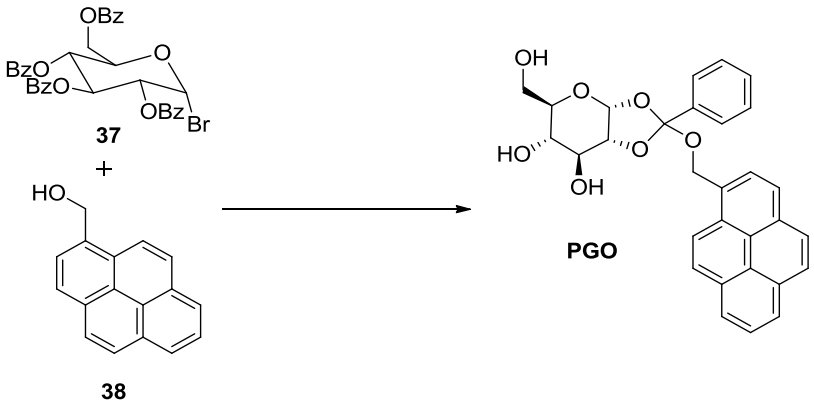

Scheme 4.8. (i) TBAB, 2,6- lutidine, MS, DCM, 50 °C, 12 h, 45 %.

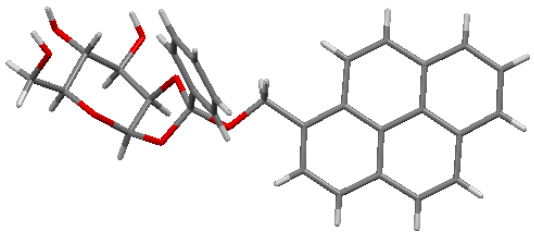

Figure 4.12. ORTEP diagram of the X-ray crystal formed from **PMO** in ethyl acetate hexane solvent system

4.3.2. Photophysical properties

Photophysical properties of the orthoester derivatives **PMO** and **PGO** were measured in different solvents (Chloroform, Tetrahydrofuran, Ethyl acetate, Ethanol and Toluene). Both these compounds did not exhibit considerable solvatochromism, except that the emission spectrum is slightly red shifted in toluene solvent. They displayed characteristic structured absorption and emission spectra of the pyrene motif. The two main peaks in the absorption spectra were located at λ_{max} = 328, 344 nm and the two main peaks in the emission spectra were observed around λ_{em} = 371, 391 nm and are representatives of monomeric absorption and emission (Figure 4.13).

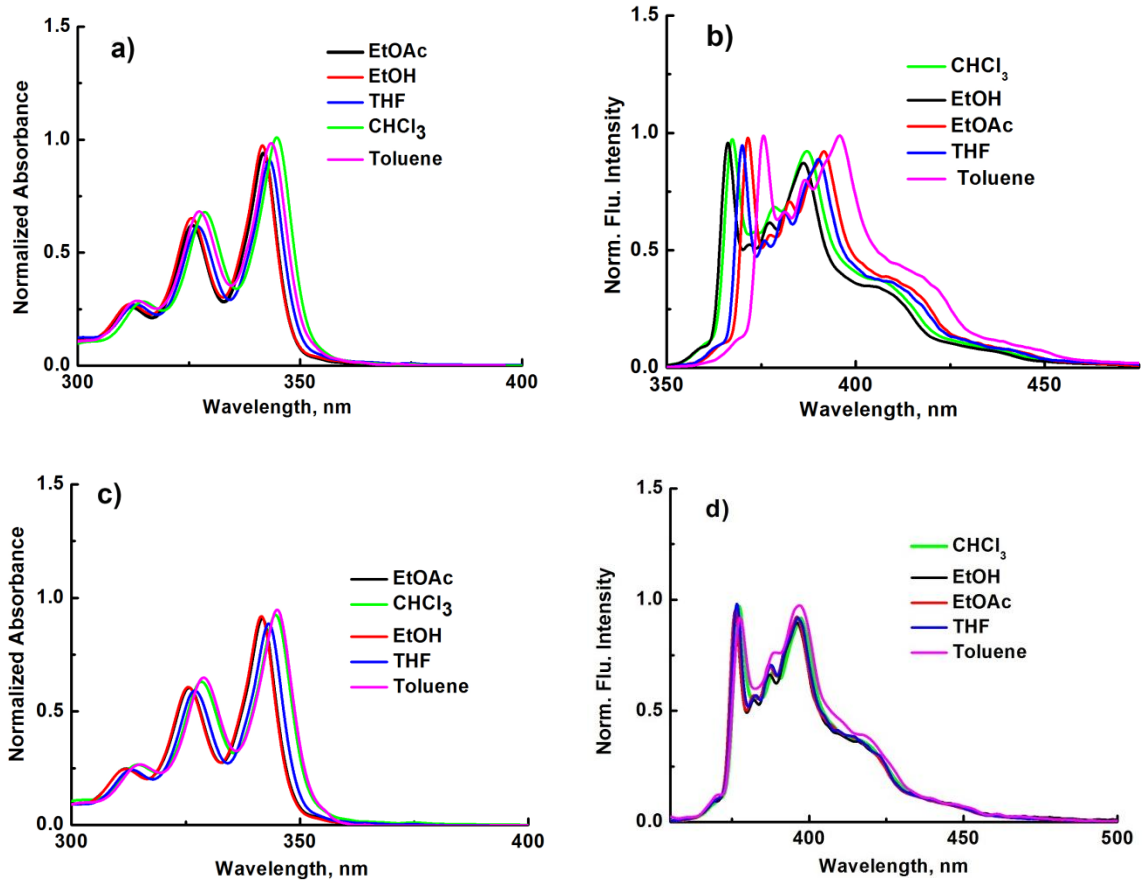

Figure 4.13. UV-Vis absorption and emission spectra of **PMO** (a and b) and **PGO** (c and d).

4.3.3. Gelation properties

The gelation properties of the compounds **PMO** and **PGO** were tested in various solvents including polar, nonpolar, aromatic and nonaromatic solvents like hexane, decane, ethanol, methanol, water, THF, DMF, DMSO, benzene, toluene, dioxane, ethyl acetate, acetone, dichloromethane, chloroform, 2-propanol, n-butanol and water. The results are listed in Table 4.1. Gelation test was performed by the "stable to inversion of a test tube" method, by inverting the material containing vial. Gels were prepared by dissolving a known amount of the sample in different solvents followed by sonication. **PMO** and **PGO** exhibited gelation behaviour in aromatic solvents such as toluene, xylene and benzene. Also, the gels formed were found to be emissive (Figure 4.14). The strength of these gels was monitored by measuring the

gel-sol transition temperatures. The lower gel-sol transition temperatures observed for **PMO** (43 °C) and **PGO** (50 °C) indicate that the gels formed from these gelators are very weak.

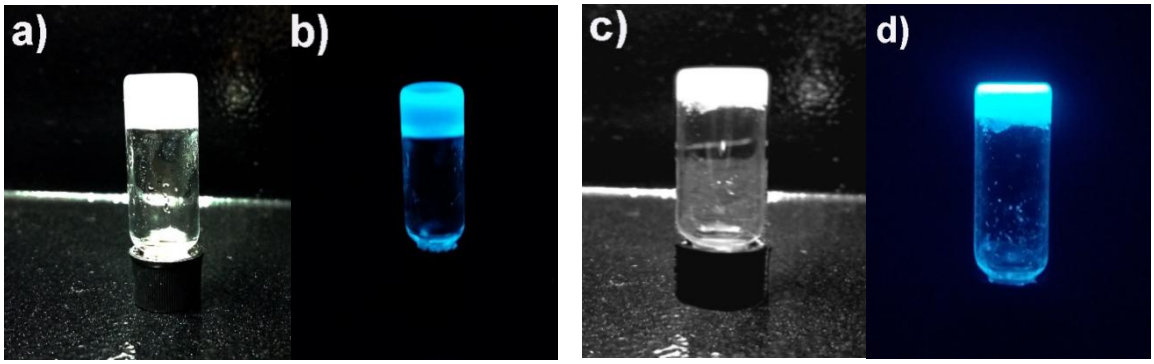

Figure 4.14. Images of the gels under normal light and UV light formed from **PMO** (a and b) and **PGO** (c and d) in toluene solution.

Table 4.1. Gelation property of **PMO** and **PGO** in different solvents

Solvent	Gelation behaviour/ Critical gelation concentration (wt %)	
	PMO	**PGO**
Hexane	Insoluble	Insoluble
Decane	Insoluble	Insoluble
Benzene	G/1.54	G/1.68
Toluene	G/1.11	G/1.26
Xylene	G/1.45	G/1.65
Acetone	Soluble	Soluble
EtOAc	P	P
MeOH	P	P
EtOH	P	P
BuOH	P	P
2-Propanol	P	P
Dioxane	Insoluble	Insoluble
Dichloromethane	P	P
Chloroform	P	P
THF	Soluble	Soluble
Acetonitrile	Soluble	Soluble
DMF	Solution	Solution
DMSO	Solution	Solution
Water	Insoluble	Insoluble

P = Precipitate, G = gel

Since the compounds **PMO** and **PGO** are forming gel in aromatic solvents, particularly showing excellent gelation properties in toluene solvent, we have chosen toluene solvent for further studies. To understand the self-assembling behaviour in toluene solvent, concentration dependent absorption and emission spectra were measured. No considerable change in the UV-Vis absorption and emission spectra was observed upon increasing the concentration of compounds, which indicate the absence of aggregate formation and excimer formation up to a concentration of 400 μM for **PMO** and **PGO** (Figure 4.15).

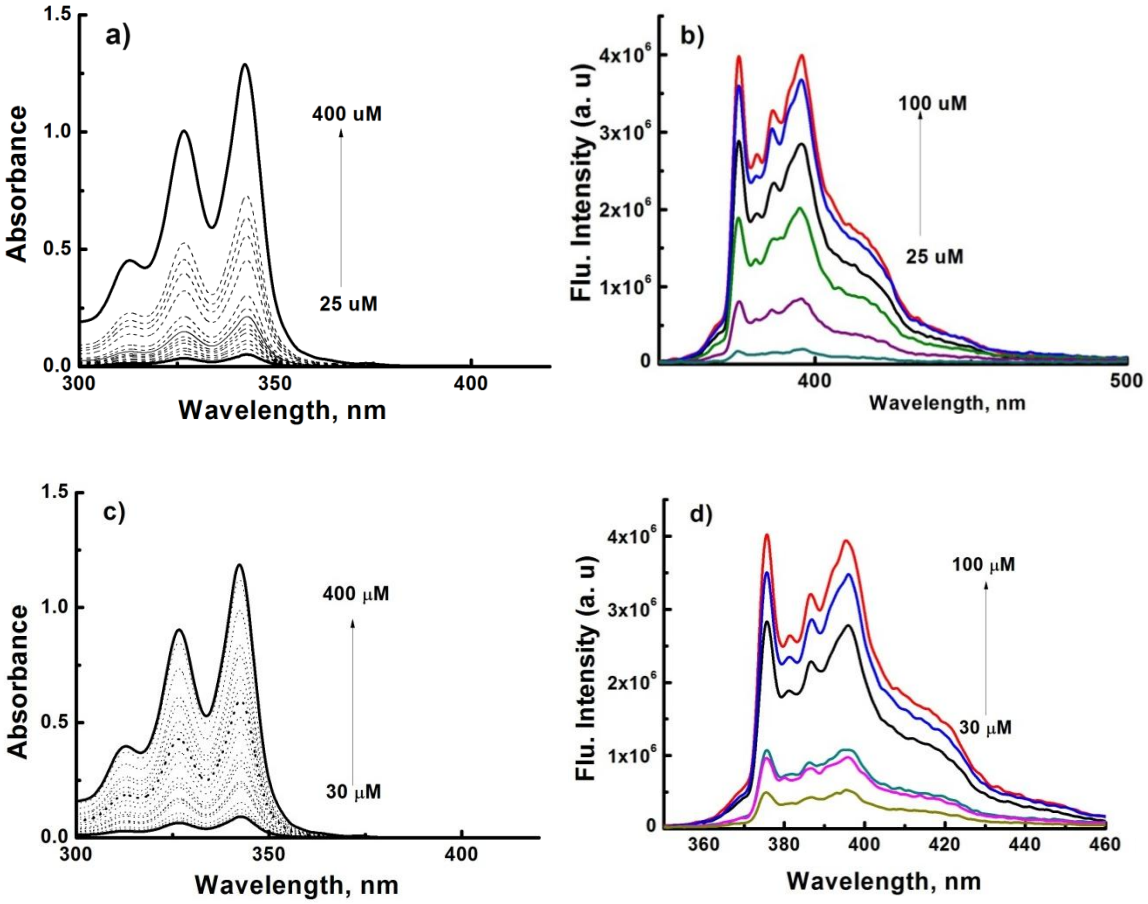

Figure 4.15. Concentration dependent UV-Vis absorption and emission spectral changes of **PMO** (a and b) and **PGO** (c and d) in toluene solution.

Morphology of the xerogels obtained from orthoester derivatives after evaporation of the toluene solvent was measured using scanning electron microscopy

(SEM) and atomic force microscopy (AFM). Both the derivatives showed high tendency to self-assemble in aromatic solvents and to form extended three dimensional structures. **PMO** showed thick fibres originating from a single point in SEM (Figure 4.16a). As with AFM, **PMO** exhibited variation in morphology with concentration (Figure 4.16b and c). At 20 μM concentration, it showed spherical morphology of micrometre size (Fig 4.16b). Whereas at high concentration-40 μM, fibres are shown to be growing from this spheres (Fig. 4.16c). In the case of **PGO**, an interstacked fibrillar network was observed for the xerogel in SEM (Fig. 4.16d). Whilst AFM images of **PGO** (40 μM) displayed spherical nanoparticles (Fig. 4.16e). Nanoparticle formation from **PGO** was confirmed by DLS analysis (Fig 4.17).

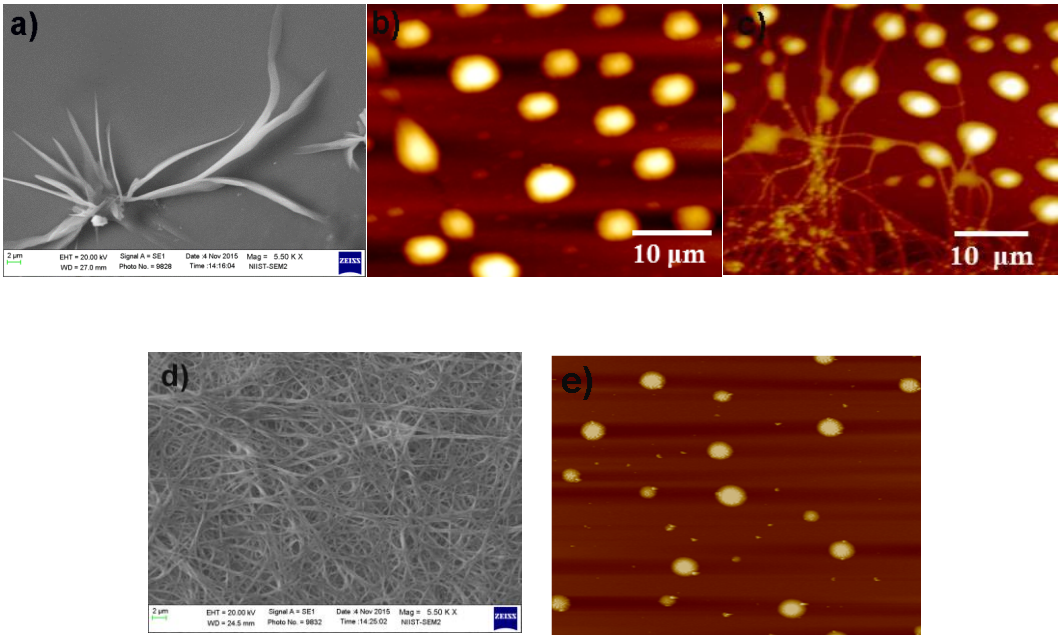

Figure 4.16. SEM images of the xerogel formed from **PMO** (a) and **PGO** (d) in toluene solution **PGO** (d), AFM images of **PMO** (b = 20 μM, c = 40 μM) and **PGO** (e = 40 μM) in toluene solution.

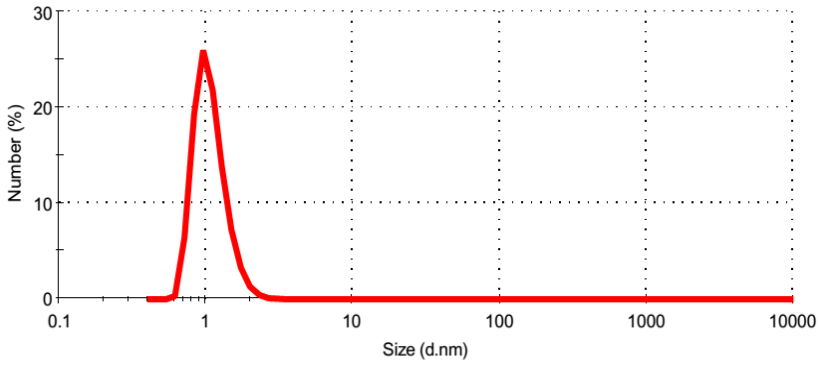

Figure 4.17. Size distribution analysis of **PGO** (40 μM, in toluene solution) by DLS.

4.3.4. Single crystal X-ray structure of PMO

Single crystals of **PMO** were grown in ethyl acetate-hexane solvent mixture and the crystal details are shown in Table 4.2. The crystal contains two molecules per unit cell (Figure 4.18) and the molecules are oriented in such a way that one pyrene core is arranged orthogonally to the adjacent one (Figure 4.19). Therefore, no effective π-π stacking is possible between the adjacent molecules. But there exists hydrogen bonding interactions between the hydroxyl groups of adjacent molecules. In toluene solvent, at higher concentrations the interactions of the solvent with solute molecules along with hydrogen bonding may contribute to the gel formation.

Table 4.2. Summary of crystallographic data.

Empirical formula	$C_{30}H_{26}O_7$
Molecular weight	498.51
Crystal system	Monoclinic
Space group	$P2_1$
Z	2
a, Å	8.642 (5)
b, Å	6.843 (4)
c, Å	20.761 (11)
α, deg	90
β, deg	99.460 (9)
γ, deg	90
V, Å^3	1211.1 (12)
Wavelength, nm	0.71073
Total reflections	5020
Final *R* indices *R1* and *wR2*	0.0537, 0.1316

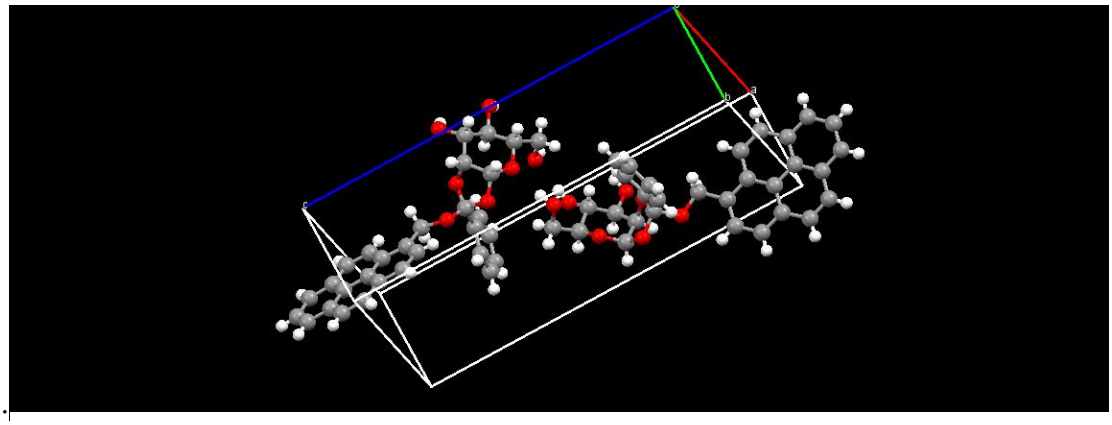

Figure 4.18. Crystal structure of **PMO** showing unit cell.

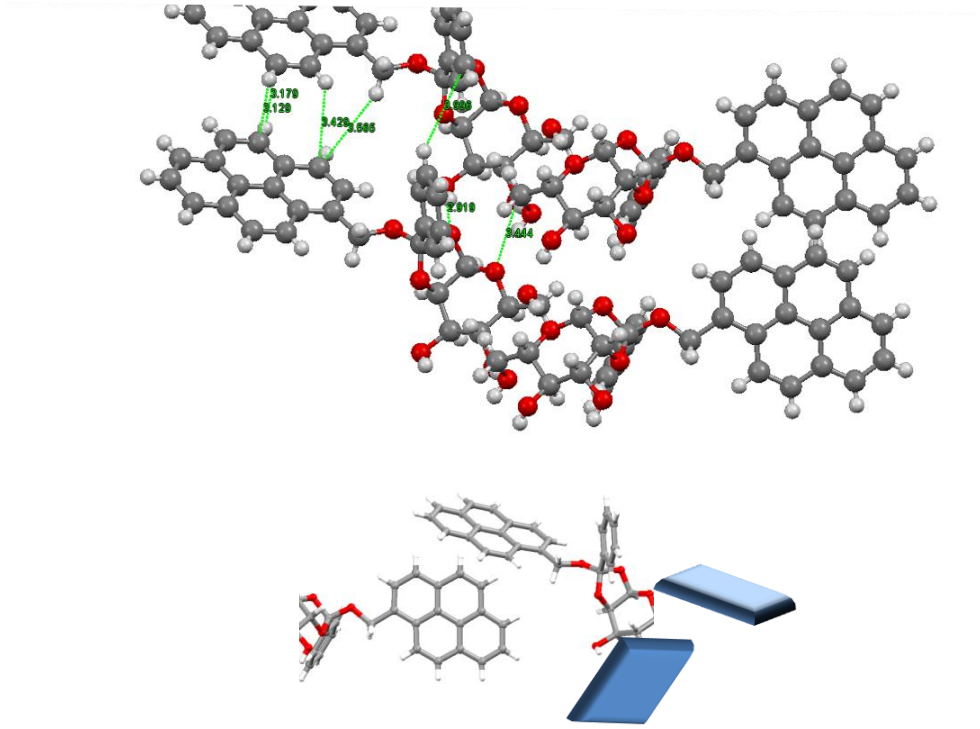

Figue 4.19. Major interactions in the crystal unit and the molecular orientation in the crystal of **PMO**.

Solid state X-ray diffraction studies of the two orthoester organogelators **PMO** and **PGO** revealed that **PMO** was crystalline in nature while **PGO** showed amorphous nature in solid state (Figure 4.20). Thermal stability of the compounds was checked using thermogravimetric analysis (TGA). TGA curve indicate that both these compounds were stable up to 300 °C (Figure. 4.21)

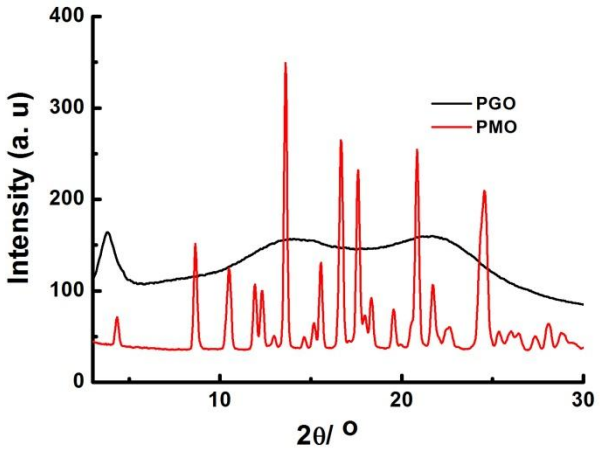

Figure 4.20. Powder X-ray diffraction studies of **PMO** and **PGO**.

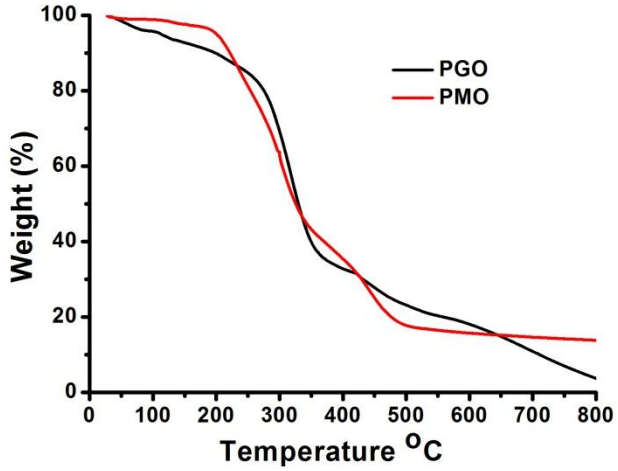

Figure 4.21. TGA thermograms for **PGO** and **PMO**.

4.3.5. Acidolysis

The response of these organogelators toward acidolysis was monitored using trifluoroacetic acid (TFA). Organogelators underwent cleavage in the presence of catalytic amount of TFA (Figure 4.22). UV-Vis spectral changes of the compounds during acidolysis were also monitored. A slight decrease in the intensity of absorption and emission was observed upon increasing the concentration of TFA in solution (Figure 4.23).

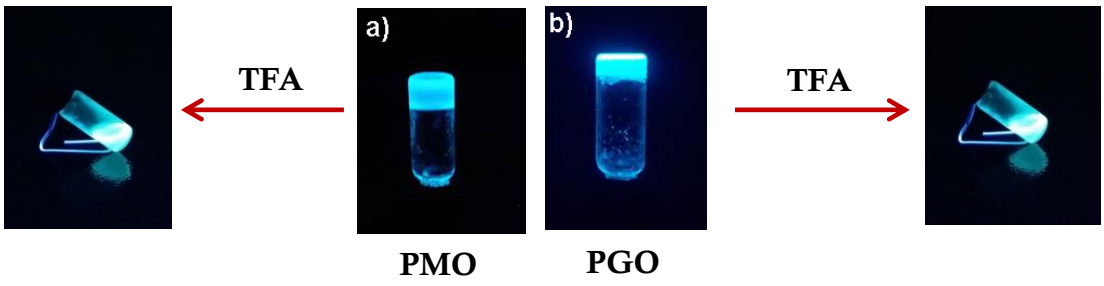

Figure 4.22. Photograph of acidolytic cleavage of the organogel formed from **PMO** (a) and **PGO** (b) in toluene in the presence of TFA.

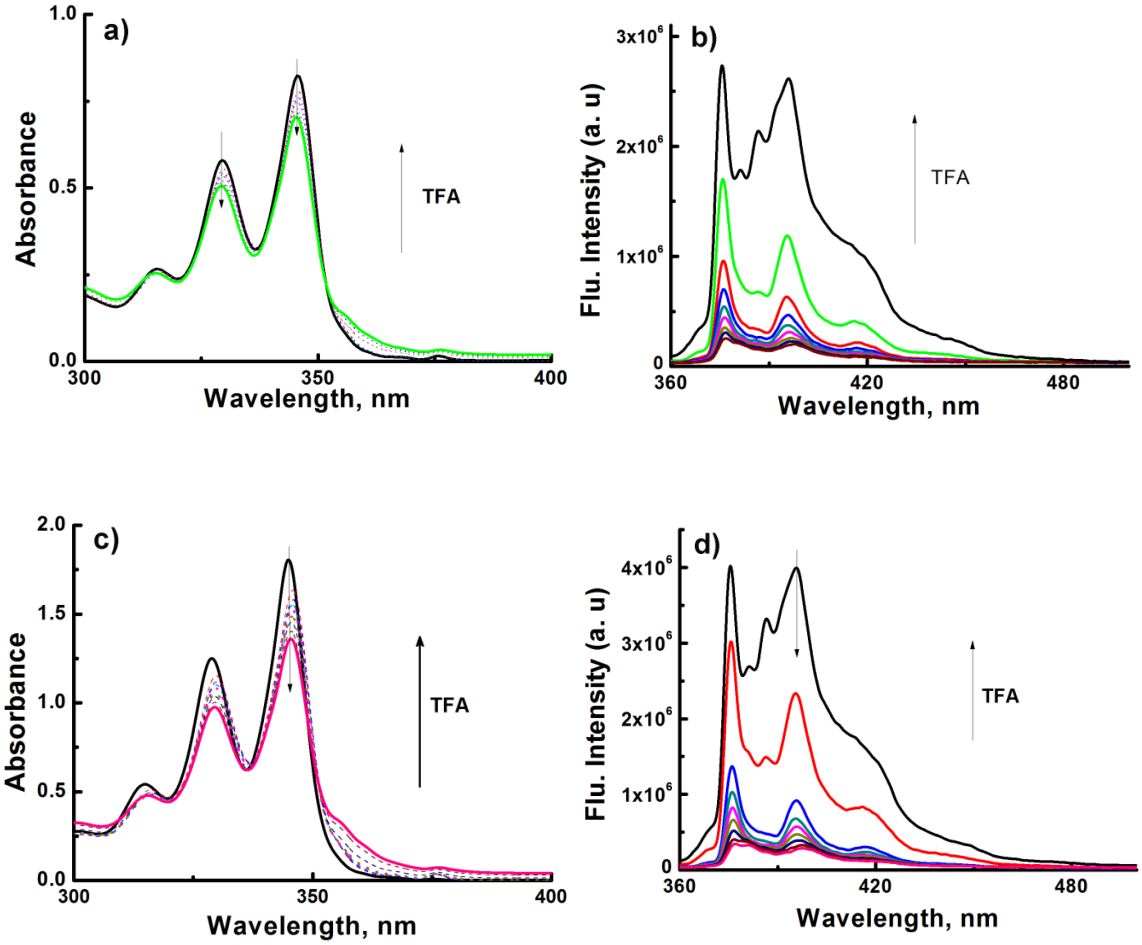

Figure 4.23. UV-Vis absorption and emission spectral changes of **PMO** (a and b) and **PGO** (c and d) in the presence of acid TFA.

This acidolytic cleavage was further confirmed with the aid of NMR spectra. In the presence of protic solvent, orthoester functional group undergoes cleavage and leads to the release of pyrenemethanol. This is evident from the ^{1}H NMR spectra before and after addition of TFA (Figure 4.24 and 4.25). A sharp singlet was appeared after addition of TFA in ^{1}H NMR spectra corresponds to the –OCH_2 of pyrene methanol. Also, shift in the peaks at the aromatic region (δ 7.2-7.8 ppm) indicates changes in the aromatic protons of benzoyl group attached to the C2 of the sugar unit. Based on the literature reports the acidolytic cleavage can be proposed as shown in scheme 4.9.[30]

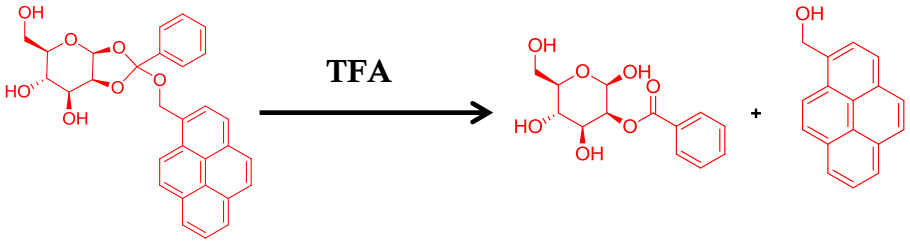

Scheme 4.9. Acidolytic cleavage of **PMO** in the presence of TFA.

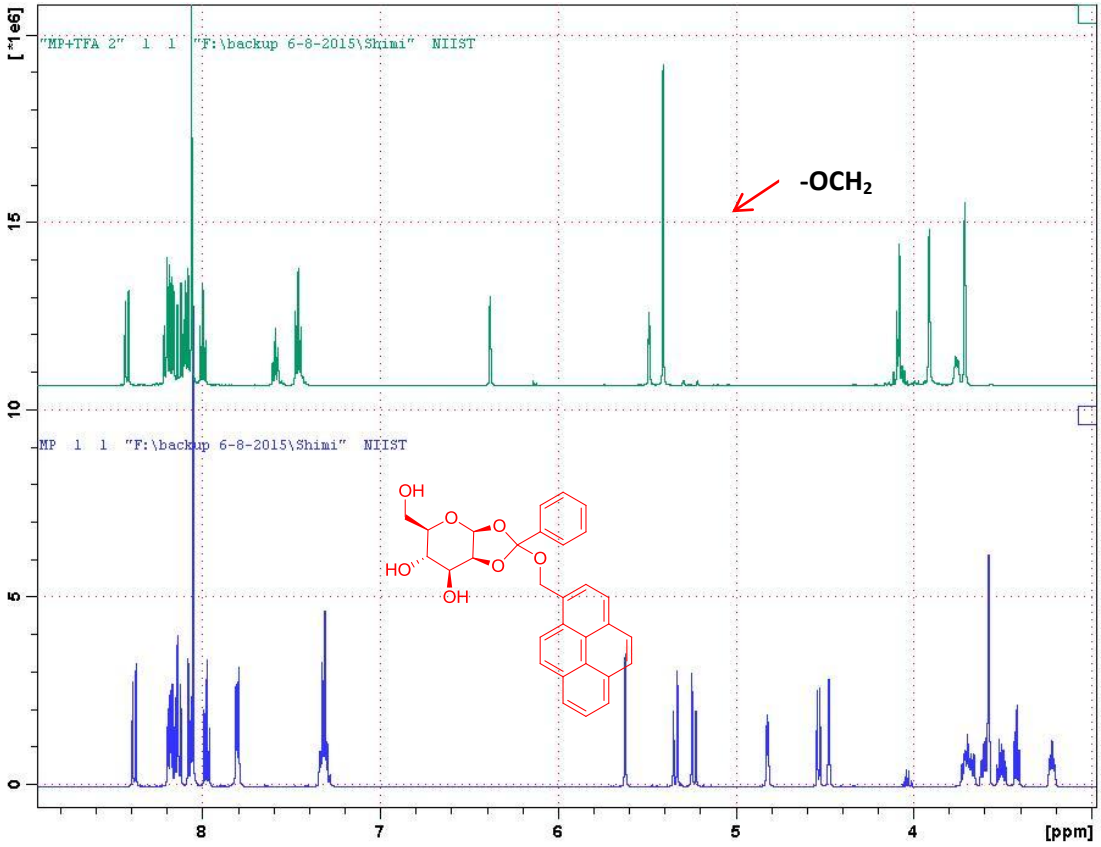

Figure 4.24. ^{1}H NMR spectra of **PMO** in deuteriated toluene solvent in the absence (a) and in the presence (b) of TFA (concentration of TFA = 10 μM).

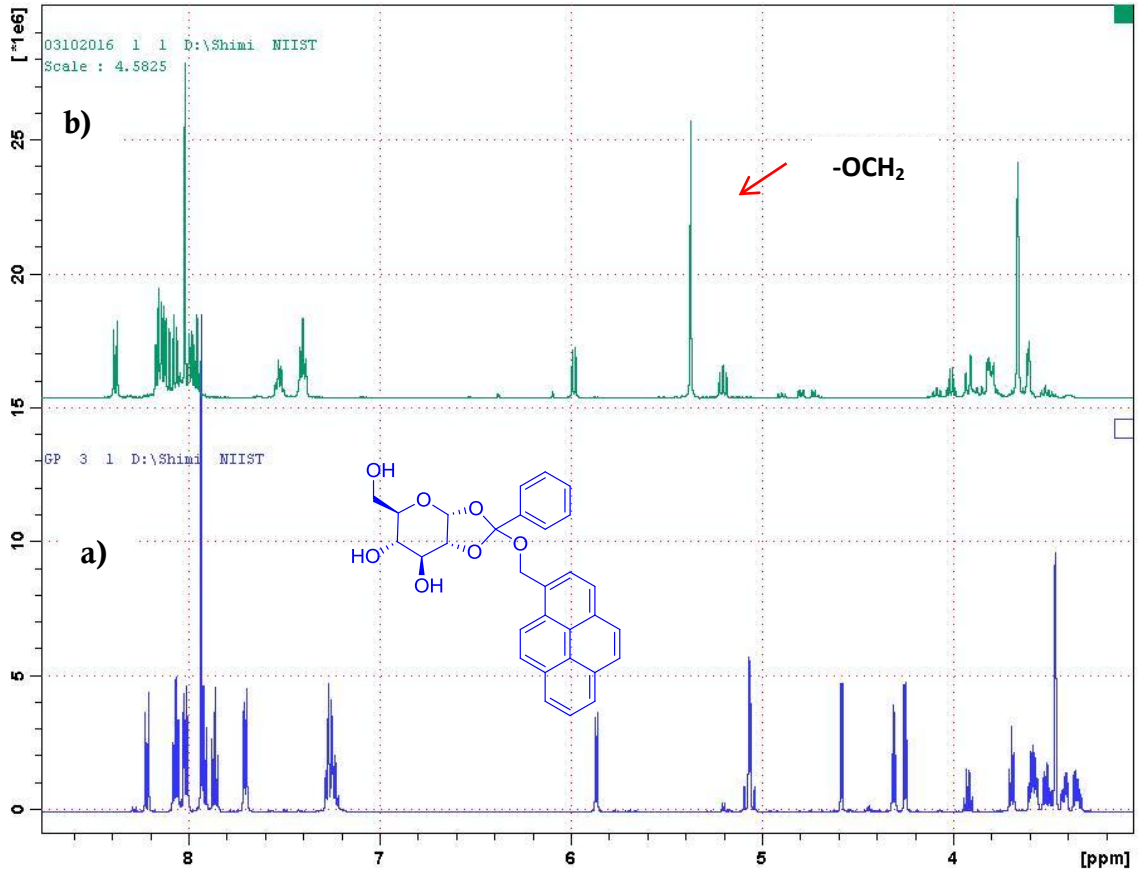

Figure 4.25. ^{1}H NMR spectra of **PGO** in deuteriated toluene solvent in the absence (a) and presence (b) of TFA (concentration of TFA = 10 μM).

4.3.6. Cytotoxicity assay

After completing all the characterisation studies and acidolysis, we checked the efficiency of the organogelators towards biological application. As a preliminary study, we checked the cytotoxicity of orthoester derivatives using MTT colourimetric assay with methylthiazolium tetrazole dye in normal cardiomyoblast cell lines (H9c2). The cytotoxicity assay was conducted using the compounds dissolved in DMSO solvent and the studies revealed that both these compounds are less cytotoxic (up to 10 μM) and the cells are viable in the presence of orthoesters (Figure 4.26, cells are incubated with compounds for a time period of 24 h). These cytotoxic studies point to the applicability of compounds **PMO** and **PGO** in biology as well.

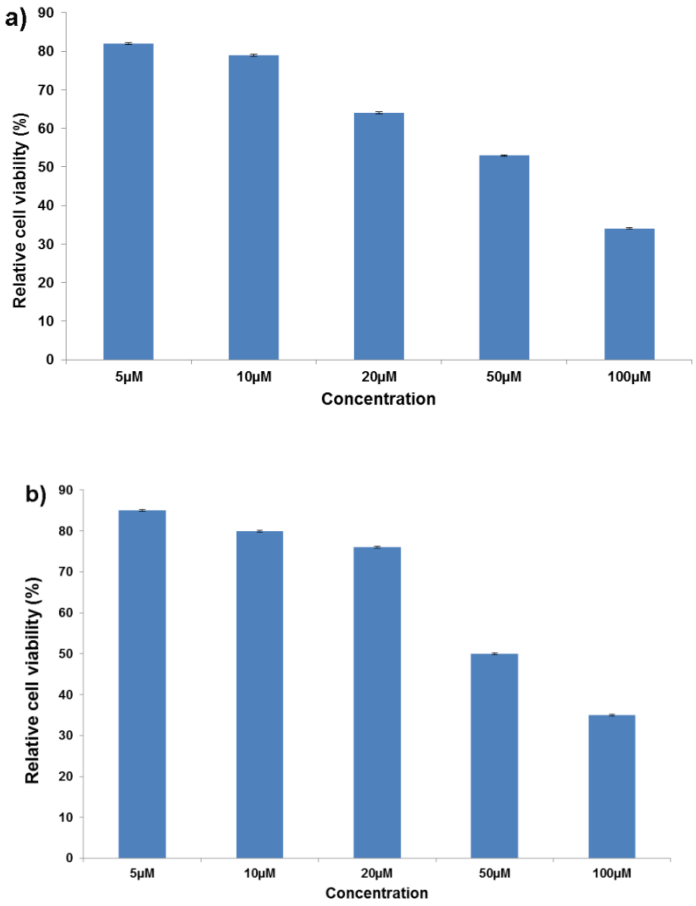

Figure 4.26. Relative cell viabilities of H9c2 cells incubated with (a) **PMO** and (b) **PGO.**

4.4. Conclusion

We have synthesized two pyrene-sugar orthoester conjugates **PMO** from mannose and **PGO** from glucose. Fluorescent organogels were formed from **PMO** and **PGO** in aromatic solvents like toluene and xylene upon heating and sonication. Photophysical properties of the synthesized pyrene-sugar conjugates were measured in various solvents and they exhibited characteristic absorption and emission properties of pyrene. Gels formed from orthoester derivatives showed pH sensitivity (acidic). Xerogels formed from both these orthoesters showed three dimensional fibre like morphology with difference in the thickness. Also these compounds are found to

be less toxic. These results disclosed the potency of carbohydrate orthoesters as new functional materials for biological studies.

4.5. Experimental section

4.5.1. Materials and methods

All the chemicals were purchased from Sigma-Aldrich, Alfa Aesar, Merck and SDFCL were used without further purification. ^{1}H and ^{13}C NMR were recorded on Bruker 500 MHz spectrometer using tetramethylsilane (TMS) as the standard. IR spectra were recorded on Bruker FT-IR spectrometer. Mass spectra were recorded under ESI/HRMS at 60,000 resolution using Thermo Scientific Exactive Mass Spectrometer. Absorption spectra were measured on a Shimadzu UV-3101 PC NIR scanning spectrophotometer and emission recorded on SPEX Fluorolog F112X spectrofluorimeter. AFM images were recorded under ambient conditions using a NTEGRA (NT-MDT) operating with a tapping mode regime. Micro-fabricated TiN cantilever tips (NSG10) with a resonance frequency of 299 kHz and a spring constant of S8 20-80 Nm^{-1} was used. AFM section analysis was done offline.

H9c2 cell lines were obtained from National Centre for Cell Science, Pune, India and also from Prof S. Murty Srinivasula of Indian Institute for Science Education and Research (IISER), Thiruvananthapuram, India. For maintenance of cell lines, Dulbeccos Modified Eagle's Medium (DMEM) *(Sigma)* containing 10 % fetal bovine serum (FBS) *(Gibco),* antibiotics (100 U/mL Penicillin and 100 µg/mL streptomycin) and amphotericin (0.25 µg/mL) *(HiMedia)* were employed. The cells were maintained in CO_2 incubators at 37 °C with 5 % CO_2 in air and 99 % humidity. Passaging of cells when confluent was carried out using 0.25 % trypsin and 0.02 % EDTA *(HiMedia)* in phosphate buffered saline (PBS). Experiments were carried out after 36 h of seeding the cells at appropriate density in suitable well plates.

4.5.2. Gelation test

5 mg of the compound was dissolved in 500 μL of the solvent in a test tube by heating and the solution was subjected to sudden sonication. The sample was classified as gel based on the inversion of test tube experiment.

4.5.3. Determination of critical gelation concentration (CGC)

5 mg of the gelator was dissolved in 100 μL of the solvent under study by heating in a test tube and gelation test was done. If it passes gelation test, further small measured volume of solvent was added and gelation test was conducted. This experiment was repeated until the gel failed inversion of test tube test. The maximum amount of solvent that can be gelated by 5 mg of the gelator was noted. From this, CGC was calculated as wt %.

4.5.4. Determination of gel transition temperature or gel melting temperature (Tgel)

The gel formed from compounds **PMO** or **PGO** in different solvents were prepared in a test tube. The test tube was heated gradually in an oil bath while observing the temperature. The temperature at which the gel melted to solution was recorded as Tgel.

4.5.5. Scanning electron microscopy (SEM)

SEM images were taken using ZEISS EVO MA and LS series scanning electron microscope. The operating range was between 100-230 V at 50-60 Hz single plane with a consumption of 2.5 kVA. The xerogels were prepared by drying the gels in toluene. A small amount of the xerogel was placed on carbon-tape pasted to a copper grid and later the sample was sputter coated with gold and directly imaged under the scanning electron microscope. The xerogels made up of **PMO** showed thick fibres whereas that from **PGO** showed interstacked fibrillar network.

4.5.6. AFM sample preparation

Dilute solutions of gelators in gelling solvents were drop casted on freshly cleaved mica sheets and allowed to dry at room temperature to form a thin layer of xerogel. These samples were viewed under Atomic Force Microscope.

4.5.7. Dynamic light scattering (DLS) analysis

The DLS studies were carried out on a Nano Zeta Sizer, Malvern instruments. The samples were prepared by dissolving in hot toluene solvent followed by sonication. The light scattering experiments were performed under low polydispersity index by using glass cuvettes.

4.5.8. General procedure for the synthesis of sugar orthoesters

Sugar bromide (1 equiv.) was dissolved in DCM solvent. 2,6-lutidine (2 equiv.) was added to the solution followed by the addition of pyrenemethanol (1.5 equiv.). The reaction mixture was refluxed for 6 h. The reaction mixture was extracted with ether and dried over Na_2SO_4 and the solvent was evaporated off completely. The crude sample on purification by silica-gel column chromatography afforded the protected sugar 1,2-orthoesters as a colorless viscous liquid. This crude was treated with sodium carbonate (4 equiv.) in methanol furnished the corresponding hydroxyl derivative of the sugar 1,2-orthoester.

((3aS,6S,7S,7aS)-5-(hydroxymethyl)-2-phenyl-2-(pyren-1-ylmethoxy)tetrahydro-3aH-[1,3]dioxolo[4,5-b]pyran-6,7-diol (PMO): Following the general procedure, glycosyl bromide, **28** (5 g, 7.5 mol), pyrenemethanol, **29** (2.6 g, 11.25 mol) and 2,6-lutidine (1.75 mL, 1.51 mmol) in 20 mL DCM solvent with 10 mol % TBAB were refluxed for 6 h. The crude product obtained from the above reaction was subjected to deprotection in the presence of Na_2CO_3 (3.2 g, 1.30 mol) in methanol to obtain hydroxylated orthoester derivative, **PMO**. The product was obtained as pale yellow solid after column chromatography using hexane-ethyl acetate solvent mixture (1.71 g, 45.3 %). **^{1}H NMR** ($CDCl_3$, 500 MHz): δ 8.37 (d, *J* = 9.0 Hz, 1 H), 8.33- 8.31 (m, 2 H), 8.18 (bs, 2 H), 8.11-8.08 (m, 2 H), 7.72-7.71 (m, 2 H), 7.39-7.38 (m, 3H), 5.71 (d, *J* = 9 Hz, 1H,), 5.41-5.39 (m, 1 H), 5.32 (d, *J* = 11 Hz, 1 H), 5.17 (d, *J* = 11.5 Hz, 1H), 5.09-5.07 (m, 1 H), 4.82-4.81 (m, 1 H), 3.78-3.77 (m, 1H), 3.69-3.65 (m, 1H), 3.42-3.39 (m, 1H), 3.30-3.26 (m, 1 H), 3.22-3.19 (m, 1H) ppm. **^{13}C NMR** ($CDCl_3$, 125 MHz): δ 139.1, 131.3, 131.1, 130.7, 129.3, 129.2, 128.3, 127.9, 127.8, 126.8, 125.9, 125.8, 125.2, 124.4, 124.3, 123.8, 97.9, 80.8, 77.1, 71.5, 67.5, 63.6, 61.7 ppm. HRMS (ESI) analysis *m/z* calcd for $C_{30}H_{26}O_7Na$: 521.1576; found 521.1589 $[M+Na]^+$.

(3aR,6S,7S,7aR)-5-(hydroxymethyl)-2-phenyl-2-(pyren-1-ylmethoxy)tetrahydro-3aH-[1,3]dioxolo[4,5-b]pyran-6,7-diol (PGO): Following the general procedure, mannosyl bromide (5 g, 7.5 mol), pyrenemethanol, **29** (2.6 g, 11.25 mol) and 2,6-lutidine (1.75 mL, 1.51 mol) in 20 mL DCM solvent with 10 mol % TBAB were refluxed for 6 h. The crude product obtained from the above react ion was subjected to deprotection in the presence of Na_2CO_3 (3.2 g, 1.30 mol) in methanol to obtain hydroxylated orthoester derivative, **PGO**. The product was obtained as pale yellow solid after column chromatography using hexane-ethyl acetate solvent mixture (2.12 g, 55.8 %). **^{1}H NMR** ($CDCl_3$, 500 MHz): δ 8.35-8.31 (m, 3H), 8.29- 8.18 (m, 2 H), 8.11-8.10 (m, 2 H), 8.08-8.06 (m, 2 H), 7.73- 7.72 (m, 2H), 7.47-7.43 (m, 3 H), 6.03 (d, *J* = 4.5 Hz, 1 H), 5.37 (d, *J* = 4 Hz, 1 H), 5.18 (m, 1 H), 4.68-4.66 (m, 1 H), 4.48-4.47 (m, 1 H), 3.63-3.60 (m, 2H), 3.48 (m, 1H), 3.47 (m, 1H), 3.29 (m, 1H) ppm. **^{13}C NMR** ($CDCl_3$, 125 MHz): δ 137.9, 130.9, 130.7, 130.2, 129.1, 128.7, 128.2, 127.7, 127.3, 126.3, 125.9, 125.4, 125.3, 124.7, 123.9, 123.8, 123.3, 119.7, 97.9, 78.3, 74.1, 72.5, 68.4, 63.0, 61.1, 59.7 ppm. HRMS (ESI) analysis *m/z* calcd for $C_{30}H_{26}O_7Na$: 521.1576; found 521.1575 $[M+Na]^+$.

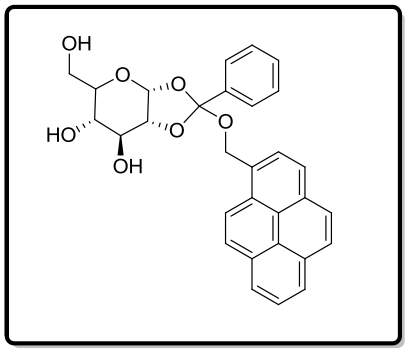

4.6. References

1. (a) G. G. Z. Zhang, S. Y. L. Paspal, R. Suryanarayanan, D. J. W. Grant, *J. Pharm. Sciences* **2003**, *92*, 1356-1366.; (b) J. Kopeček, P. Kopečková, T. Minko, Z. R. Lu, C. M. Peterson, *J. Control. Release* **2001**, *74*, 147-158.; Y. Takakura, M. Hashida, *Pharm. Res.* **1996**, *13*, 820-831.; (c) C. J. Pedersen, *J. Am. Chem. Soc.* **1967**, *89*, 7017-7036.; (d) J.-M. Lehn, in *Supramolecular Chemistry*, Wiley-VCH Verlag GmbH & Co. KGaA, **2006**, pp. 1-281.
2. (a) S. S. Babu, V. K. Praveen, A. Ajayaghosh, *Chem. Rev.* **2014**, *114*, 1973-2129.; (b) D. Zhai, W. Xu, L. Zhang, Y.-T. Chang, *Chem. Soc. Rev.* **2014**, *43*, 2402-2411.; (c) Y. Peng, Y. Feng, G.-J. Deng, Y.-M. He, Q.-H. Fan, *Langmuir* **2016**, *32*, 9313-9320.
3. (a) F. J. M. Hoeben, P. Jonkheijm, E. W. Meijer, A. P. H. J. Schenning, *Chem. Rev.* **2005**, *105*, 1491-1546.; (b) A. P. H. J. Schenning, E. W. Meijer, *Chem. Commun.* **2005**, 3245-3258.; (c) J.-H. Wan, W.-F. Fang, Y.-B. Li, X.-Q. Xiao, L.-H. Zhang, Z. Xu, J.-J. Peng, G.-Q. Lai, *Org. Biomol. Chem.* **2012**, *10*, 1459-1466.; (d) M. Shirakawa, S.-i. Kawano, N. Fujita, K. Sada, S. Shinkai, *J. Org. Chem.* **2003**, *68*, 5037-5044.
4. H. Jintoku, T. Sagawa, T. Sawada, M. Takafuji, H. Hachisako and H. Ihara, *Tetrahedron Lett.* **2008**, *49*, 3987-3990.
5. (a) L. Zhang, C. Liu, Q. Jin, X. Zhu, M. Liu, *Soft Matter* **2013**, *9*, 7966-7973.; (b) N. Yan, Z. Xu, K. K. Diehn, S. R. Raghavan, Y. Fang, R. G. Weiss, *Langmuir* **2013**, *29*, 793-805.
6. X. Lin, M. Hirono, H. Kurata, T. Seki, Y. Maruya, K.-i. Nakayama, S. Yagai, *Asian J. Org. Chem.* **2014**, *3*, 128-132.

7. V. K. Praveen, S. J. George, R. Varghese, C. Vijayakumar, A. Ajayaghosh, *J. Am. Chem. Soc.* **2006**, *128*, 7542-7550.
8. X. Cao, N. Zhao, A. Gao, H. Lv, Y. Jia, R. Wu, Y. Wu, *Mater. Sci. Eng. C* **2017**, *70, Part 1*, 216-222.
9. (a) L. A. Estroff, A. D. Hamilton, *Chem. Rev.* **2004**, *104*, 1201-1218.; (b) L. Qin, P. Duan, F. Xie, L. Zhang, M. Liu, *Chem. Commun.* **2013**, *49*, 10823-10825.; (c) A. Vintiloiu, J.-C. Leroux, *J. Control. Release* **2008**, *125*, 179-192.
10. (a) N. S. S. Kumar, S. Varghese, G. Narayan, S. Das, *Angew. Chem. Int. Ed.* **2006**, *45*, 6317-6321.; (b) S. Wang, W. Shen, Y. Feng, H. Tian, *Chem. Commun.* **2006**, 1497-1499.
11. (a) J. W. Chung, B.-K. An, S. Y. Park, *Chem. Mater.* **2008**, *20*, 6750-6755.; (b) A. Y.-Y. Tam, K. M.-C. Wong, V. W.-W. Yam, *J. Am. Chem. Soc.* **2009**, *131*, 6253-6260.
12. (a) Y. Li, K. Liu, J. Liu, J. Peng, X. Feng, Y. Fang, *Langmuir* **2006**, *22*, 7016-7020.; (b) N. E. Shi, H. Dong, G. Yin, Z. Xu, S. H. Li, *Adv. Funct. Mater.* **2007**, *17*, 1837-1843.; (c) D.-C. Lee, K. K. McGrath, K. Jang, *Chem. Commun.* **2008**, 3636-3638.
13. (a) S.-i. Kawano, N. Fujita, S. Shinkai, *J. Am. Chem. Soc.* **2004**, *126*, 8592-8593.; (b) C. Wang, Q. Chen, F. Sun, D. Zhang, G. Zhang, Y. Huang, R. Zhao, D. Zhu, *J. Am. Chem. Soc.* **2010**, *132*, 3092-3096.; (c) J. E. A. Webb, M. J. Crossley, P. Turner, P. Thordarson, *J. Am. Chem. Soc.* **2007**, *129*, 7155-7162.
14. (a) W. Busa, R. Nucitelli, *Am. J. Physiol.* **1984**, *246*, R409–R438.; (b) W. Busa, *Annu. Rev. Physiol.* **1986**, *48*, 389–402.; (b) E. M. Bachelder, T. T. Beaudette, K. E. Broaders, J. Dashe, J. M. J. Fréchet, *J. Am. Chem. Soc.* **2008**, *130*, 10494-10495.

15. E. M. Bachelder, T. T. Beaudette, K. E. Broaders, J. Dashe, J. M. J. Fréchet, *J. Am. Chem. Soc.* **2008**, *130*, 10494-10495.

16. (a) Z. L. Cheng, A. Al Zaki, J. Z. Hui, V. R. Muzykantov, A. Tsourkas, *Science* **2012**, *338*, 903-910.; (b) S. M. Nie, Y. Xing, G. J. Kim, J. W. Simons, *Annu. Rev. Biomed. Eng*. **2007**, *9*, 257-288.; (c) S. M. Lee, H. Park, J. W. Choi, Y. N. Park, C. O. Yun , K. H. Yoo, *Angew. Chem., Int. Ed*. **2011**, *50*, 7581-7586.

17. (a) L. Cui, J. A. Cohen, K. E. Broaders, T. T. Beaudette, J. M. J. Fréchet, *Bioconjug. Chem.* **2011**, *22*, 949-957.; (b) J. A. Cohen, T. T. Beaudette, J. L. Cohen, K. E. Brooders, E. M. Bachelder, J. M. J. Frechet, *Adv. Mater.* **2010**, *22*, 3593−3597.

18. (a) Y. M. Zhang, Q. Lin, T. B. Wei, X. P. Qin and Y. Li, *Chem. Commun.* **2009**, 6074-6076; (b) J. Boekhoven, J. M. Poolman, C. Maity, F. Li, L. van der Mee, C. B. Minkenberg, E. Mendes, J. H. van Esch and R. Eelkema, *Nat. Chem.* **2013**, *5*, 433-437. (c) H. Qian, I. Aprahamian, *Chem. Commun.* **2015**, *51*, 11158-11161.

19. E. R. Gillies, A. P. Goodwin, J. M. J. Fréchet, *Bioconjug. Chem.* **2004**, *15*, 1254-1263.

20. G. Leriche, M. Nothisen, N. Baumlin, C. D. Muller, D. Bagnard, J.-S. Remy, S. A. Jacques, A. Wagner, *Bioconjug. Chem.* **2015**, *26*, 1461-1465.

21. J.-L. Pozzo, G. Michel Clavier, J.-P. Desvergne, *J. Mater. Chem.* **1998**, *8*, 2575-2577.

22. C. Zhou, W. Gao, K. Yang, L. Xu, J. Ding, J. Chen, M. Liu, X. Huang, S. Wang, H. Wu, *Langmuir* **2013**, *29*, 13568-13575.

23. P. Rajamalli, P. S. Sheet, E. Prasad, *Chem. Commun.* **2013**, *49*, 6758-6760.

24. S. Datta, S. Bhattacharya, *Chem. Soc. Rev.* **2015**, *44*, 5596-5637.

25. J. H. Fuhrhop, C. Boettcher, *J. Am. Chem. Soc.* **1990**, *112*, 1768-1776.

26. (a) O. Gronwald, S. Shinkai, *Chem. Eur. J.* **2001**, *7*, 4328-4334.; (b) K. Yoza, Y. Ono, K. Yoshihara, Y. Ono, T. Akao, H. Shinmori, M. Takeuchi, S. Shinkai, D. N. Reinhoudt, *Chem. Commun.***1998**, 907-908.; (c) K. Yoza, N. Amanokura, Y. Ono, T. Akao, H. Shinmori, M. Takeuchi, S. Shinkai, D. N. Reinhoudt, *Chem. Eur. J.* **1999**, *5*, 2722-2729.; (d) N. Amanokura, K. Yoza, H. Shinmori, S. Shinkai, D. N. Reinhoudt, *J.Chem. Soc., Perkin Trans. 2* **1998**, 2585-2592.; (e) O. Gronwald, K. Sakurai, R. Luboradzki, T. Kimura, S. Shinkai, , *Carbohydr. Res.* **2001**, *331*, 307-318.

27. (a) J. H. Jung, G. John, M. Masuda, K. Yoshida, S. Shinkai, T. Shimizu, *Langmuir* **2001**, *17*, 7229-7232.; (b) Q. Ji, S. Kamiya, J.-H. Jung, T. Shimizu, *J. Mater. Chem.* **2005**, *15*, 743-748.; (c) J. H. Jung, J. A. Rim, W. S. Han, S. J. Lee, Y. J. Lee, E. J. Cho, J. S. Kim, Q. Ji, T. Shimizu, *Org. Biomol. Chem.* **2006**, *4*, 2033-2038.

28. (a) A. Srivastava, S. Ghorai, A. Bhattacharjya, S. Bhattacharya, *J. Org. Chem.* **2005**, *70*, 6574-6582.; (b) S. Bhattacharya, S. N. G. Acharya, *Chem. Mater.* **1999**, *11*, 3504-3511.

29. J. Cui, A. Liu, Y. Guan, J. Zheng, Z. Shen, X. Wan, *Langmuir* **2010**, *26*, 3615-3622.

30. (a) E. Pacsu, in *Advances in Carbohydrate Chemistry, Vol. Volume 1* (Eds.: W. W. Pigman, M. L. Wolfrom), Academic Press, **1945**, pp. 77-127.; (b) F. Kong, , *Carbohydr. Res.* **2007**, *342*, 345-373.

31. (a) T. Ogawa, K. Beppu, S. Nakabayashi, *Carbohydr. Res.* **1981**, *93*, C6-C9.; (b) Z. Yang, W. Lin, B. Yu, , *Carbohydr. Res.* **2000**, *329*, 879-884.; (c) F. J. Urban,

B. S. Moore, R. Breitenbach, *Tetrahedron Lett.* **1990**, *31*, 4421-4424.; (d) W. Wang, F. Kong, *J. Org. Chem.* **1998**, *63*, 5744-5745.

32. B. Valeur, *Molecular Fluorescence: Principles and Applications*, Wiley-VCH Verlag GmbH, **2001**
33. T. M. Figueira-Duarte, K. Müllen, *Chem. Rev.* **2011**, *111*, 7260-7314.
34. (a) C.-B. Huang, L.-J. Chen, J. Huang, L. Xu, *RSC Adv.* **2014**, *4*, 19538-19549; (b) Y. Kamikawa, T. Kato, *Langmuir* **2007**, *23*, 274-278.

List of publications

1. Jijy, E.; Praveen, P.; **Shimi, M**.; Pihko, P. M.; Nayana Joseph.; and Radhakrishnan, K.V. *Rhodium catalyzed oxidative coupling of salicylaldehydes with diazabicyclic olefins: a one pot strategy involving aldehyde C-H cleavage and π-allyl chemistry towards the synthesis of fused ring chromanones*. *Chem. Commun***. 2013,** *49*, 7349-7351.

2. Jijy, E.; Praveen, P.; **Shimi, M**.; Saranya, S.; Preethanuj, P.; Pihko, P. M.; Sunil, V. and Radhakrishnan, K.V. *Rhodium(III)-catalysed ring opening of strained olefins through C-H activation of O-acetyl ketoximes: an efficient synthesis of trans-functionalized cyclopentenes and spiro[2.4] heptenes*. *Tetrahedron Lett.* **2013,** *54*, 7127-7131.

3. Prakash, P.; Jijy, E.; **Shimi, M**.; Aparna, P. S.; Suresh, E. and Radhakrishnan, K. V. *Mild rhodium(I) catalysed ring opening of cyclopropane appended spirocyclic olefins through C-H activation of aryl boronic acids. RSC Adv.* **2013,** *3*, 19933-19936.

4. Ajesh Vijayan; Jijy, E.; Praveen Prakash; Baiju, T. V.; **Shimi, M.**; Petri P. M.; Nayana Joseph and Radhakrishnan, K. V. *Rhodium catalyzed oxidative coupling of salicylaldehydes with heterobicyclic olefins towards the synthesis of fused chromanones*. *Tetrahedron* **2016**, *72*, 4007-4015.

5. **Shimi, M.**; Vandana, S.; Rahim, M .K.; and Nitha, P. R.; Suresh Das.; Radhakrishnan, K. V. and Raghu, K. G. *Novel glyco-conjugated squaraine dyes for selective tumor imaging. Chem. Commn.* **2017**, *53*, 5433-5436.

6. **Shimi M**.; Preethanuj P.; Nitha P. R.; Santhini P. V.; Suresh Das and Radhakrishnan K. V. *pH responsive fluorescent organogels derived from pyrene-sugar orthoesters. (To be communicated)*

Papers presented at conferences

1. Near infrared fluorescent glycoconjugated squaraine dyes for targeted tumour optical imaging, **Shimi M**.; Vandana Sankar, Suresh Das; Radhakrishnan, K. V.; K. G. Raghu, a poster presented at International Symposium on Photonics Applications and Nanomaterials, Thiruvananthapuram, December **2015**.

2. A facile route towards fused chromanone derivatives *via* rhodium catalyzed oxidative coupling of salicylaldehydes with diazabicyclic olefins, **Shimi**, **M**.; Jijy, E.; Praveen Prakash and Radhakrishnan, K. V. a poster presented at National Symposium on Transcending Frontiers in Organic Chemistry, held at CSIR-National Institute for Interdisciplinary Science & Technology, Thiruvananthapuram, October **2014**.